

**System-Level Ventilation Considerations for Thermal Risk Assessment
of Aircraft Systems in Conceptual Design**

Abdul Malik Huzaifa

A Thesis

in

The Department of

Mechanical, Industrial and Aerospace Engineering

**Presented in Partial Fulfillment of the Requirements for the Degree of
Master of Applied Science (Mechanical Engineering) at Concordia University**

Montreal, Quebec, Canada

June 2021

© Abdul Malik Huzaifa, 2021

Concordia University
School of Graduate Studies

This is to certify that the thesis prepared

By: Abdul Malik Huzaifa

Entitled: System-Level Ventilation Considerations for Thermal Risk Assessment of Aircraft Systems in Conceptual Design

and submitted in partial fulfillment of the requirements for the degree of

Master of Applied Science (Mechanical Engineering)

complies with the regulations of this University and meets the accepted standards with respect to originality and quality. Signed by the Final Examining Committee:

_____ Chair
Dr. Brian Vermeire

_____ External Examiner
Dr. Liangzhu Wang

_____ Examiner
Dr. Brian Vermeire

_____ Supervisor
Dr. Susan Liscouët-Hanke

Approved by

Dr. Martin D. Pugh, Chair
Department of Mechanical, Industrial and Aerospace Engineering

30 June 2021

Dr. Mourad Debbabi, Dean
Gina Cody School of Engineering and Computer Science

Abstract

System-Level Ventilation Considerations for Thermal Risk Assessment of Aircraft Systems in Conceptual Design

Abdul Malik Huzaifa

The aviation industry is moving towards an environment-friendly future. Therefore, aircraft manufacturers are investigating new technologies to make future aircraft more efficient while striving at the same time to reduce development time and cost. These new technologies, such as more electric or hybrid-electric aircraft, require novel design tools to improve different aspects of aircraft design. One important aspect is the thermal analysis for aircraft systems, usually implemented during later stages as they require detailed information. The late consideration of thermal aspects can lead to delays due to redesign. With the recently developed Thermal Risk Assessment (TRA) approach, thermal architectures for systems can be defined in conceptual design. This thesis contributes to developing these conceptual thermal design tools by improving the TRA. The focus of this thesis is on system-level ventilation aspects; a so-called mainstream flow analysis is introduced. This analysis investigates the relationship between the location of the aircraft systems within equipment bays and the characteristics of the ventilation sources. New dimensionless numbers (DN) are defined to capture the effects of the mainstream flow. The development of the DN, their integration, and validation into the TRA is performed through several case studies using computational fluid dynamics (CFD). As a result, this new system-level ventilation analysis is introduced successfully into the TRA. The improved TRA shows satisfactory results for real-world aircraft equipment bays. As the analysis is based on DN, which is much faster than conventional CFD analysis and requires fewer inputs, suitable cooling strategies can now be developed during the conceptual design phase. In this way, thermal analyses can be integrated into a multidisciplinary design analysis and optimization framework, helping aircraft manufacturers develop more mature concepts with fewer iterations, particularly important for future unconventional, more electric, hybrid-electric, or all-electric aircraft configurations.

Acknowledgments

In the name of God, the Most Beneficent, the Most Merciful.

I dedicate this thesis to my parents for enabling me to think, persevere and work towards my goals. I have gained invaluable experiences over the last few years at Concordia, which have helped me grow as a person. I would like to thank Dr. Susan Liscouët-Hanke for providing me the opportunities to look into the fascinating world of aerospace. I am grateful for her patience and her constant support in times both tough and jolly. I would also like to thank Dr. Florian Sanchez, who was my co-researcher on the topic. He mentored me and helped me with minutest of problems related to my research. I would also like to thank my colleagues in the lab: Andrew, Vijesh, Shakti and others for making work seem like fun. Finally, I would like to thank my parents for being the beacon of support during my masters.

Table of Contents

List of Figures	vii
List of Tables	x
Nomenclature	xi
1 Introduction.....	1
1.1 Background and Motivation.....	1
1.2 Thesis Scope and Objectives.....	5
1.3 Organization of the Thesis	6
2 State of the Art.....	7
2.1 Thermal Considerations in Aircraft Design	7
2.2 Use of Dimensionless Numbers (DN) in Thermal Analyses	9
2.3 Prior Work in Thermal Risk Assessment (TRA) in Aircraft Conceptual Design.....	11
2.3.1 Existing TRA Workflow.....	12
2.3.2 Need for Enhanced System-Level Analyses.....	17
2.4 Literature Review on Enhanced System-Level Thermal Analyses.....	17
2.4.1 Background on Mainstream Flow Analysis.....	18
2.4.2 Other System-Level Analyses: Heat Removal Potential Analysis	20
3 Methodology for the Integration of Mainstream Flow Analysis in the Existing Thermal Risk Assessment.....	22
3.1 Adaption of Mainstream Flow Analysis to Conceptual Design of Aircraft Equipment Bays	22
3.1.1 Overview of Case Studies.....	23
3.1.2 Overview of CFD Simulation Approach Used for Development and Validation ..	24
3.2 Preliminary development: First Iteration of the Development of Mainstream Numbers Using a Simplified 2D Case Study	27
3.2.1 Simple 2D Case Studies Using a Single System	29
3.2.2 Design Study to Define the Boundaries of S_1 and S_2	31
3.2.3 Limitations of the First Iteration.....	36
3.3 Enhanced Formulation of the Mainstream Numbers MS	36
3.3.1 Formulation of the Streamwise Number SW	38
3.3.2 Formulation of the Cross-Stream Number CS	38
3.3.3 Mainstream Flow Analysis Using Cross-Stream and Streamwise Numbers.....	40

3.3.4	Examples of Mainstream Flow Prediction Using the Mainstream Numbers.	42
3.3.5	Conclusion	48
3.4	Updated Thermal Risk Assessment.....	48
3.4.1	Thermal Risk Scoring Workflow with Mainstream Flow Analysis	48
3.4.2	Ventilation Analysis Scoring (TR ₁).....	51
3.4.3	Temperature Stratification Analysis Scoring (TR ₂).....	51
3.4.4	Mainstream Flow Analysis Scoring (TR ₃).....	51
3.4.5	Temperature Limits Scoring (TR ₄).....	53
3.4.6	System Integration Scoring (TR ₅).....	53
3.4.7	Heat Removal Potential Scoring (TR ₆).....	53
3.4.8	Thermal Interaction Scoring (TR ₇).....	54
3.4.9	Conclusion	54
4	Application of the Updated Thermal Risk Assessment on Aircraft Equipment Bays.....	55
4.1	Aircraft Avionics and Their Thermal Management.....	56
4.2	Aircraft Avionics Bay with Multiple Systems and a Single Inlet/Outlet Configuration	57
4.2.1	Description of the Configuration	58
4.2.2	Mainstream Flow Analysis	60
4.2.3	Thermal Risk Prediction and Comparison with CFD.....	64
4.3	Aircraft Avionics Rack with Multiple Systems and Multiple Outlets	68
4.3.1	Description of the Cases	69
4.3.2	Mainstream Flow Analysis	71
4.3.3	Thermal Risk Prediction and Comparison with CFD.....	76
4.4	Conclusion.....	83
5	Conclusion and Future Work	85
5.1	Summary of Contributions	85
5.2	Limitations	86
5.3	Future Work	86
5.4	Conclusion.....	87
	Bibliography	88
	Publications Associated with This Thesis.....	93
	Appendix.....	94

List of Figures

Figure 1: Evolution of electrification for commercial aircraft [8]. 2

Figure 2: Electronics bays and their possible locations in an aircraft; nose, underfloor, as racks, or in the aft. Under hot conditions, these densely packed bays need efficient cooling requirements or risk operating outside their prescribed temperature range. 3

Figure 3: TRA at the top introduced for aircraft conceptual design. More complex methods can be implemented in preliminary and detailed design stages [11]. 4

Figure 4: Overview of the thermal risk assessment approach [1] and the scope of the research conducted. 5

Figure 5: Block diagram of a typical thermal management system model [19]. The different colored lines represent fuel (red), refrigerant (blue), and air (green). 7

Figure 6: Dimensionless parameters illustration for two entities A and B. The length of A and B in vertical directions are compared using just one dimensionless parameter, h^* 9

Figure 7: A simplified 3D aircraft zone with a single system. The arrows represent the direction of the inlet and outlet flows. The input data related to the aircraft zone characteristics can also be seen. 12

Figure 8: Initial TRA workflow from [1] before integrating system-level ventilation analysis developed in this thesis. 13

Figure 9: Values of Richardson number corresponding to the different states of ventilation in the aircraft zone. The blue curved arrows represent the flow due to natural convection. 14

Figure 10: State of stratification depending on the wall temperatures and source of stratification (R_{nat}). 14

Figure 11: Two systems at different distances to the inlet (green), their thermal risk can be compared using thermal interactions analysis. 15

Figure 12: Illustration of the mainstream (parallel streamlines seen in blue) and its distance from Systems 1 and 2. 17

Figure 13: Mainstream current of a river illustrated with the eddies near the riverbanks. 18

Figure 14: Cross-section of fluid flow near the wall shows the velocity boundary layer and the mainstream flow. 18

Figure 15: Mainstream flow in a zone with an inlet and an outlet along with the system. 19

Figure 16: Geometry tree of the model. Split surfaces of each part; 2D mesh generated for the Base surface. 25

Figure 17: The aircraft zone housed inside a fuselage. The different environmental conditions affecting the temperature of the zone are seen. 26

Figure 18: Geometrical parameters associated with the system and the aircraft zone to derivate the mainstream numbers. 27

Figure 19: Visual representation of the ranges of S_1 and S_2 are shown; a) System locations according to different values of S_1 , b) System locations according to different values of S_2 28

Figure 20: The different values of S^* and its related influences on the mainstream, red indicates no mainstream influence, yellow means a weak influence, and green means the influence of mainstream is strong. 29

Figure 21: The baseline CFD model, along with the values of its geometrical and physical parameters	30
Figure 22: The 2D mesh generated for the baseline model, prism layers are applied at the walls of the CFD model.....	30
Figure 23: The velocity and temperature plots of the baseline CFD simulation, the red area in the velocity plot represents the mainstream flow.	31
Figure 24: A sample variable LHS design space.....	32
Figure 25: Systems of different sizes represented as either lying or not lying on the mainstream, the velocity of the mainstream is normalized with the inlet flow velocity. The cooler regions of the bay are near the mainstream.....	34
Figure 26: System-bay configurations corresponding to S^* values; velocity plots help in visualizing the mainstream predictions.....	35
Figure 27: a) Both System 1 and 2 are under the influence of mainstream but comparing the relative influence between these 2 systems is difficult. b) A configuration where the system's bounds would be under the influence of mainstream but not the centroid	36
Figure 28: 2D Geometrical Configuration used to derive the cross-stream and stream-wise numbers: the square shaded area in the middle represents the system housed in the bay.	37
Figure 29: Definition of the CS number for six cases: 1-System close to the inlet, not influenced by the mainstream, 2-System close to the inlet, partially influenced by the mainstream, 3-System close to the inlet, engulfed by the mainstream, 4-System close to the outlet, engulfed by the mainstream, 5-System close to the outlet, partially influenced by the mainstream, 6-System close to the outlet, not influenced by the mainstream.	40
Figure 30: 2D graphical representation of the mainstream flow analysis	41
Figure 31: Geometrical description of the 2D case study with different inlet and outlet positions.	42
Figure 32: 2D mesh shown with prism layers at the walls for the case study, only applied to the fluid region.....	43
Figure 33: Mainstream numbers for the 2D case study for Cases 1-12: the grey shaded area is not under the mainstream influence, the area under the partial influence is yellow, and the area where the mainstream has a considerable influence is green.	45
Figure 34: Velocity fields obtained from the CFD simulations of Cases 1-12 for the 2D multi-systems case study; the black streamlines indicate the mainstream flow.	46
Figure 35: Temperature plots obtained from the CFD simulations of Cases 1-12 for the 2D multi-systems case study; the white streamlines indicate the mainstream flow.....	47
Figure 36: Flowchart for the thermal risk scoring with mainstream flow analysis; the steps to be followed are highlighted in yellow.	49
Figure 37: The MS scoring flowchart. The logic of scoring is shown along with each possible score.	52
Figure 38: Configurations of the aircraft equipment bays considered and their possible locations inside an aircraft seen from a side view.....	55
Figure 39: Schematic of a test chamber for thermal testing for aircraft systems; the temperature probes are inserted in the ambient zone.....	56
Figure 40: MCUs and their dimensions.....	58

Figure 41: Supporting rack modeled for supporting the systems (translucent).....	58
Figure 42: 3D Model of the avionics bay and the three-view representation with the associated geometrical parameters shown.....	59
Figure 43: Mesh plane of the avionics bay in the front view, prism layers seen near the walls...	60
Figure 44: Mainstream numbers mapping for Systems 1 to 9: the grey shaded area is not under the mainstream influence, the area under the partial influence is yellow, and the area with considerable mainstream influence is in green.	62
Figure 45: Velocity streamlines normalized with inlet flow speed. The mainstream flow moves along the bottom and right walls towards the outlet.	63
Figure 46: Velocity plots along different section planes in the front and top views; Systems far away from the mainstream experience very little flow.....	64
Figure 47 Temperatures of the systems from the CFD results in different views; surfaces of the systems closer to the mainstream are at lower temperatures.	66
Figure 48: Temperature plot of the bay section in the front view; the regions close to the mainstream are shown cooler. Hotspots can be seen around System 4.	68
Figure 49: 3D Model of the aircraft avionics rack with multiple outlets and three-view representation with the geometrical parameters.	69
Figure 50: The different cases for which the TRA is applied are shown in the side view.	70
Figure 51: Mapping of the CS and SW numbers for different ventilation sources; green region indicates a strong mainstream influence. Orange indicates that the mainstream influence is weak. In the grey region, the mainstream influence is negligible.....	73
Figure 52: Velocity streamlines and velocity plots in the side view for Case 1 containing all outlets; a) Streamlines show originating from the inlet and moving across the curved wall of the bay Velocity plots for the b) aft section, c)mid-section, and d) fore section of the bay are also seen.	74
Figure 53: Side views of the velocity plots shown; changes in ventilation configuration change the mainstream flow. Systems 5, 8, and 11 are discussed.	75
Figure 54: Comparison of thermal risk prediction for each system between all configurations ..	77
Figure 55: Temperature plot showing the hot spots formed near System 7, while Systems 8 and 9 have a cooler surrounding region.....	80
Figure 56: Comparison of predicted thermal risk and thermal risk from CFD for all configurations; green color indicates low thermal risk and yellow indicates medium thermal risk.	83

List of Tables

Table 1: Overview of relevant existing dimensionless numbers for this thesis.....	10
Table 2: Thermal risk scoring, introduced in prior work [1].	16
Table 3: Simplified equipment bays used in the development and application of the TRA.	23
Table 4: Description and ranges (min, max) of all the selected parameters for the design study.	33
Table 5: Limits of S_1 and S_2	35
Table 6: 2D case study with multiple systems: Geometrical parameters and boundary conditions.	44
Table 7: Inlet and outlet locations for the 2D case study.....	44
Table 8: Thermal risk scores for all modules.....	50
Table 9: The maximum allowed heat dissipation with and without cooling air for a given size of the avionics system [64].....	57
Table 10: Mainstream numbers for each system with respect to the inlet and outlet.	61
Table 11: Thermal risk assessment for Systems 1 to 9; scores listed for all the conducted analyses.	65
Table 12: Comparison of thermal risk predictions and CFD results.	67
Table 13: Mesh cells generated for CFD model of each configuration.	70
Table 14: MS scores for all the systems in four cases.	71
Table 15: Systems grouped by ventilation source for HR potential calculations.	78
Table 16: Thermal risk derived from the CFD results using ambient temperatures.....	82

Nomenclature

Symbols

a	The lower limit of S_1
b	The upper limit of S_1
c	The lower limit of S_2
d	The upper limit of S_2
g	Gravity
h	Heat transfer coefficient
k	Thermal conductivity
q	Rate of heat transfer
v	Velocity
x	Dimension in x-axis
y	Dimension in y-axis
z	Dimension in z-axis
C	Celsius
D	Depth of an entity
H	Height of an entity
L	Length of an entity
M	Mass flow rate
Q	Heat load of an entity
R	Radius of an entity
T	Temperature of an entity
U	Inertial flow velocity
W	Width of an entity
X	X axis
Y	Y axis
Z	Z axis

kW	kilowatt
Re	Reynolds number
Ri	Richardson number
Gr	Grashof number
S_1	The vertical ratio of a system and the ventilation source
S_2	The horizontal ratio of a system and a ventilation source
S^*	Ordered pair
ρ	Density
β	Coefficient of fluid thermal expansion
ΔT	Temperature difference
ε	Emissivity
μ	Dynamic viscosity
C_p	Specific heat of a fluid

Subscripts

l	Subscript related to the lower bound of an entity
u	Subscript related to the upper bound of an entity
x	Subscript related to X-axis
y	Subscript related to Y-axis
z	Subscript related to Z-axis
amb	Subscript related to ambient
bay	Subscript related to the bay
bot	Subscript related to an entity on bottom
env	Subscript related to the environment
in	Subscript related to inlet
lim	Subscript related to limit used in temperature limits
out	Subscript related to outlet
sky	Subscript related to the sky

<i>solar</i>	Subscript related to sun
<i>sys</i>	Subscript related to system
<i>top</i>	Subscript related to an entity on top
<i>wall</i>	Subscript related to the wall

Acronyms

APU	Auxillary Power Unit
CAD	Computer Aided Design
CFD	Computation Fluid Dynamics
COP	Coefficient of Performance
CS	Cross-Stream
DN	Dimensionless Numbers
DOE	Design of Experiments
ECS	Environmental Control System
FEM	Finite Element Method
HR	Heat Removal
HVAC	Heating Ventilation and Air-Conditioning
LHS	Latin Hyper-cube Sampling
LRU	Line Replaceable Unit
MAAXIMUS	More Affordable Aircraft through eXtended, Integrated and Mature nUmerical Sizing
MCU	Modular Concept Unit
MDAO	Multidisciplinary Design Analysis and Optimization
MEA	More Electric Aircraft
MS	Mainstream
MTOW	Maximum Takeoff Weight
NCD	Nearest Cross-stream Distance
OAT	Outside Ambient Temperature

SAE	Society of Automotive Engineers
SST	Shear Stress Transport
SW	Stream Wise
TOICA	Thermal Overall Integrated Conception of Aircraft
TRA	Thermal Risk Assessment

1 Introduction

During the design phase of an aircraft, a good understanding of its thermal environment is required. The thermal management of aircraft systems, such as electrical and electronic equipment, has a significant impact on the reliability and safety of the aircraft. For future more electric or all-electric aircraft, the importance of good thermal management becomes even more critical.

In this context, the Aircraft Systems Lab at Concordia University investigates new methodologies to integrate thermal analysis better in the traditional design process. A novel thermal risk assessment (TRA) approach was introduced by Sanchez et al. [1,2] as part of a collaborative research project with Bombardier Aviation. The method predicts the thermal risk for components such as avionics boxes housed in aircraft equipment bays. *Thermal risk* is defined as the potential of non-compliance with thermal requirements (e.g., an electronic device not complying with its range of operating temperatures would increase the thermal risk of the said device). This thesis further contributes to the prior work while focusing on ventilation-related aspects. This chapter presents the context and motivations, along with the scope and the organization of this thesis

1.1 Background and Motivation

Aircraft operate in a wide range of temperatures. Both military and commercial aircraft operate in regions with outside ambient temperatures (OAT) ranging from -70°C to 60°C . While the OAT can vary, the inside thermal environment of the aircraft must be maintained within fixed temperature ranges for both pressurized and unpressurized zones.

Unpressurized aircraft zones encounter large variations in temperature. The thermal environment in these aircraft zones depends on the equipment heat loads, the OAT, solar loads, and the ventilation flowrate. While very low temperatures occur during flight, high temperatures will occur while the aircraft is on the ground on a hot day. Hot temperatures on the ground may lead to ambient conditions that can cause equipment to exceed its survival temperatures. To avoid overheating of equipment, thermal analysis is required, and, if necessary, ventilation needs to be provided or increased, equipment cooling solutions need to be implemented, or equipment needs to be relocated.

Pressurized regions include the cockpit, cabin and can also include pressurized electronic equipment (E/E) bays. Human comfort drives the temperature requirements in the cockpit and the cabin. The allowable temperature range is much smaller and usually maintained around $23\text{-}28^{\circ}\text{C}$. Other vital factors such as humidity, oxygen levels, and air purity also play a factor while designing their ventilation systems. [3,4]. Electronic bays, on the other hand, have larger temperature variations. These bays house the aircraft electronics and other systems critical for an aircraft's operation. Unless specified, the upper operating limit for the electronics in these bays is 70°C .

The equipment in both pressurized and unpressurized regions is designed to operate for extended periods (8-10 hours in a single operation) and is expected to last for years. The criticality of these systems (such as flight control, engine control, navigation, or flight management) makes it

essential to maintain the temperature below their specified limit. Thus, any heat loads produced by them must be effectively dissipated.

Dedicated cooling systems, which use the cabin exhaust air as the inlet, are designed for the electronic equipment bays. A fan is usually placed either as a blower or an exhaust to ventilate these regions. However, fans can only operate if the aircraft is supplied with external power or runs an auxiliary power unit. These regions are usually tightly packed with electronic boxes [3]. The need for more optimized and fuel-efficient aircraft creates tighter and smaller spaces to house these electronics. An inefficient ventilation system may result in more weight added, which indirectly increases the fuel consumption of the aircraft.

In addition, the dependence on electronics in aircraft is increasing. Figure 1 illustrates the evolution of the electrical power capacity of aircraft over time. The electrical power use in aircraft is growing exponentially. The most recent aircraft, the Airbus A380 and the Boeing 787, are so-called More Electric Aircraft (MEA) [5]. The MEA concept is a move towards electrification of systems usually using centrally distributed hydraulic or pneumatic power. The MEA concept has the potential to improve various aspects of future aircraft, such as their efficiency, emissions, reliability, and maintenance costs. Currently, this electrification trend expands also to the propulsion systems. Many aircraft and engine manufacturers see future aircraft with hybrid-electric or engines [6,7].

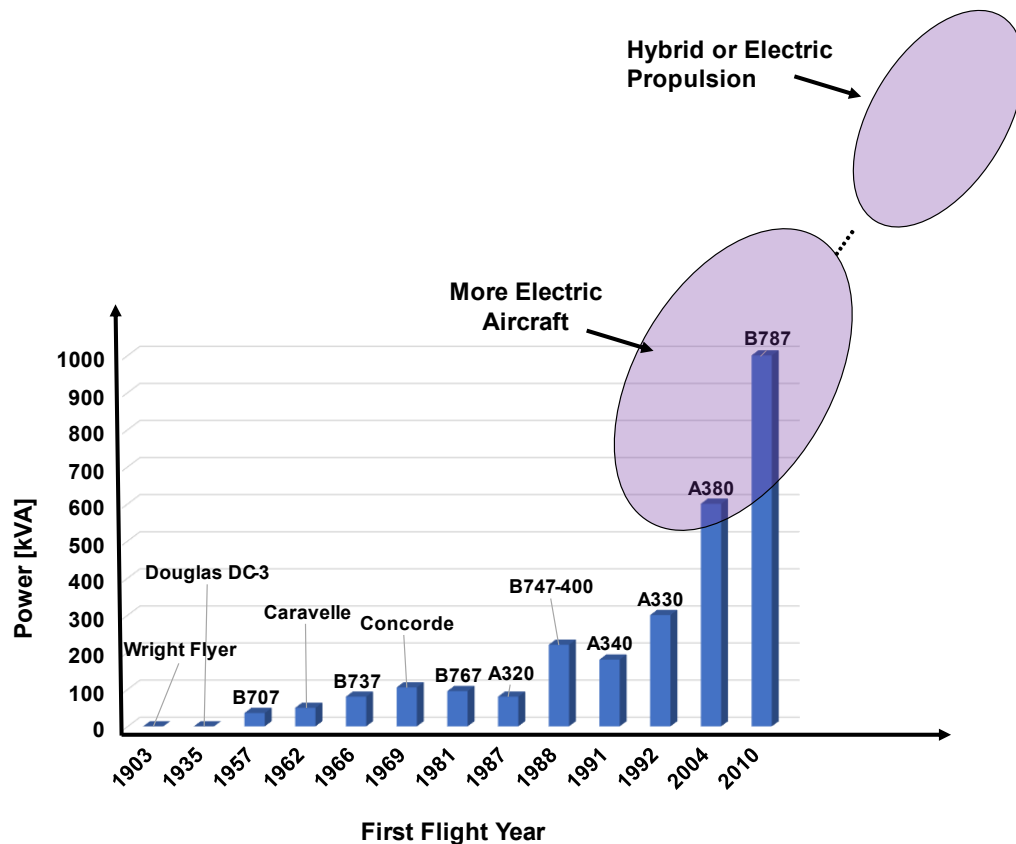


Figure 1: Evolution of electrification for commercial aircraft [8].

In the current generation of aircraft such as the Boeing 787 Dreamliner, the pneumatic systems (such as the environmental control system (ECS) and the ice protection system) as well as the spoiler actuation and the Auxiliary Power Unit (APU) are electrified [8]. These systems use power electronics for control, located in the equipment bays present in the fore and aft of the aircraft. The increased amount of power electronics, their higher power capability, and increased local heat loads from more-electric systems lead to thermal challenges. Avionics racks or the aft equipment bay, as illustrated in Figure 2, are densely packed. Most of the electronics have to dissipate their heat, and with adverse outside temperatures, the ambient temperatures inside these bays may exceed the operating ranges. More systems with higher electric power would result in higher heat loads. The chances of hotspots in these electronics thus increase. So does the chance of failure due to thermal reliability issues. Thus, cooling configurations must be updated accordingly

Due to these challenges, assessing the thermal risk of aircraft equipment bays, and particularly those containing electronic components, is a priority. In addition, an effective ventilation system must be designed for safe operating [9]. At the same time, the increase of ventilation or the addition of dedicated cooling systems also leads to increased aircraft weight and drag, thus increasing fuel consumption. Therefore, a multidisciplinary analysis is required to optimize the thermal architecture at the aircraft level.

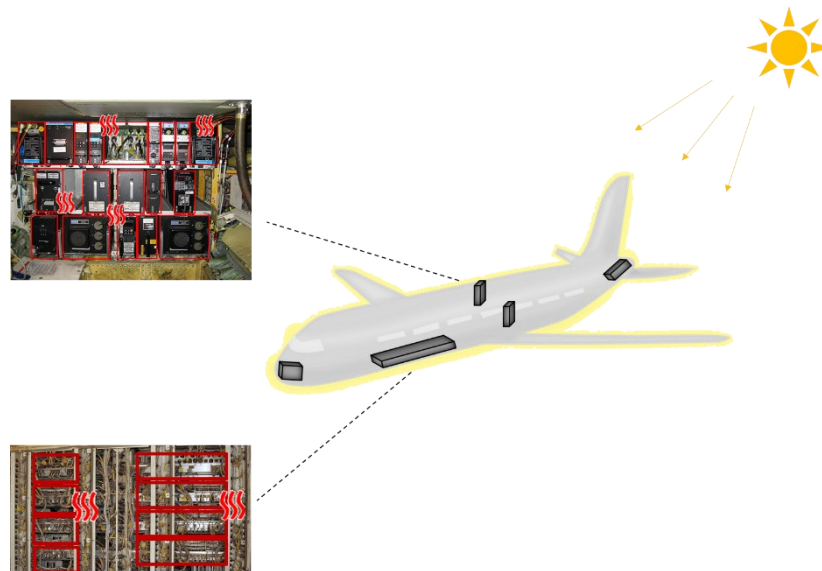


Figure 2: Electronics bays and their possible locations in an aircraft; nose, underfloor, as racks, or in the aft. Under hot conditions, these densely packed bays need efficient cooling requirements or risk operating outside their prescribed temperature range.

It is essential to discuss the overall aircraft design process to understand the thermal management of these electronics. The aircraft design process typically consists of three stages [10].

1. Conceptual Design
2. Preliminary Design
3. Detailed Design.

Conceptual design deals with aircraft level requirements and specifications such as the payload, range, Maximum Takeoff Weight (MTOW), or speed. System-level specifications are developed in the preliminary design phase. It includes individual systems such as flight control, environmental control, landing gear, and electrical systems. Individual subsystems and components are designed, and specifications are provided to the suppliers in the detailed design phase [10]. Thus, the thermal analysis of these components is traditionally performed in the detailed design phase. The thermal analysis consists of complex Computational Fluid Dynamics (CFD) and experimental thermal analyses. Changes in the detailed design stage are undesirable as it leads to increased cost and introduces major redesigns in aircraft systems. For more mature requirements to be sent to the component suppliers, thermal analyses must be introduced in early stages, preferably conceptual design. Defining thermal architecture at conceptual stages is challenging as there is limited information available about the aircraft systems, their placement, and their associated heat loads. Thus, CFD and experimental analyses cannot be performed at this stage.

Sanchez et al. [1] developed the so-called Thermal Risk Assessment (TRA) for aircraft conceptual design to close this gap. Figure 3 shows the scope of the TRA in aircraft design. The TRA uses limited data available at the conceptual design. It is based on dimensionless numbers (DN) to conduct qualitative analyses at both aircraft zonal and component levels. This thesis aims to add more analyses to the existing TRA and improve its thermal risk predictions. Thus, it deals with thermal analyses conducted at aircraft conceptual design.

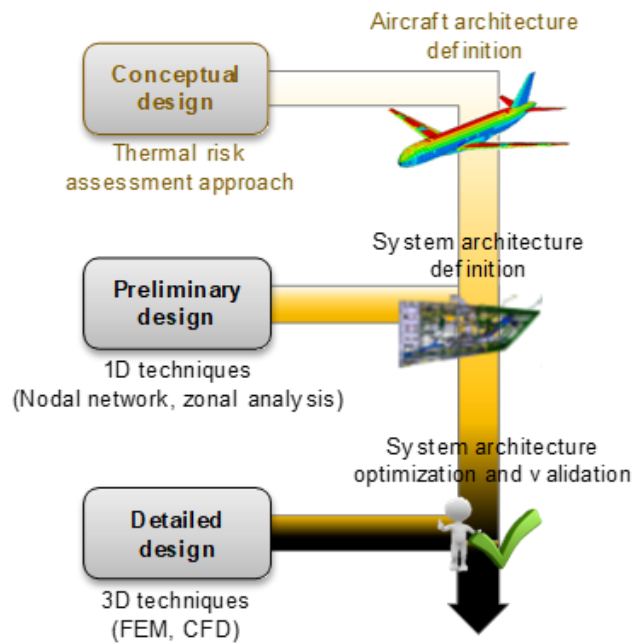


Figure 3: TRA at the top introduced for aircraft conceptual design. More complex methods can be implemented in preliminary and detailed design stages [2].

1.2 Thesis Scope and Objectives

The previous work on TRA focused on the aircraft zone level, namely ventilation and stratification analyses, shown in Figure 4. It also introduced a thermal risk scoring procedure. The scope of this thesis includes expanding the existing TRA and improving the thermal risk scoring procedure. TRA is enhanced by adding more component (*system*) level analyses in the existing workflow. The thermal risk scoring is enhanced as well. While a few *system*-level analyses have already been introduced in [1], there exists a need for ventilation-based *system*-level analyses. These analyses are validated via case studies conducted on aircraft equipment bays.

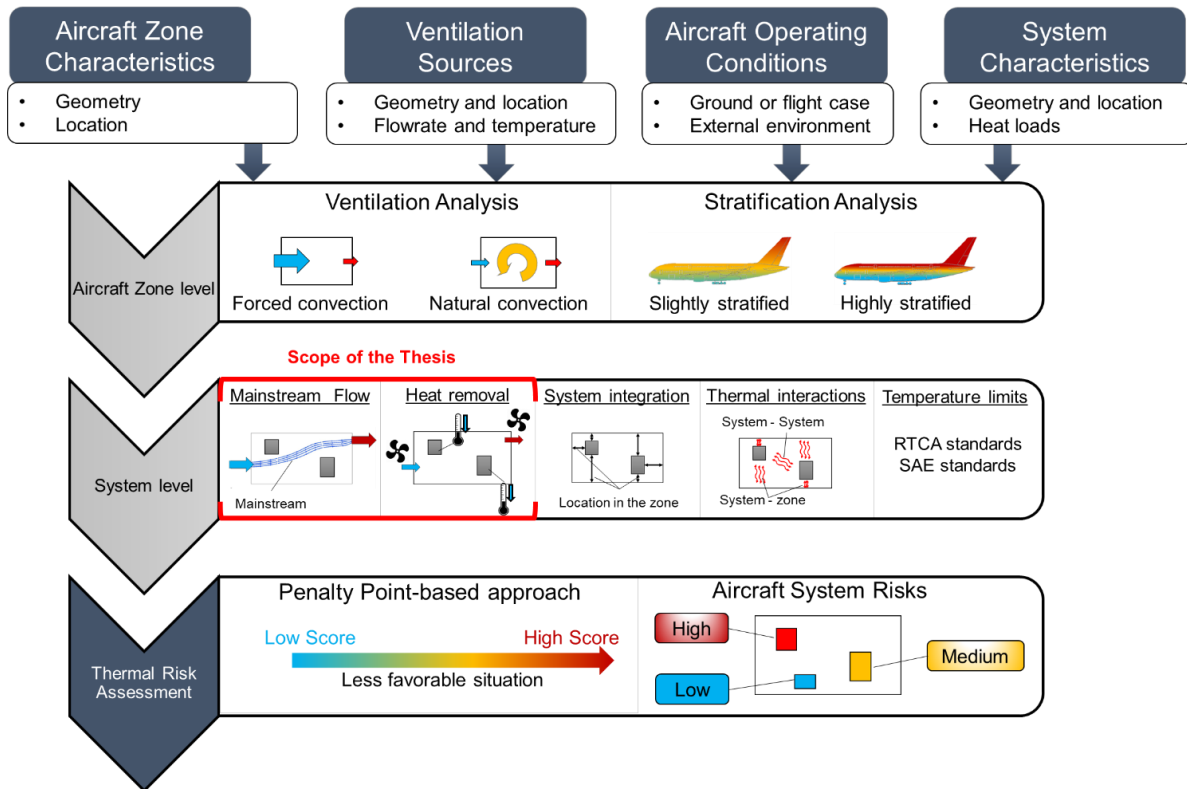


Figure 4: Overview of the thermal risk assessment approach [1] and the scope of the research conducted.

The addition of a ventilation-based system-level analysis to the TRA would result in:

1. Ventilation effects being accounted for component level thermal analyses in conceptual design.
2. Case studies on aircraft equipment bays would demonstrate the benefits of the updated TRA.
3. Better specifications to be sent to the component suppliers by the integrator.
4. Finally, this would help to handle the increasing heat loads due to the increasing electrification of aircraft.

1.3 Organization of the Thesis

This thesis is structured as follows. Chapter 2 provides state of the art in thermal analyses in aircraft design. It also discussed in more detail the current TRA and the need for improvement. Chapter 3 introduces the methodology applied in this thesis to improve the TRA by focusing on ventilation aspects at the system level. Chapter 4 discusses the so-called mainstream flow analysis. Chapter 5 discusses the improved TRA and Chapter 6 applies this updated TRA on aircraft equipment bays for validation. Chapter 7 concludes this thesis and discusses the future work.

2 State of the Art

This chapter covers the state of the art in thermal analyses in the design of aircraft systems. First, an overview of thermal considerations in aircraft design is presented. Then, the use of dimensionless numbers is discussed, followed by a detailed review of the prior work performed in the Aircraft Systems Lab, i.e., the novel thermal risk assessment method for aircraft conceptual design. Finally, this chapter closes by explaining the need to introduce a better system-level ventilation analysis, introducing the so-called mainstream flow analysis for the thermal risk assessment.

2.1 Thermal Considerations in Aircraft Design

This section discusses conventional methods of thermal analyses in aircraft system design.

Thermal analyses of aircraft can be categorized into two categories:

- 1) Thermal integration of systems at the aircraft level
- 2) Thermal analyses conducted at subsystem or component level

Traditionally, both types of analyses take place at the end of the detailed design [11,12].

The thermal integration of systems at the aircraft level follows a so-called one-dimensional (1D) thermal network using tools developed by the integrator for a comprehensive thermal management system [13–17]. A 1D model of a thermal management system substitutes a component with an equation, and the output of that equation forms the input for the next component. It is similar to an electrical network consisting of different components such as resistors, capacitors, and batteries. Figure 5 shows a typical 1D thermal network model for an aircraft. In this network, each component can be replaced by a set of governing equations and implemented using a tool such as MATLAB. The final output can be either in the form of maximum temperatures reached or the power required to cool these systems.

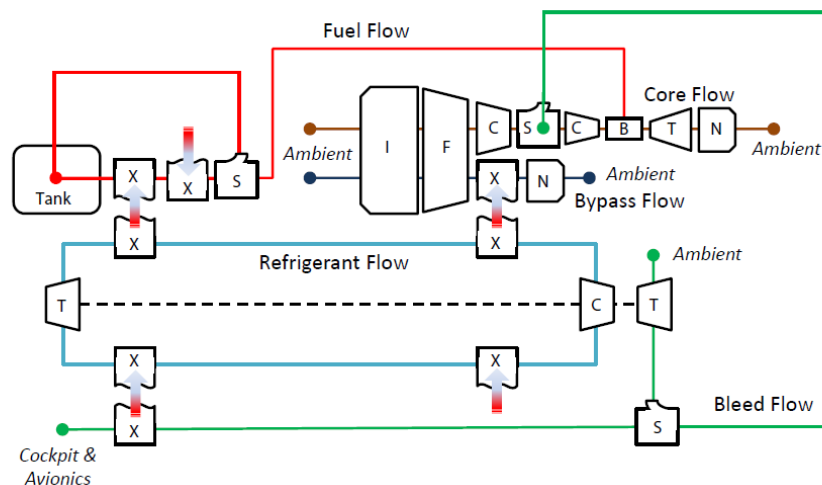


Figure 5: Block diagram of a typical thermal management system model [18]. The different colored lines represent fuel (red), refrigerant (blue), and air (green).

Some studies focus on integrating systems in conceptual design using the so-called “tip-to-tail” thermal models of the aircraft [11]. These models allow conducting aircraft-level trades from the outcomes of the system-level thermal model. System-level thermal models are developed in SIMULINK [19,20]. They consist of governing equations of each set of components and integrate engine models that simulate the effect of engine bleed and shaft power offtake demands integrating full flight dynamics model to simulate the various phases [19].

However, these systems contain a wide range of subsystems and components certified to various operating conditions and thus are too complex for reduction into a 1D set of equations. Their design uses costly and time-intensive methods such as CFD, as is the case in the detailed design phase [21]. Moreover, the modeling strategies adopted for such analyses focus on system and component-level interaction and are typically steady-state [22]. As a result, this often excludes the thermal effect of dynamic interactions between systems during various phases of an aircraft mission, such as start-up, takeoff, landing, and the transition between these phases.

Additionally, their thermal analyses are conducted in late aircraft design stages where a system architecture has already been selected. As thermal analyses are carried out in the detailed design stages, the results may have aircraft-level effects such as added system weight, unsatisfactory performance, and non-compliance with certification. Thus, it either results in overdesign or having to change the system architecture towards the end.

Projects such as Thermal Overall Integrated Conception of Aircraft (TOICA) [23] and More Affordable Aircraft through eXtended, Integrated and Mature nUmerical Sizing (MAAXIMUS) [24] have resulted in the development of several thermal modeling capabilities for aircraft design. These modeling capabilities include the aircraft system architecture and system heat loads from flight data as inputs. Both projects mainly worked on the preliminary and detailed stages of aircraft design. Butler et al. [25] studied the optimization of locations of sensitive electrical equipment inside an aircraft compartment. Similarly, Akin et al. [26] conducted an optimization study for a rotorcraft avionics bay cooling. These studies used expensive CFD simulations that are unsuitable for conceptual design phases.

The advantage of CFD is that it provides an accurate map of flow characteristics and heat transfer around the systems and in the system environment. Furthermore, CFD results can be validated against the wealth of flight test data available [22,27], thereby reducing the uncertainty of the numerical schemes. When compared to 1D modeling, CFD offers more accuracy but is cost and time-intensive. Additionally, CFD models require the details of system location, but conversely, this can skew the results of the other modeling techniques.

Conceptual stages must include thermal analyses of systems to support the overall aircraft thermal design process. Recent industry trends towards model-based engineering have pushed both researchers and aircraft designers to consider system-level disciplines in the conceptual design phase of the aircraft [16,17]. The advantages of doing so are numerous, such as cost-saving and defining more mature aircraft-level requirements. Efforts have been made to integrate system sizing and performance methods into the conceptual design process [28,29]. Early geometric modeling of system components within the aircraft has been explored in the conceptual design

stage [30]. Increased definition of system architectures in the conceptual design stages eases the integration of novel system architectures such as MEA. Numerous system components in MEA tend to have higher heat loads with increasing electrification, as discussed before in section 1.1.

The system architecture definition in conceptual design includes the aircraft zone, the various components housed in the said aircraft zone, and the air distribution system involving cool air inlets and outlets for exhaust. One of the challenges is that at the conceptual stage, limited information is available. The lack of information regarding the system skin temperatures, local heat transfer coefficients, and temperature of the aircraft zone makes it difficult to predict accurately the temperatures encountered while operating. The only information available would be the location of the subsystems (components) and a few other thermal parameters such as ventilation characteristics, solar loads, fuselage skin temperatures. Therefore, a need arises to develop a methodology that can work with this limited information and conduct thermal analyses in conceptual design.

Indeed, variable parameters have been reduced historically via the dimensionless numbers strategy [31]. Fluid dynamics and heat transfer use this method, where the number of unknowns is large. As discussed in Chapter 1, the TRA was developed using dimensionless numbers (DN) to make it suitable for conceptual design [1,32]. Using DN is a good approach as the information is limited, and thus other numerical methods (CFD) cannot be used. The following section provides background to the concept of DN and describes some dimensionless numbers relevant to thermal engineering and this thesis.

2.2 Use of Dimensionless Numbers (DN) in Thermal Analyses

Dimensionless numbers (DN) are numbers without any dimension. They are derived using dimensional analysis [31]. Figure 6 shows the dimensionless length (h^*), obtained as the ratio of two lengths, h_a , and h_b . The value of h^* depends on these lengths and can be used to compare them. Thus, the measurement of the system (A, B) is represented by just one dimension (h^*).

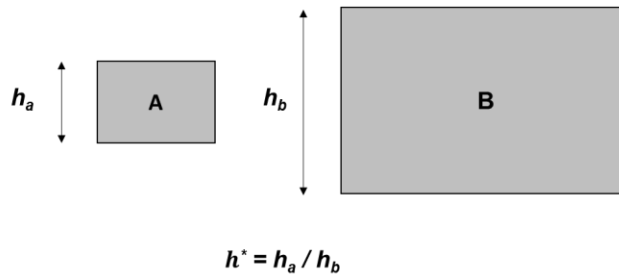


Figure 6: Dimensionless parameters illustration for two entities A and B. The length of A and B in vertical directions are compared using just one dimensionless parameter, h^* .

Dimensionless numbers have been widely used in the field of fluid mechanics and heat transfer. The field of thermo-fluids must deal with many physical parameters. Instead of using n parameters to describe the properties of a fluid, p ($p < n$) dimensionless parameters can be used [31]. Thus, these numbers condense the information and can be used to describe fluid properties. The study of heat transfer is also closely related to fluid mechanics as fluids are used widely in thermal

engineering. Different heat transfer phenomena such as conduction, convection, and radiation can be compared using DN. Table 1 lists some of the DN widely used in thermal engineering, along with their physical interpretations. Three widely used DN are explained in detail next.

Table 1: Overview of relevant existing dimensionless numbers for this thesis.

DN	Expression	Definition
Reynolds [33]	$Re = \frac{\rho UL}{\mu}$	The ratio of inertial forces to viscous forces
Grashof [33]	$Gr_{\Delta T} = \frac{\rho^2 g \beta \Delta T L^3}{\mu^2}$ $Gr_q = \frac{\rho^2 g \beta q L^4}{k \mu^2}$	The ratio of buoyant forces to viscous forces
Richardson [33]	$Ri_{\Delta T} = \frac{Gr_{\Delta T}}{Re^2}$ $Ri_q = \frac{Gr_q}{Re^2}$	The ratio of buoyant forces to inertial forces
Stratification Factor [34]	$S = \frac{qL}{k\Delta T}$	The ratio of imposed heat flux to the temperature difference
MIX [35]	$MIX = \frac{(M_{E, strat} - M_{E, act})}{(M_{E, strat} - M_{E, mixed})}$ $M_E = \sum y_i E_i = \sum y_i \rho u_i C_p T_i$	Indicates the level of stratification; $MIX = 0$ is perfectly stratified, $MIX = 1$ is fully mixed

The most known among the DN is Reynold's number (Re), characterizing fluid flow. This number indicates whether the flow is laminar or turbulent. The numerator is a product of the fluid density (ρ), fluid velocity (u), and the characteristic length (L) of the surface relative to which the fluid flows. The denominator is the dynamic viscosity (μ) of the fluid. For flow over flat plates, a small Re ($Re < 10^5$) indicates that the flow is ordered and laminar. A large Re ($Re > 10^6$) indicates that the flow is turbulent. Using Re , similarity can be obtained for flow over different sized bodies. This similarity is beneficial in applications like the wind tunnel, where smaller-scale models can simulate the flow over actual-sized bodies.

Grashof number (Gr) describes natural convection phenomena. Heating a fluid causes its density to reduce, and the resultant buoyant forces cause it to come into motion; the viscous forces of the fluid oppose this motion. Depending on the heat source, this number is either based on the temperature gradient ($Gr_{\Delta T}$) or the heat loads responsible for the fluid motion (Gr_q). The numerator for $Gr_{\Delta T}$ is the product of the square of the fluid density (ρ^2), gravitational acceleration (g), the coefficient of thermal expansion of the fluid (β), the temperature gradient (ΔT) and the cube of characteristic length (L^3) of the surface relative to which the fluid motion occurs. The denominator consists of the square of the dynamic viscosity (μ^2). In Gr_q , all other terms remain the same except

that the heat load (q) replaces the temperature gradient (ΔT), and the denominator contains the thermal conductivity of the fluid (k).

The Richardson number (Ri) is the ratio of the Grashof number (Gr) and the square of Reynolds number (Re^2). This number determines the nature of convection through which heat transfer occurs in a system. The convection can be forced ($Ri < 1$), natural ($Ri > 1$), or mixed ($Ri \approx 1$). Mixed convection is a combination of forced and natural convection. Ri has been used by Castell et al. [36] to characterize the stratification in water tanks. It is widely used in building engineering, where optimal Heating, Ventilation, and Air Conditioning (HVAC) solutions are required [37].

These numbers can characterize flows and are particularly useful for this thesis, where the ventilation effects are studied. While these are some of the widely used DN, others have also been introduced in various research works related to thermal analysis.

Duval et al. introduced the Stratification Factor [34] while assessing the temperature stratification in cryogenic water tanks. This factor indicates whether the source of stratification is the heat loads (q) or the temperature difference (ΔT). Davidson et al. [35] used the MIX number to investigate the temperature stratification in a tank

Although the research above uses DN, the applications are relatively simple, compared to complex aircraft zones housing various systems and featuring multiple ventilation sources. Also, the studies involve tanks [34,35] and air-conditioned rooms [37] with well-defined geometries of the zones and the inlets and outlets. Studies involving electronic chipset design investigated the effects of changing the location of ventilation sources while keeping the location of the heat source fixed [38] and vice-versa [39]. Both these studies concluded that changing geometries can have considerable influences on cooling.

TRA extends the current use of DN for a thermal risk prediction for aircraft systems in conceptual design. The following section explains prior work done in TRA.

2.3 Prior Work in Thermal Risk Assessment (TRA) in Aircraft Conceptual Design

This section describes the TRA developed in Aircraft Systems Lab at Concordia University in the past years in more detail. An initial part of the work was performed in collaboration with Bombardier Aerospace. The concept of the TRA was first introduced as the final part of multi-level thermal modeling methodology by Sanchez et al. in [40]. A first complete study on TRA, including different sub-analyses, was validated with CFD and aircraft test data for an aft equipment bay of an aircraft and was presented in [32].

Further development in TRA [1] included improvements in its thermal risk scoring and definition of system-level analyses and its application to a nose equipment bay of a rotorcraft. In collaboration with other members of the lab to further developed the methodology, this thesis contributed to two publications [41,42].

In the following, the TRA inputs and the workflow are presented. Then, a brief overview of the existing analyses (before the contribution of this thesis) of the TRA is presented, followed by the TRA scoring approach. Finally, the need for a more detailed ventilation analysis is discussed.

2.3.1 Existing TRA Workflow

The overall TRA approach was illustrated in Figure 4. TRA uses DN for qualitative thermal analyses of aircraft equipment bays. Analyses are conducted for both the zonal and component level. This method deals with an aircraft zone which is a whole or a part of an aircraft, including usually several systems (e.g., the under-floor zone of the aft equipment bay in the tail). In this context, the word *system* refers to the individual component housed in the aircraft zone. The input data needed for these analyses are three types, the aircraft zonal inputs, the aircraft operating conditions, and the system characteristics data. [32] describes all of these in detail. A zonal-level analysis deals with the whole aircraft zone. Therefore, it uses aircraft-level inputs. System-level analyses are local analyses that apply to an individual system inside the aircraft zone. These analyses use both aircraft-level and system-level inputs. Figure 7 shows a simplified aircraft zone in 3D, including only one system for simplicity. The figure describes both the zone and the ventilation sources that form the zonal inputs.

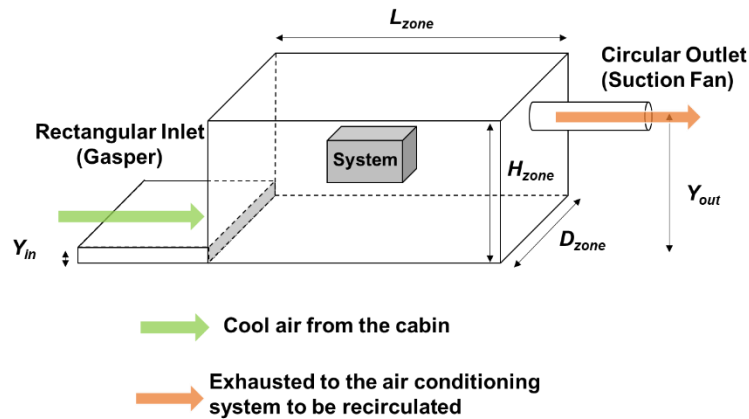


Figure 7: A simplified 3D aircraft zone with a single system. The arrows represent the direction of the inlet and outlet flows. The input data related to the aircraft zone characteristics can also be seen.

On top of these inputs, many uncertainties are related to the structural and thermal aspects of the aircraft. These may include structural components such as frames and stringers. At the system level, this includes the system wiring and its supports. However, information about these components is not available in conceptual design, and thus, these are not modeled in the conceptual TRA. Aircraft systems are certified for thermal safety using the standard DO-160 [9] or the standard SAE AIR1168/6A [43].

Five analyses are carried out using the inputs described before. These analyses are described in detail next, starting with the ventilation analysis. Figure 8 describes the TRA workflow.

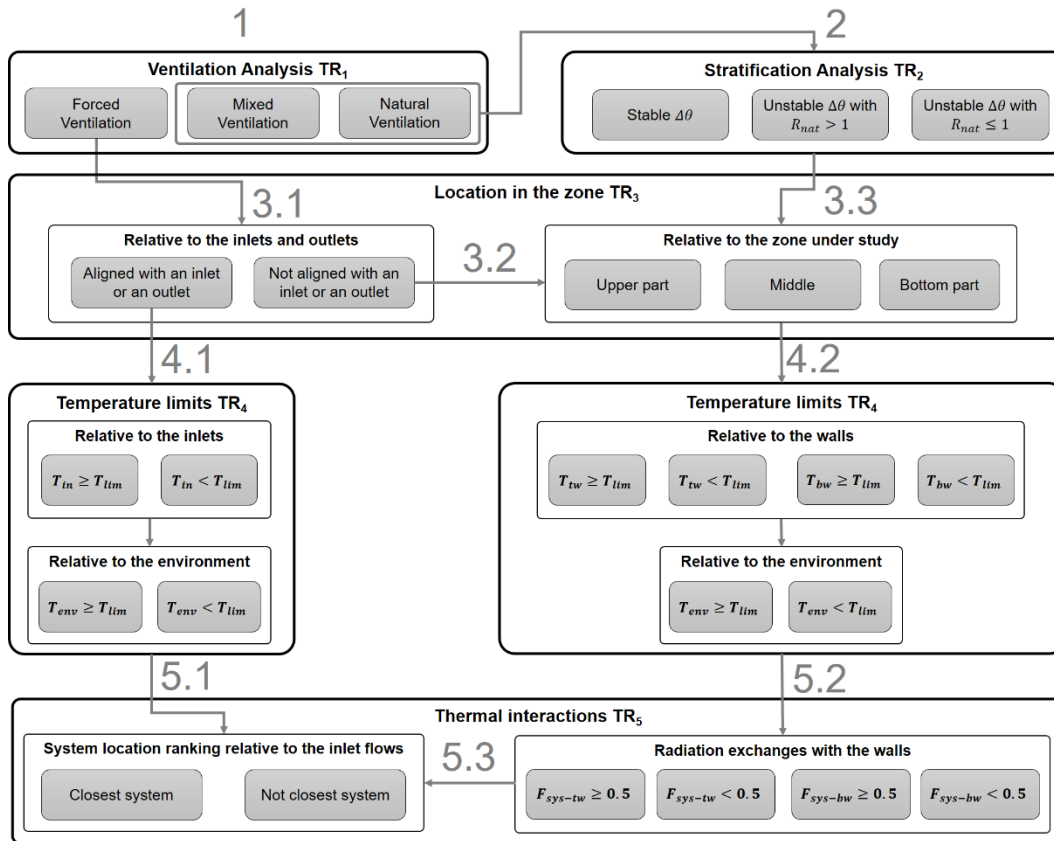


Figure 8: Initial TRA workflow from [1] before integrating system-level ventilation analysis developed in this thesis.

1. Ventilation Analysis

Ventilation analysis is the first analysis conducted in the TRA and identifies the forces that drive the aircraft zone's ventilation. The Richardson number (Ri) compares the buoyant and the inertial forces of the airflow.

- $Ri > 1$ indicates that natural convection is the dominant part.
- $Ri = 1$ indicates that there is a combination of both natural and forced convection.
- $Ri < 1$ indicates that the flow from the inlet is stronger than the buoyant flow inside the zone.

Based on the aircraft zone shown in Figure 7, the various cases of ventilation for a single inlet and outlet are shown in Figure 9.

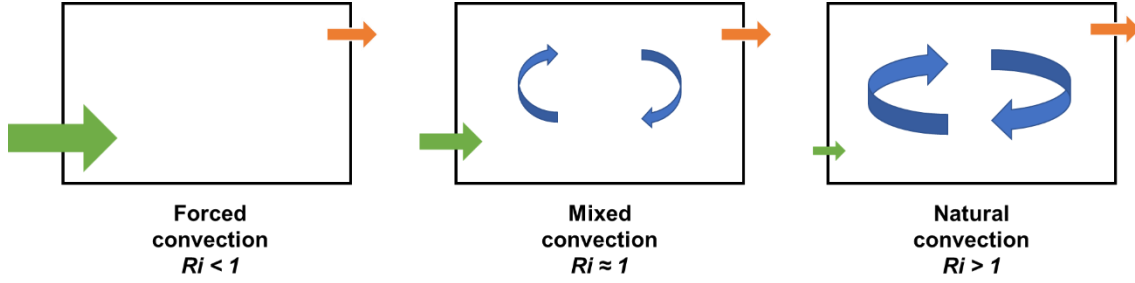


Figure 9: Values of Richardson number corresponding to the different states of ventilation in the aircraft zone. The blue curved arrows represent the flow due to natural convection.

2. Temperature Stratification Analysis

The subsequent analysis described in TRA is the temperature stratification analysis, identifying the type of thermal stratification in the aircraft zone and its cause. Here the primary source of the natural convection is considered using the Gr numbers. Eq. (1) introduces R_{nat} as the ratio of $Gr_{\Delta T}$ to Gr_q .

$$R_{nat} = Gr_{\Delta T} / Gr_q \quad (1)$$

In cases of a stable thermal gradient, the recirculation flow is generated due to the heat loads generated by the system and thus aids in better cooling.

In case of an unstable thermal gradient, R_{nat} is used to assess the driver of the natural convection. When the temperature difference drives the unstable thermal gradient ($R_{nat} > 1$), a much larger recirculation flow occurs between the zone's top and bottom walls. It ensures air mixing, as seen in Figure 10. On the other hand, when the unstable thermal gradient is driven by the heat loads ($R_{nat} \leq 1$), the zone is highly stratified. This leads to the creation of hot spots due to a lack of recirculation flow.

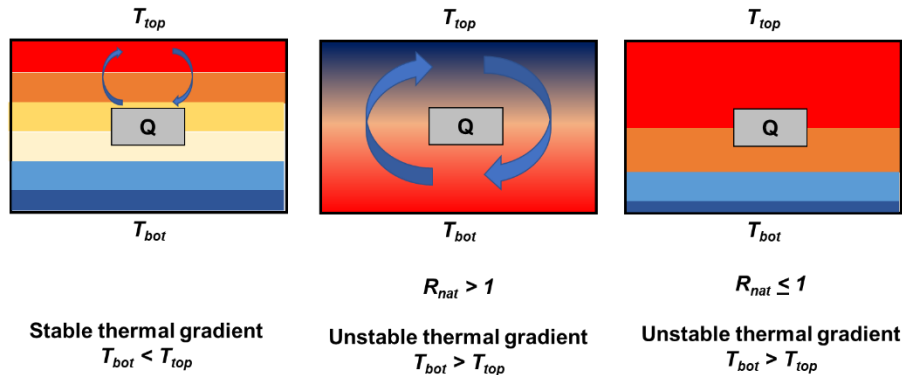


Figure 10: State of stratification depending on the wall temperatures and source of stratification (R_{nat}).

In the following paragraphs, system-level analyses compare a system's location in the bay with its dimensions (system integration), compare the maximum allowable system temperatures with other entities (temperature limits analysis), and discuss the system to wall radiations (thermal interactions analysis).

3. Temperature Limits Analysis

The temperature limits analysis compares the maximum allowable system temperature, known as the system temperature limit (T_{lim}), to the available input temperatures. These include the inlet(s) temperature (T_{inlet}), the temperature of the walls of the aircraft zone (T_{top} , T_{bot}), and the outside ambient temperature (T_{amb}).

4. System Integration Analysis

This analysis compares the locations of the system with inlet, outlet, and relative to the bay.

The location of the system and the inlet/outlets are compared in 3 dimensions (Y_{sys}/Y_{inlet} , X_{sys}/X_{inlet} , and Z_{sys}/Z_{inlet}). If both the system and inlet are aligned ($Y_{sys}/Y_{inlet} = 1$ or $X_{sys}/X_{inlet} = 1$ or $Z_{sys}/Z_{inlet} = 1$), the system is more likely to receive air from the inlet and thus has a lower thermal risk. Next, the vertical location of the system in the aircraft zone is compared to the height of the aircraft zone (Y_{sys}/H_{zone}). A system placed higher in the zone would be more likely to receive rising hot air and miss the cold air from the inlet.

5. Thermal Interactions Analysis

In aircraft zones with multiple systems, there is thermal interaction among systems and between systems and their environment. Thermal interactions analysis tries to deal with an approach that quantifies such interactions. For the thermal interactions between systems, earlier work [1] focussed on the relative location of the system concerning the inlet. It ranked systems based on the closeness to the inlet. A 2D cross-section of an aircraft zone can be seen in Figure 11. Two systems are shown along with the inlet and the outlet. The system (1) closer to the inlet is more likely to receive cold air. Thus, its thermal risk is lower than the system (2), far from the inlet.

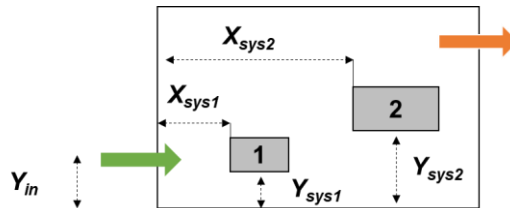


Figure 11: Two systems at different distances to the inlet (green), their thermal risk can be compared using thermal interactions analysis.

The other part of this analysis deals with a system's thermal interaction with the zone walls. These systems interact with the walls through radiation heat transfer. The inputs to radiation include the emissivity of the system and the walls (ε), their temperatures (T_{sys} , T_{walls}), the heat exchange surface areas (A), and the view factor ($F_{sys-wall}$) of the considered system with the wall. Wall temperatures, heat exchange areas, and emissivity form the inputs, whereas the view factor needs to be calculated. These view factors are derived using the Hottel crossed string method [44]. If the view factor is high (close to 1), the radiation heat exchange between the system and the wall is significant. Also, if the wall is at a higher temperature than the systems (refer to temperature limits analysis), the system may receive heat from the wall and thus be at a higher thermal risk. This analysis is not applicable in cases where the wall temperatures are lower than the system limit

temperatures. Thus, using the view factor as the DN, the thermal interactions between the system and the wall can be ranked and quantified. Further work on radiation view factors has been performed by fellow members of the aircraft systems lab [45].

Sanchez et al. proposed a thermal risk scoring methodology using all the analyses mentioned above. Each analysis is scored based on its considered dimensionless numbers (e.g., Ri in ventilation analysis). Table 2 gives the scoring chart.

Table 2: Thermal risk scoring, introduced in prior work [1].

Thermal risk assessment parameter	Score	Thermal risk assessment parameter	Score
Ventilation analysis		Temperature stratification analysis	
Natural convection: $Ri_\phi \gg 1$	3	Unstable thermal gradient: $R_{nat} \leq 1$	3
Mixed convection: $Ri_\phi \sim 1$	2	Unstable thermal gradient: $R_{nat} > 1$	2
Forced convection: $Ri_\phi \ll 1$	1	Stable thermal gradient	1
Location in the zone		Temperature limits	
Relative to ...		Relative to an inlet	
...an inlet	TR_{3.1}	Hot inlet: $T_{in}/T_{lim} \geq 1$	TR_{4.1}
Not aligned: $Y_{sys}/Y_{in} \neq 1$ or $X_{sys}/X_{in} \neq 1$ or $Z_{sys}/Z_{in} \neq 1$	2	Cold inlet: $T_{in}/T_{lim} < 1$	1
Aligned: $Y_{sys}/Y_{in} \sim 1$ or $X_{sys}/X_{in} \sim 1$ $Z_{sys}/Z_{in} \neq 1$	1	Relative to the bay	
...an outlet		Hot bottom wall: $T_{bw}/T_{lim} > 1$	TR_{4.2}
Not aligned: $Y_{sys}/Y_{out} \neq 1$ or $X_{sys}/X_{out} \neq 1$ $Z_{sys}/Z_{out} \sim 1$	2	Hot top wall: $T_{tw}/T_{lim} > 1$	2
Aligned: $Y_{sys}/Y_{out} \sim 1$ or $X_{sys}/X_{out} \sim 1$ $Z_{sys}/Z_{out} \sim 1$	1	Cold bottom wall: $T_{bw}/T_{lim} < 1$	
Relative to the bay		Cold top wall: $T_{tw}/T_{lim} < 1$	1
Top of the bay: $Y_{sys}/H_b \sim 1$	TR_{3.2}	Relative to the environment	
Middle of the bay: $Y_{sys}/H_b \sim 0.5$	3	Hot environment: $T_{env}/T_{lim} > 1$	TR_{4.3}
Bottom of the bay: $Y_{sys}/H_b \ll 1$	2	Warm environment: $T_{env}/T_{lim} \sim 1$	2
	1	Cold environment: $T_{env}/T_{lim} < 1$	1
Thermal interactions		TR₅	
System to system flow interactions		Wall to system radiations (only if $TR_{4.2} > 1$)	
System located after other system(s) in the flow direction	TR_{5.1}	$F_{sys-tw} \geq 0.5$	TR_{5.1}
First system in the flow direction: $\min(Y_{sys}/Y_{in})$ or $\min(X_{sys}/X_{in})$ or $\min(Z_{sys}/Z_{in})$	2	$F_{sys-bw} \geq 0.5$	2
	1	$F_{sys-tw} < 0.5$	1
		$F_{sys-bw} < 0.5$	
Total thermal risk score		$TR_{tot} = f(TR_1, TR_2, TR_3, TR_4, TR_5)$	
Low risk		$TR_{tot} < 5$	
Medium risk		$5 \leq TR_{tot} \leq 10$	
High risk		$TR_{tot} > 10$	

Thermal risk scoring follows a penalty-point system where a higher score indicates a higher thermal risk. Each analysis is scored individually, and the scores are multiplied at the end. The resulting score is categorized into low, medium, or high thermal risk.

2.3.2 Need for Enhanced System-Level Analyses

The TRA introduced by Sanchez et al. laid the groundwork and established the methodology for predicting thermal risk in conceptual design. Overall, the methodology yields satisfactory results in predicting thermal risk. However, the validation with CFD simulations showed some potential for improvement [1,32]. In most cases, the system is in the flow, which cools the system and keeps the temperature well below the temperature limit. The thermal risk from the CFD is low. When the flow influences a particular system, the thermal risk score is predicted higher than the CFD results.

The TRA assesses the state of ventilation at the zonal level and does not capture the flow effect on individual systems. Therefore, the system-level influences of the ventilation flow must be studied.

2.4 Literature Review on Enhanced System-Level Thermal Analyses

The ventilation considerations at the system level are two types.

- The first consideration is location-based; it uses locations of the system and the flow as inputs and estimates the relative distance of the system to the flow (Mainstream flow analysis).
- The second consideration is effectiveness-based; it uses the inlet/outlet temperatures and the system heat load as the inputs and assesses the system cooling potential (Heat Removal Potential analysis).

The distance of the flow to the system is the first indicator of how strong it influences the system temperature. Figure 12 shows an aircraft zone with two systems and a single inlet and outlet. The flow comes in from the inlet and exits through the outlet. System 2 is closer to the flow and, thus, under its influence. Suppose all other parameters are similar for both systems (heat loads and dimensions), System 2 would be at a lower thermal risk.

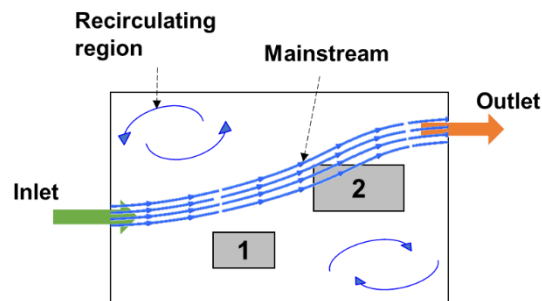


Figure 12: Illustration of the mainstream (parallel streamlines seen in blue) and its distance from Systems 1 and 2.

Thus, the distance of the system to the flow needs to be calculated. The location of the ventilation sources must be known to get the location of the flow. In system integration analysis, the system's

location was compared to both the inlet and outlet (Y_{sys}/Y_{in} , Y_{sys}/Y_{out}). While this was a good start, a more in-depth analysis is needed for assessing the influence of the flow using its location.

Ventilation effects are studied in detail using the mainstream flow analysis in this thesis (Figure 4). ‘*Mainstream flow*’ is most of the inlet flow which exits through the outlet. It is a novel approach that uses the ventilation sources as inputs and the zone-system configuration to characterize the mainstream influence. This analysis forms the central part of the thesis. Mainstream flow analysis is defined, and its significance is discussed in the next section.

2.4.1 Background on Mainstream Flow Analysis

This section introduces background on mainstream flow analysis. The Oxford dictionary defines *mainstream flow* as “The portion of the fluid flow away from a surrounding surface and thus not under the influence of any boundary layer” [46]. In Figure 13, the term “main current” can be replaced with the mainstream flow. Mainstream flow is a uniform flow where the flow velocity is not affected by the riverbanks. The eddies formed near the riverbanks are recirculation flows because of the fluid interacting with the coast. These eddies are not part of the mainstream flow.

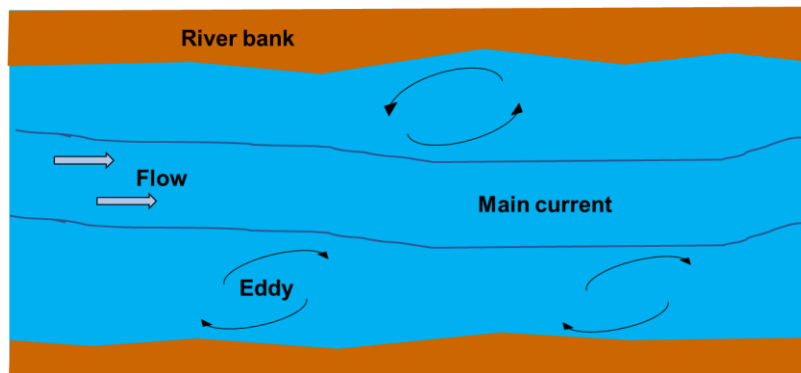


Figure 13: Mainstream current of a river illustrated with the eddies near the riverbanks.

Figure 14 shows a 2D cross-section of a laminar fluid flow profile, where the velocity increases from zero, the bulk velocity moving away from the wall. The portion of the flow with a constant velocity at the end of the boundary layer is called the mainstream flow.

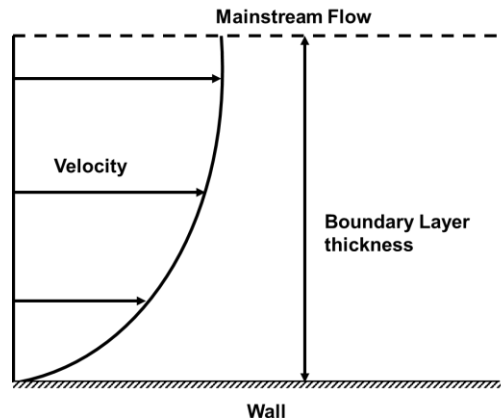


Figure 14: Cross-section of fluid flow near the wall shows the velocity boundary layer and the mainstream flow.

The term mainstream flow is also used by Sinha et al. in a building engineering study [37]. This paper identifies three main regions for the flow: an upper recirculating region, a lower recirculating region, and the mainstream region. This mainstream region, which accounted for 70-80% of the total inlet flow, was flowing straight from the inlet towards the outlet. The mainstream flow can thus be defined as the bulk of inlet flow, unaffected by the surroundings and going directly from the inlet towards the outlet. Figure 15 shows in a simplified manner the mainstream flow in a 2D zone. This simple 2D zone also houses one system and has a single inlet and an outlet. The blue lines represent the mainstream region of the flow, flowing largely unaffected from the inlet to the outlet.

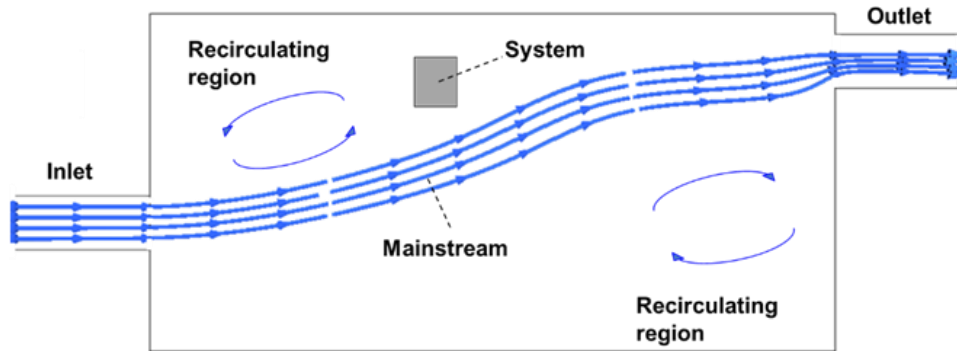


Figure 15: Mainstream flow in a zone with an inlet and an outlet along with the system.

Mainstream flow is crucial in cooling. Consider air flowing over a heated flat plate. Convective heat transfer happens due to random molecular motion (conduction), which occurs near the surface, and the fluid's bulk motion, which dominates further away from it [33]. This bulk motion of the fluid cools the heated surface continuously.

Eq. (2) gives the expression for convective heat transfer via Newton's law of cooling. The heat flux (q) depends on the temperature gradient ($T_{hot} - T_{cold}$) and the heat transfer coefficient (h). h increases with the increase in fluid velocity [33].

$$q = h(T_{hot} - T_{cold}) \quad (2)$$

As the mainstream contains the bulk/macroscopic motion of the fluid and is free of boundary layer interactions, the flow velocity in the mainstream is the highest. Thus, convection heat transfer should be higher near the mainstream. A system close to the mainstream is expected to be more efficiently cooled via convection.

The literature offers several studies that demonstrate the benefits of having a system located on the mainstream flow. Farj et al. [47] discuss the effects of the location of an air inlet for an operating room in a hospital. They perform a 3D CFD study to optimize the location of the inlet. The best cooling configuration is achieved when the airflow is directly on top of the heat source, with the heat source being on the mainstream. Ling et al. [48] study the effect of natural vs. forced cooling on lithium-ion batteries. The introduction of forced cooling directly on the batteries improves their reliability. While inefficiently cooling them using natural convection causes thermal system failures. In a mixed convection study by Fontana et al. [49], the heat source location

is varied vertically along with the Reynolds number. The cooling design improved when the heat source was placed close to the cold stream inlet opening. CFD and experimental studies of a large industrial hall conducted by Jankes et al. [50] show that the best location for heat extraction is directly above the heat source.

To summarize, a hot body is most effectively cooled if placed on the mainstream of the cooling fluid. In the scope of aircraft equipment bays, which are often cooled by forced ventilation, this mainstream flow would be of utmost importance. The distance of the aircraft equipment from the mainstream would determine the cooling effectiveness of their ventilation system. A system that is closer to the mainstream flow could potentially have a higher rate of heat transfer than the system far away from it.

To determine if a system is closer or farther away from the mainstream, one must estimate its location. The mainstream path could be roughly estimated in ventilation systems with forced or mixed convection ($Ri \leq 1$), meaning that the flow is strong enough to move directly from the inlet to the outlet. In a CFD study of flow in a room with varying inlet and outlet locations by Babu in [51], the aim was to estimate the most optimum locations for the inlet and outlet for uniform temperature distribution. Multiple configurations were used, each with different locations of inlet/outlet. In every configuration, most of the flow moved directly from inlet to outlet. The location of the inlet and outlet can be used as a start and endpoint of the mainstream path. The relative location of the system to the mainstream can be estimated using the system's location and the locations of the inlet and outlet. Also, in a configuration with multiple systems, some systems may fall directly on the mainstream path. They act as obstacles to the flow.

The mainstream flow path can be detected and estimated using costly CFD and experimental methods. Most of these studies have well-defined geometrical configurations. The locations of the inlet, outlet, and heat sources are fixed [37,47,48,52]. Although there are some cases where the inlet/outlet locations are varied, these happen in the absence of heat sources [53]. In the context of conceptual design, there is limited availability of inputs. As a result, the geometry is not fixed, and the locations of different entities (inlets, outlets, and heat sources) can change. CFD is time-consuming and expensive at this stage, where the information is limited, and design is ever-evolving.

Thus, a novel approach needs to be developed to integrate the changing of geometries and heat loads present in an aircraft zone. This approach requires DN to rank systems based on their closeness to the mainstream and is discussed in Chapter 3.

2.4.2 Other System-Level Analyses: Heat Removal Potential Analysis

Introduced by Sanchez et al. in [42], this consideration analyzes the cooling potential of ventilation sources at the system level. It was developed in parallel to the mainstream flow analysis approach. The principal behind analyzing the cooling potential is quantifying the maximum heat a particular ventilation source can remove. It uses temperatures of the inlet, outlet, and the environment as input temperatures. It also uses mass flow rate for each ventilation source and system heat loads as inputs. This forms the heat removal potential analysis given in Figure 4. Section 2.4.1 discusses the mainstream flow and its importance in system cooling. However, the cooling performance of

the ventilation source for a particular system is not assessed. This cooling performance depends on the heat removal potential of the said ventilation source. It is modeled on the Coefficient of Performance (COP), used extensively for refrigeration systems [54]. The COP of a refrigerator is the ratio of heat (Q) extracted to work (W) done by the refrigerator. Eq. (3) gives the formula for COP of a refrigerator.

$$COP = \frac{Q_{extracted}}{W_{done}} \quad (3)$$

Thus, COP is a useful parameter for assessing the efficiency of a ventilation source. This section derives the potential with which a ventilation source extracts heat from a system using COP.

In the scope of this thesis, the desired result is to assess the performance of a ventilation source for a given system. In Eq. (4), the advection energy ($M_{source} * C_p * \Delta T$) exchanged by the said ventilation source is compared to heat dissipated by the system (Q_{sys}). This depends on its mass flow rate (M_{source} , here the subscript *source* implies the ventilation source), its operating temperature (T_{source}), and the limit temperatures of the systems influenced by it ($T_{lim, sys}$), given that air is incompressible (C_p is constant). If this advection energy is small compared to Q_{sys} , the heat removal potential is low.

Thus, the heat removal number (HR) of a ventilation source for a system is given by Eq. (4). This number is inversely proportional to the heat removal potential. The lower this number, the higher the ventilation source's performance for that system.

$$HR = \frac{Q_{sys}}{M_{source} C_p (T_{lim,sys} - T_{source})} \quad (4)$$

The next chapter introduces a methodology to integrate the mainstream flow analysis in the existing TRA. Finally, an enhanced thermal risk scoring is presented.

3 Methodology for the Integration of Mainstream Flow Analysis in the Existing Thermal Risk Assessment

This chapter discusses the methodology used to integrate the mainstream flow analysis with the existing TRA. Section 3.1 describes the case study approach and the CFD validation strategy used. Sections 3.2 and 3.3 present the development of new dimensionless numbers (DN) used for the mainstream flow analysis. Finally, section 3.4 presents the TRA enhanced with the integration of mainstream flow analysis.

3.1 Adaption of Mainstream Flow Analysis to Conceptual Design of Aircraft Equipment Bays

Mainstream flow analysis for aircraft equipment bays is complex. Each system and ventilation source involves several geometrical parameters (size, location) and thermal parameters (accompanying heat loads, temperature limits, mass flow rate).

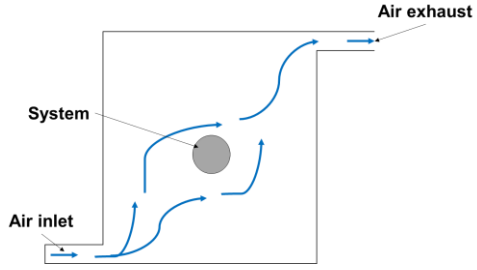
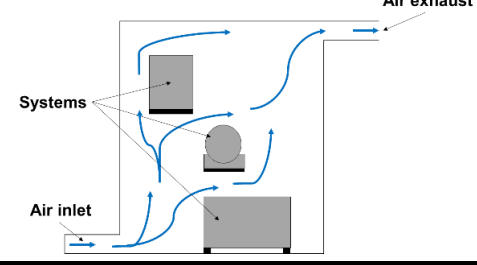
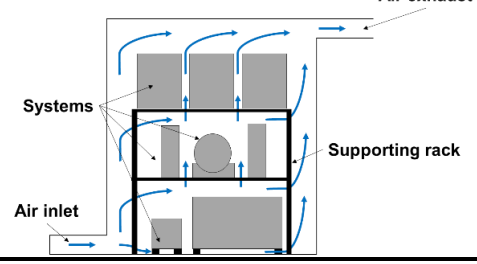
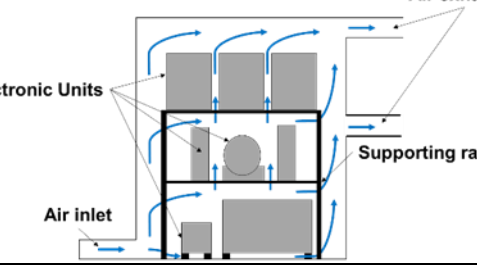
This thesis proposes using dimensionless numbers (DN). Establishing DN to characterize the mainstream allows condensing the geometrical parameters associated with an aircraft zone and its systems to assess the effects of the mainstream. These new DN should be valid for different geometrical configurations and multiple heat sources and help in ranking various systems based on the influence of the mainstream. It is proposed to name these numbers as mainstream (*MS*) numbers.

Due to the large design space and the complexity of the problem, *MS* numbers are developed using a step-by-step approach. Section 3.1.1 gives a brief overview of the case studies and the level of complexity involved with each. Section 3.1.2 discusses the methodology of the CFD simulations conducted for all the case studies.

3.1.1 Overview of Case Studies

Table 3 presents an overview of the case studies used to develop and validate the mainstream flow analysis and the improved TRA. It is proposed to use four different models with increasing levels of complexity.

Table 3: Simplified equipment bays used in the development and application of the TRA.

Characteristics		Geometrical description
Systems complexity	Single system	
Number of inlets/outlets	Single inlet/outlet	
Supporting rack	No	
Considered dimensions	2D	
Systems complexity	Multiple systems	
Number of inlets/outlets	Single inlet/outlet	
Supporting rack	No (2D supports)	
Considered dimensions	2D	
Systems complexity	Multiple systems	
Number of inlets/outlets	Single inlet/outlet	
Supporting rack	Yes	
Considered dimensions	3D	
Systems complexity	Multiple systems	
Number of inlets/outlets	Single inlet, multiple outlets	
Supporting rack	Yes	
Considered dimensions	3D	

While simple 2D case studies are used to establish the mainstream flow concept, the application of the updated TRA involves 3D close to real-world aircraft equipment bays. The 2D case studies are numerous to explore the design space and establish the range of the dimensionless MS numbers. The case studies at the end, in contrast, are fewer, with established design configurations and

thermo-physical conditions derived from standards. They aim to prove that this system-level integration to the TRA can be used in a real case scenario.

The following section discusses the CFD simulation methodology used throughout this thesis.

3.1.2 Overview of CFD Simulation Approach Used for Development and Validation

In this thesis, CFD is used to understand the thermal and flow phenomena in simple to more realistic aircraft equipment bays. STAR-CCM+ [55] is used for the CFD simulations. As described in Table 3, the first case studies are in 2D and numerous. Thus, multiple configurations are run in STAR-CCM+ 's design manager module. Also, different design parameters are varied to cover the large design space. These CFD simulations are faster as they contain simple geometry. The faster speed of these simulations allows for multiple cases to be run where the geometry and the boundary conditions can be varied. Running a design study involves the following steps.

1. Creating a baseline CFD model
2. Selecting the parameters which would be varied for the design study
3. Using the design of experiments (DOE) to choose the number of configurations to be studied and defining the values of each parameter selected
4. Providing the input to STAR-CCM's Design Manager module and running the design study

STAR-CCM+ offers an integrated CAD modeler, which makes it easy to construct the baseline model. In addition, the in-house meshing tool uses polyhedral elements for automated meshing. For a CFD simulation, the following steps are performed.

1. Pre-processing: This includes the creation of the geometry and generation of the mesh.
2. Setting up physics: This step includes selecting the correct physics models and applying the boundary conditions.
3. Solving: Here, the type of solver is specified along with the number of iterations. It also includes creating reports and monitors such as residuals, mass-flow, temperature, and pressure. The software then starts solving the Navier-Stokes equations.
4. Post-processing: The final step of a CFD simulation requires checking if the solution is correct and makes sense physically. This is verified by analyzing the convergence of the residuals and other monitors. Plots of mass flow and pressure also indicate if there is a discontinuous solution in the domain. Finally, the results are plotted, and the data is extracted for further analysis.

The geometry is created using the CAD modeler of STAR-CCM+, and the dimensions of the model are exposed as design parameters. These design parameters are varied when running multiple cases. Parts are then imported from the CAD model. The surfaces of the parts are split. Parts are then assigned to a specific region, aircraft bay to fluid, system to solid. The geometrical parameters chosen are a random starting point for the design study. For example, the system could

be placed anywhere in the bay. After assigning parts to regions, a mesh is created automatically. Figure 16 below shows the geometry tree of the different parts for a 2D example from the software user interface. The mesh is generated at the base surface of each part.

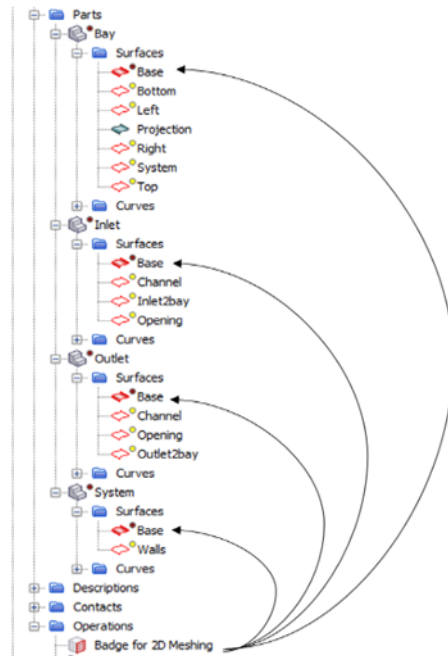


Figure 16: Geometry tree of the model. Split surfaces of each part; 2D mesh generated for the Base surface.

STAR-CCM+ solves boundary layer flows using the *Prism Layer* mesh. This mesh increases the number of elements present in the boundary layer. Prism layers are created at the walls for increased magnification at the boundaries. As this layer sees a rapid change in fluid properties (temperature, velocity), capturing the boundary layer effects is crucial.

STAR-CCM+ contains a wide range of physics models and methods to simulate single and multiphase fluid flow. The model is divided into two regions, solid and fluid. The system belongs to the solid region. As air flows in the inlet, the bay, and the outlet, these parts are assigned to the fluid region. The physics of each region is established using the models present in the software. The following assumptions are attached to each region:

- The fluid region contains air which is assumed to be an ideal gas. It is also incompressible as its velocity is well below the compressibility limit.
- Gravity is selected to act in the negative Y-axis. Thereby, the Y-axis refers to the coordinate system of the aircraft zone, where gravity is acting downwards.
- The simulation is assumed to have reached a steady state to replicate the operating periods of the equipment (8-10 hours). Steady-state simulations are faster and give mean values of flow properties developed over long periods. In addition, these type of simulations replicate the certification tests performed by the suppliers [9].

- Radiation heat transfer is considered, as the heat exchanged between the systems and the walls is significant.
- The solid region is assumed to be of constant density as thermal expansion is minimal in the scope of TRA.

The boundary conditions selected for the CFD simulations replicate the environmental conditions developed in the aircraft bay and include information on the airflow inlet temperature and mass flow rate. Figure 17 gives a better idea about the type of boundary conditions to be used. The various case studies replicate the ventilation conditions of equipment bay configurations at a steady-state condition. These case studies also model the heat load (Q) of a system. Q is the heat dissipated by the system while operating. It depends on their state of operation and could be higher during peak performance. The aircraft zone (bay) has different wall temperatures due to the different operating conditions (ground, takeoff, cruise, and landing.). An inlet duct is attached through which cool air is passed and exhausted through the ventilation outlet. The exhausted air is recirculated using the air conditioning system.

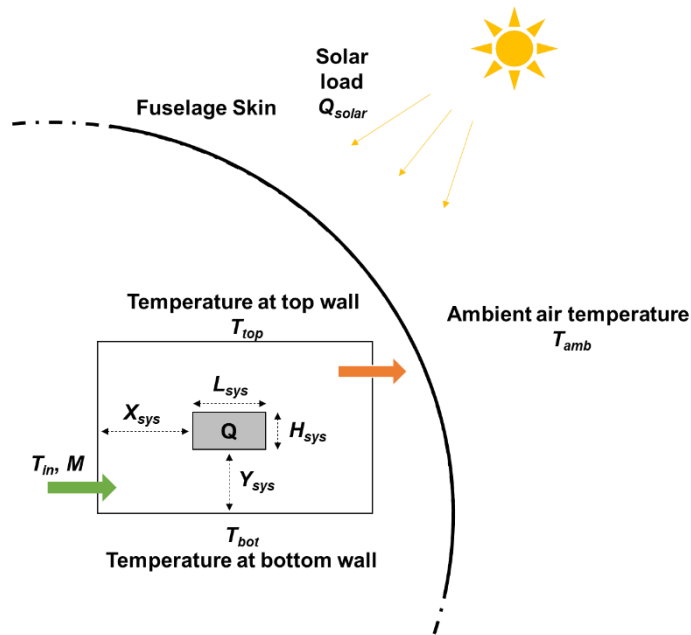


Figure 17: The aircraft zone housed inside a fuselage. The different environmental conditions affecting the temperature of the zone are seen.

STAR-CCM+ is a finite volume solver. A finite volume solution either uses a segregated or a coupled flow solver. The coupled flow solver calculates both the pressure and momentum equations simultaneously and is slower than the segregated solver. The CFD studies use coupled solver for the 2D cases as the time difference is negligible, but a segregated solver is used for the 3D cases as it is much faster. SST $k-\omega$ model is used to solve the turbulence. The temperature distribution and near-wall predictions are better in $k-\omega$ models compared to others [56].

Post-processing for CFD simulations includes plotting the velocity and temperature data. Also, checking for convergence of residuals is performed. Several reports (heat transfer coefficient, mass

flow rate, temperatures, and continuity) are created. The data from these reports is used for analysis and validation of the TRA results.

The next sections discuss the development of MS numbers.

3.2 Preliminary Development: First Iteration of the Development of Mainstream Numbers Using a Simplified 2D Case Study

The MS numbers are condensed geometrical parameters of the aircraft zone and its components. As DN, they needed to be defined via simple geometrical ratios. This section describes an approach that uses the centroid of the components to derive these numbers, using the first level of CFD case studies.

The first iteration in the development of the MS numbers involves using the position of the systems with respect to the cool air inlet and outlet in an aircraft zone. Figure 18 illustrates a simple 2D representation of an aircraft zone with a single system inside, and the aircraft zone has one inlet and one outlet for ventilation.

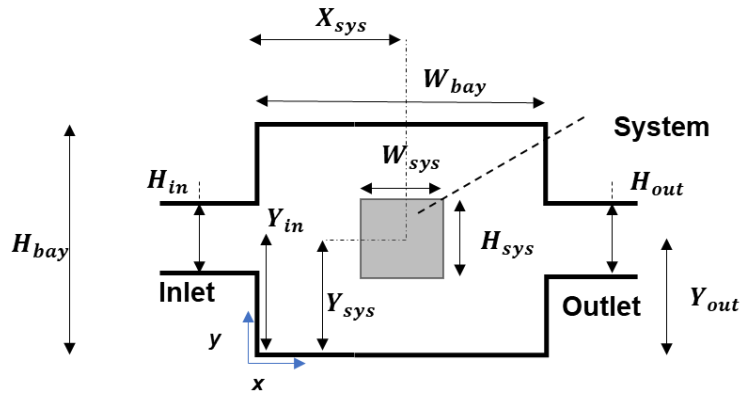


Figure 18: Geometrical parameters associated with the system and the aircraft zone to derive the mainstream numbers.

In the 2D representation given above in Figure 18, the relative location of the system to the inlet/outlet is determined using their centroids in the Y direction. The ratio of these centroids (Y_{sys}/Y_{in} , Y_{sys}/Y_{out}) determines how far the system is from these openings vertically. When this ratio is 1, the system and the respective opening are coincident in Y . The first MS number (S_1) defined by Eq. (5) uses the product of these ratios. Here, the value of S_1 closer to 1 indicates a vertical coincidence to both inlet and outlet.

$$S_1 = \frac{(Y_{sys})^2}{Y_{in} * Y_{out}} \quad (5)$$

The horizontal location of the system (X_{sys}) with respect to the width of the bay (W_{bay}) can be used to determine if the system is near or far away from either inlet or outlet. Assuming that the openings are situated at the bay walls, the ratio X_{sys}/W_{bay} normalizes the horizontal location of the system in the bay. If this ratio is close to 0 or 1, it means that the system is at either end of the bay where the inlet and outlet are located.

The second MS number (S_2) is defined by Eq. (66) using the horizontal location of the system in the bay.

$$S_2 = \frac{X_{sys}}{W_{bay}} \quad (6)$$

These numbers can have varying values depending on the geometry. S_1 close to 1 is desirable as it makes the inlet/outlet coincident vertically to the system. S_2 close to either 0 or 1 is desirable as it places the system near the walls containing the inlet/outlet. Thus, ranges are defined for these numbers. From both these numbers, S^* is created. It is an ordered pair whose values depend on the satisfaction of the following ranges. Eq. (7) gives all the possible values of S^* .

$$S^* = (m, n) = \begin{cases} (0, 0) & (a > S_1 \parallel S_1 > b) \parallel (c < S_2 < d) \\ (0, 1) & (a > S_1 \parallel S_1 > b) \parallel (S_2 < c \parallel d < S_2) \\ (1, 0) & (a \leq S_1 \leq b) \parallel (c < S_2 < d) \\ (1, 1) & (a \leq S_1 \leq b) \parallel (S_2 < c \parallel d < S_2) \end{cases} \quad (7)$$

In the expressions above, a , b , c , and d are constant values. These values define the ranges in the 2D space where the mainstream exerts influence on the system. The constants are further discussed and chosen based on simple 2D case studies conducted in 3.2.1.

Figure 19 illustrates how the location of the system changes with different values of S_1 and S_2 . For S_1 , Systems 1 and 3 would not be under the influence of mainstream in Y as they are not closer to the inlet/outlet vertically. For S_2 , Systems 1 and 3 lie close to the inlet and outlet, respectively. Thus, they are influenced by the mainstream in X .

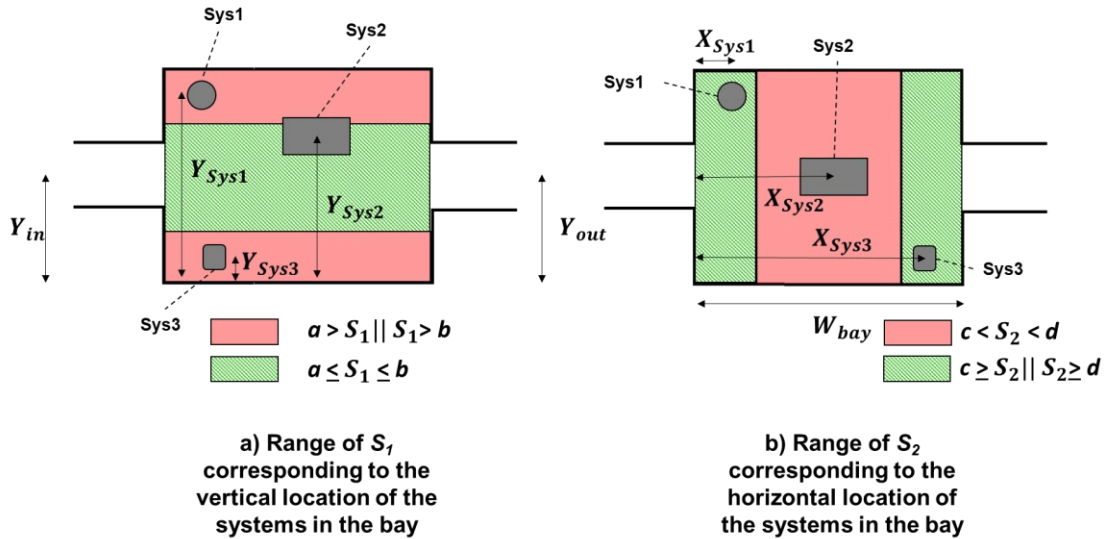


Figure 19: Visual representation of the ranges of S_1 and S_2 are shown; a) System locations according to different values of S_1 , b) System locations according to different values of S_2 .

Figure 20 illustrates all possible cases of S^* .

- $S^* = (1, 1)$ predicts that a system is under a strong influence of the mainstream.
- $S^* = (1, 0)$ and $S^* = (0, 1)$ predict that a system is under a weak influence of the mainstream.

- $S^* = (0,0)$ predicts that a system is not under any mainstream influence

Systems 1 and 2 are under a weak influence of the mainstream. System 3 is right in front of the inlet, and thus, the mainstream influence is strong. System 4 is under no influence of the mainstream as it lies in a region where $S^* = (0,0)$.

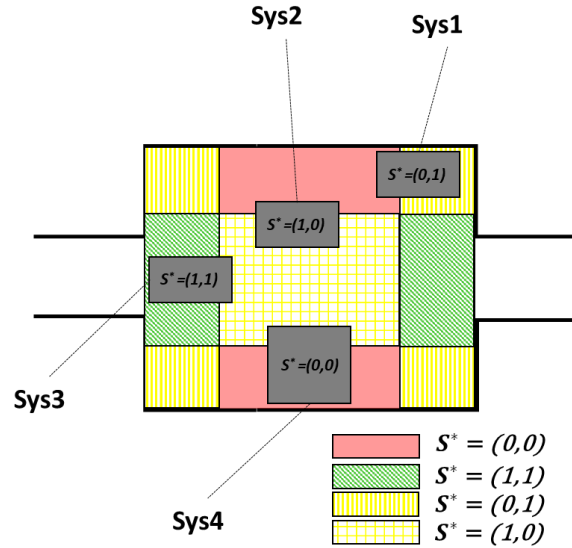


Figure 20: The different values of S^* and its related influences on the mainstream, red indicates no mainstream influence, yellow means a weak influence, and green means the influence of mainstream is strong.

S^* depends on S_1 and S_2 , which in turn depend on the limits a , b , c , and d as seen in Eq. (7). The values of these limits are determined using a simple case study in the following section.

3.2.1 Simple 2D Case Studies Using a Single System

In this section, the mainstream is visualized in 2D. The limits of S_1 and S_2 are defined and validated using 2D CFD simulations of a cylinder in a rectangular zone. This is a very simple representation of an aircraft system in an aircraft zone. As this is the first level of complexity from Table 3, a simplified equipment bay is used for the following goals:

- To validate the mainstream flow concept.
- To define the first set of MS numbers.
- To refine the mainstream definition, its applicability, and its limitations.

A design study is constructed, and mainstream numbers are predicted for each case. CFD simulations are run for each design. Results from the CFD are used to:

- Visualize the mainstream flow.
- Illustrate its importance in TRA.
- Validate the MS number predictions.

Both physical and geometrical parameters are varied in the design study. The 2D model, along with all the design parameters, is shown in Figure 21 below. The thermal parameters are the inlet

temperature (T_{in}), inlet mass flow rate (M), the system heat load (Q_{sys}) temperature of the top wall (T_{top}), and the temperature of the bottom wall (T_{bot}). The two other bay walls are considered adiabatic.

The rationale for the specific values of the thermal parameters is discussed already in Section 3.1.2. The chosen mass flow rate represents a forced convection regime in the bay ($Ri = 0.053$). The temperatures of the walls correspond to a hot day on the ground, with the aircraft is parked at a runway [3]. The top wall is at a higher temperature than the bottom wall due to it being near the aircraft skin, exposed to the sun. The inlet temperature is close to the cabin temperature assuming cabin outflow is used for cooling the bay [43].

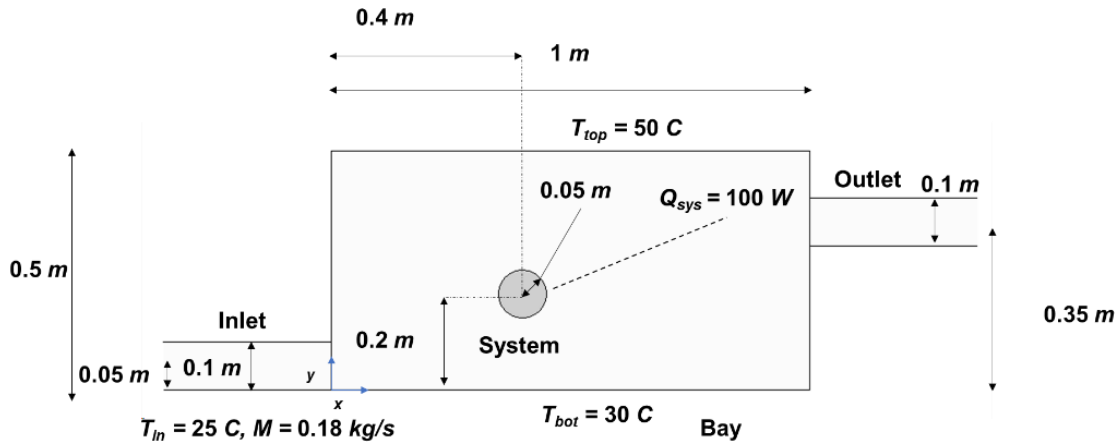


Figure 21: The baseline CFD model, along with the values of its geometrical and physical parameters

Figure 22 illustrates the 2D mesh generated for the CFD model of a sample configuration. The mesh becomes fine near the system boundaries and near the walls, thus making the solution as accurate as possible. The mesh contains 6822 cells in total.

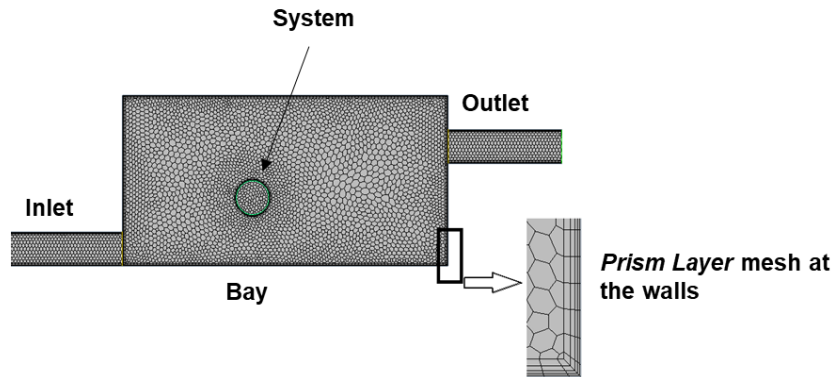


Figure 22: The 2D mesh generated for the baseline model, prism layers are applied at the walls of the CFD model.

The mainstream numbers S_1 and S_2 of the baseline model are calculated using Eq. (1) and (2) and listed below:

- $S_1 = 0.76$
- $S_2 = 0.4$

The limits of S_1 and S_2 are estimated using the CFD results.

The residuals are well converged. In Figure 23, velocity is normalized with the inlet velocity ($V_{inlet} = 1.5m/s$). The mainstream is represented by the red region; a large recirculation flow can also be observed before the outlet. The temperature plot of the bay signifies the importance of being close to the mainstream as regions near the mainstream flow are at a lower temperature compared to regions away from it. One can see from the velocity plot that the system does not lie on the mainstream. The following can be concluded for the limits of S_1, S_2 .

- $0.76 \notin [a, b]$
- $0.4 \notin [c, d]$

A parametric study is conducted, and its results are used to define the limits $a, b, c,$ and d .

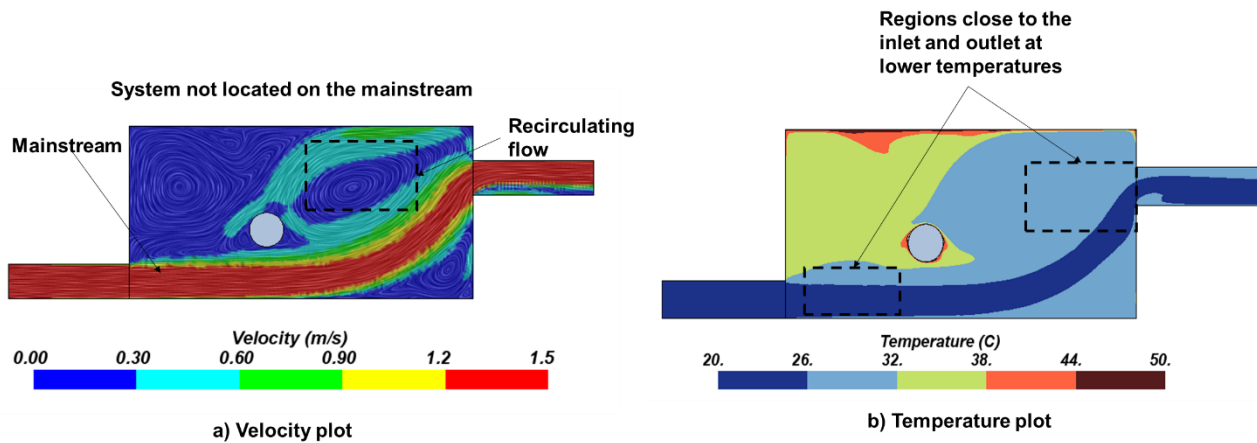


Figure 23: The velocity and temperature plots of the baseline CFD simulation, the red area in the velocity plot represents the mainstream flow.

3.2.2 Design Study to Define the Boundaries of S_1 and S_2

A parametric study is the study of the influence of different geometrical or physical parameters on the design. This study is used to estimate the values of $a, b, c,$ and d , defined in Eq.(7) by varying geometrical and physical parameters listed in Table 4.

The Design of Experiments (DOE) technique is used to define the range of the parameters so that the best design space is constructed with the least amount of CFD simulations. DOE can be defined as the strategy for setting up experiments so that the information required is obtained as efficiently and precisely as possible [57].

The DOE technique used here is a Latin Hyper-Cube Sampling (LHS) technique associated with a space-filling criterion to cover all the design space. LHS is a popular space-filling design technique and is used widely in computational experiments. It involves the generation of n samples using u variables. It, therefore, creates an $n*u$ matrix with variable values normalized from 0 to 1. The main advantage is that it does not require more samples as the variables keep increasing because n and s are independent of each other [58]. Figure 24 below illustrates a sample design space-filling capability of LHS with a 2-variable system. In the design space, $n = 10$ and $u = 2$

(U_1, U_2) , therefore the number of points is $n * u = 20$, thus allowing for the design study to be more comprehensive.

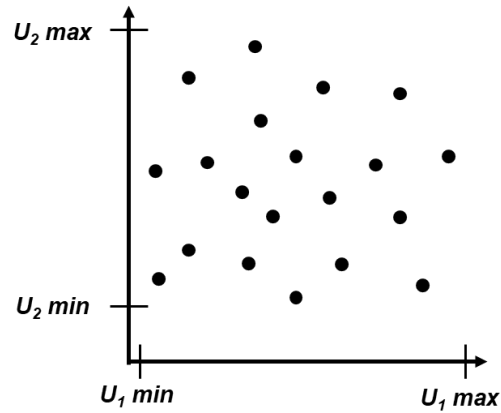


Figure 24: A sample variable LHS design space.

The ranges of each parameter are listed in Table 4. On observing the list, system size, height, and width of the bay can be excluded from the LHS technique. It leaves 11 parameters ($u = 11$), and number of samples is chosen equal to 20 ($n = 20$)

Table 4: Description and ranges (min, max) of all the selected parameters for the design study.

Description	Type	Label	Type	min	max	min	max
System size	Geometrical	$R_{sys} (m)$	Constant	0.05	0.05	0.1	0.1
Inlet position	Geometrical	$Y_{in} (m)$	Variable	0.00001	0.5	0.00001	0.5
Outlet position	Geometrical	$Y_{out} (m)$	Variable	0.00001	0.5	0.00001	0.5
System X position	Geometrical	$X_{sys} (m)$	Variable	0.1	0.9	0.15	0.85
System Y position	Geometrical	$Y_{sys} (m)$	Variable	0.1	0.4	0.15	0.35
Inlet size	Geometrical	$H_{in} (m)$	Variable	0.05	0.25	0.05	0.25
Outlet size	Geometrical	$H_{out} (m)$	Variable	0.05	0.25	0.05	0.25
Bay height	Geometrical	$H_{bay} (m)$	Constant	0.5	0.5	0.5	0.5
Bay width	Geometrical	$W_{bay} (m)$	Constant	1	1	1	1
Mass flow rate	Physical	$M (kg/s)$	Variable	0.15	0.5	0.15	0.5
Top wall temp.	Physical	$T_{top} (^{\circ} C)$	Variable	30	80	30	80
Bottom wall temp.	Physical	$T_{bot} (^{\circ} C)$	Variable	20	60	20	60
System heat load	Physical	$Q_{sys} (W)$	Variable	100	2000	100	2000
Inlet air temp.	Physical	$T_{in} (^{\circ} C)$	Variable	15	30	15	30

A (20,11) matrix of the input variables is created using MATLAB's in-built Latin Hypercube Design (LHD) function. The output is de-normalized, and an input table is created for each system size.

The input table is loaded into STAR-CCM's Design Manager module, a total of 20 configurations for each system size are simulated. The velocity and temperature plots of a selected sample of the configurations are presented in Figure 25. Table I in the Appendix provides an exhaustive summary of all the data for all the cases and their associated mainstream numbers.

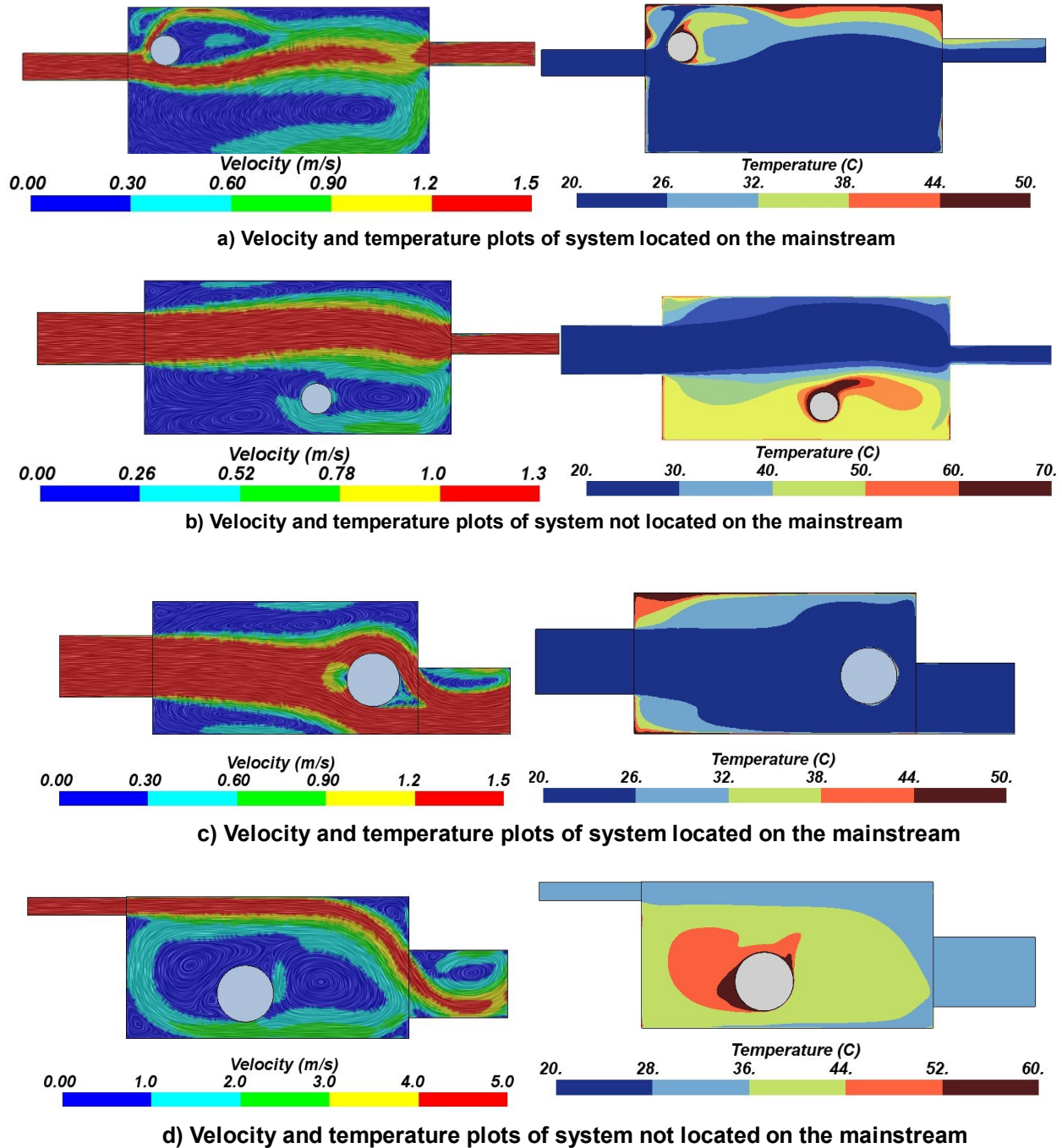


Figure 25: Systems of different sizes represented as either located or not located on the mainstream, the velocity of the mainstream is normalized with the inlet flow velocity. The cooler regions of the bay are near the mainstream.

The following observations can be made from Figure 25 and Table I from the Appendix

- All the configurations with either a mixed or a forced ventilation regime ($Ri \leq 1$) are selected for analyzing the mainstream interactions with the system.
- Both systems sizes ($R_{sys} = 0.05 m, 0.1 m$) are shown.
- A system close to either inlet/outlet is under the mainstream influence.

- The temperature plots for systems lying on the mainstream indicate they are in a cooler environment.
- The temperature plots for systems not under the mainstream influence indicate that they are present in a hotter environment.

Visual inspection of the streamlines in the velocity and temperature plots show that if the system's vertical position (Y_{sys}) is 0.8 to 1.3 times that of either the inlet's (Y_{in}) or the outlet's vertical position (Y_{out}), then the system can be seen interacting with the flow. Similarly, if the system's horizontal position (X_{sys}) is closer either to the inlet ($X_{sys}/W_{bay} \leq 0.3$) or the outlet ($0.7 \geq X_{sys}/W_{bay}$), it can be seen interacting with the mainstream flow. Thus, the limits from Eq. (7) can be listed in Table 5.

Table 5: Limits of S_1 and S_2 .

Limit	Value
a	0.64
b	1.69
c	0.3
d	0.7

The values of S^* corresponding with different system-bay configurations are given in Figure 26.

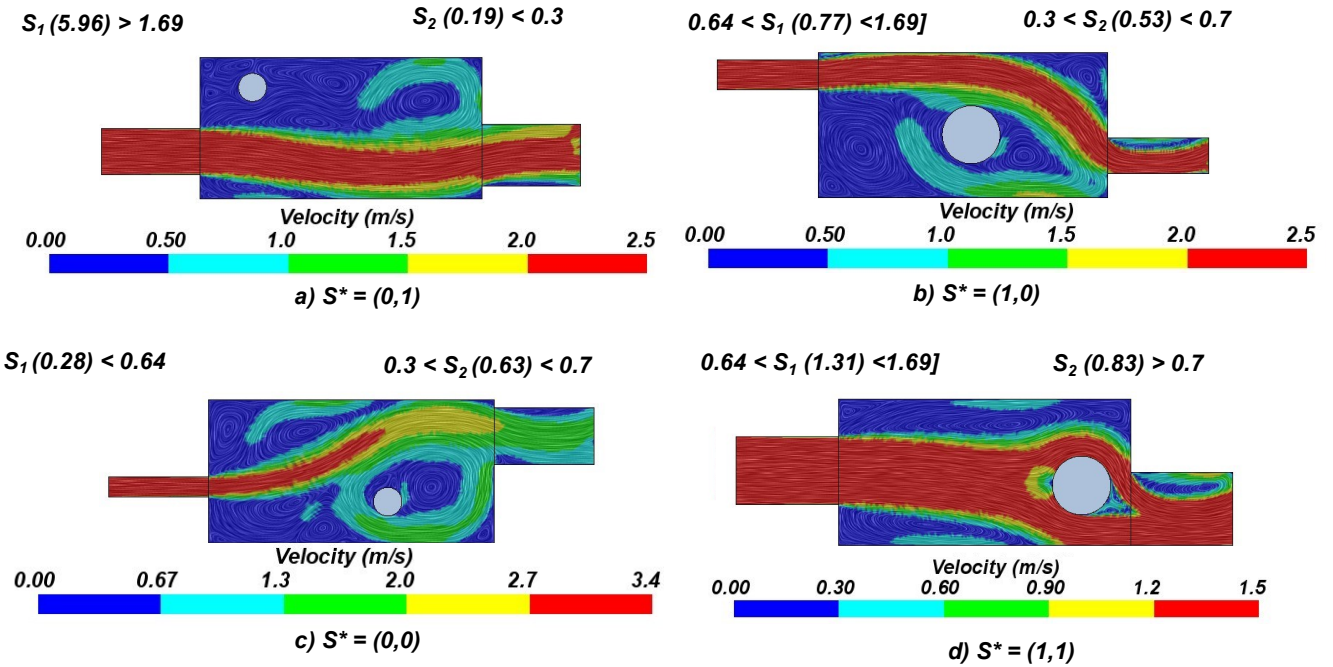


Figure 26: System-bay configurations corresponding to S^* values; velocity plots help in visualizing the mainstream predictions.

Thus, using S_1 , which uses the centroids of the system and the ventilation sources, and S_2 , which uses the system's horizontal location in the bay, the relative distance to the mainstream can be

predicted. However, there are some drawbacks to using these numbers. These drawbacks are listed in the next section. Steps taken to mitigate these drawbacks are then discussed in 3.3.

3.2.3 Limitations of the First Iteration

S^* provides information about the system's relative location in a bay concerning the inlet and the outlet. Nevertheless, it has the following limitations:

- S^* is not a single number but an ordered pair, which works on a True/False logic. Not being a single DN leads to difficulties when comparing two systems, both on the mainstream or vice-versa. In
- Figure 27-a, the mainstream influences Systems 1 and 2, but S^* cannot predict which system is under a greater influence.
- a , b , c , and d are not universal values and depend on the geometry used.
- S^* is based on a system's centroid. Thus, the bounds of the system are neglected. For example, Figure 27-b shows the case of System 3, which is engulfed by the mainstream but not at its centroid.

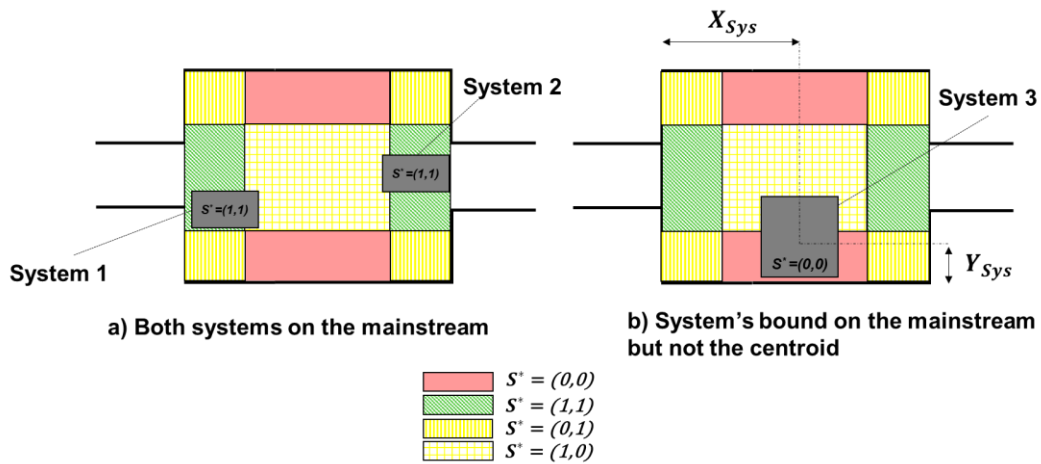


Figure 27: a) Both System 1 and 2 are under the influence of mainstream but comparing the relative influence between these 2 systems is difficult. b) A configuration where the system's bounds would be under the influence of mainstream but not the centroid

In the following Section 3.3., the MS numbers are reformulated to address the drawbacks discussed above. The reformulated numbers are continuous, which allows for the comparison of mainstream influences between different systems. They also allow being easily manipulated and interpreted in conceptual design.

3.3 Enhanced Formulation of the Mainstream Numbers MS

Two new dimensionless numbers, the cross-stream number (CS) and the streamwise number (SW), are introduced to address the drawbacks of S^* . The CS number predicts the influence of the mainstream in the cross-stream direction (vertical in fig). The SW number considers the mainstream influence in the streamwise direction (horizontal in Figure 28).

Figure 28 shows a simplified 2D representation of an aircraft bay with a single inlet and outlet and one rectangular system. To define these numbers, one needs information on the system's locations, inlet, and outlet. All these entities' locations are based on their centroid, defined according to the Cartesian frame of reference, with the origin's location outside of the aircraft bay (Figure 28).

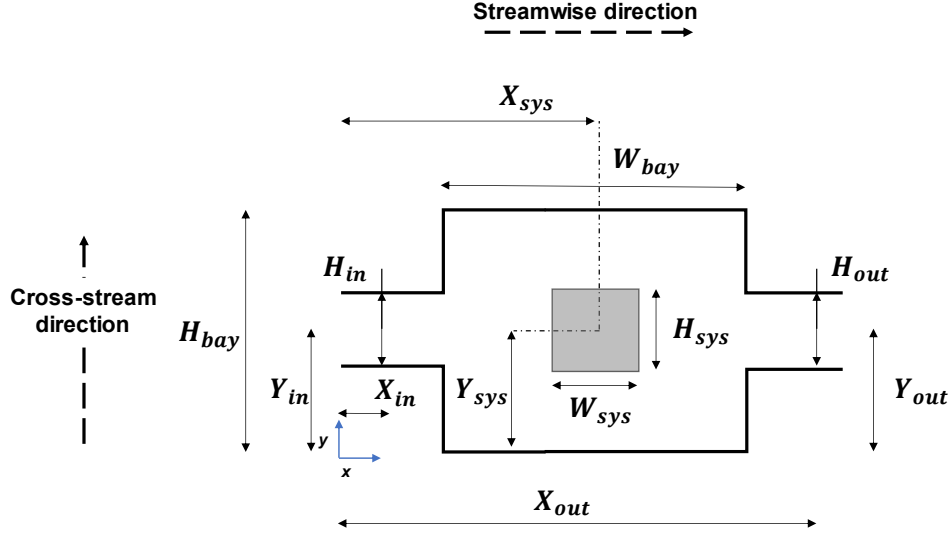


Figure 28: 2D Geometrical Configuration used to derive the cross-stream and stream-wise numbers: the square shaded area in the middle represents the system housed in the bay.

Eq. (8) and (9) define the lower-case parameters x_{sys-in} and $x_{sys-out}$ which are the coordinates of the system's bounds in the streamwise direction supported by the X -axis. They also define the system sides that face the inlet and outlet in the streamwise direction. Similarly, Eq. (10) and (11) define the lower-case parameters x_{in-sys} and $x_{out-sys}$ which are the coordinates of the inlet and outlet openings that face the system in the streamwise direction supported by the X -axis here.

$$x_{sys-in} = X_{sys} - \frac{W_{sys}}{2} \quad (8)$$

$$x_{sys-out} = X_{sys} + \frac{W_{sys}}{2} \quad (9)$$

$$x_{in-sys} = X_{in} + \frac{L_{in}}{2} \quad (10)$$

$$x_{out-sys} = X_{out} - \frac{L_{out}}{2} \quad (11)$$

Eq. (12) - (17) define the coordinates of the upper and lower bounds of the system, the inlet, and the outlet in the cross-stream direction supported by the Y -axis.

$$y_{sys,u} = Y_{sys} + \frac{H_{sys}}{2} \quad (12)$$

$$y_{sys,l} = Y_{sys} - \frac{H_{sys}}{2} \quad (13)$$

$$y_{in,u} = Y_{in} + \frac{H_{in}}{2} \quad (14)$$

$$y_{in,l} = Y_{in} - \frac{H_{in}}{2} \quad (15)$$

$$y_{out,u} = Y_{out} + \frac{H_{out}}{2} \quad (16)$$

$$y_{out,l} = Y_{out} - \frac{H_{out}}{2} \quad (17)$$

Defining the upper and lower bounds makes it easier to calculate the nearest distances, both vertically and horizontally, in the case of Figure 28. The nearest distance is the quantitative synonym for closeness and must be assessed in the three dimensions for three-dimensional case studies. Thus, the SW number's formulation uses the nearest distances in the streamwise direction, while the CS number uses the nearest distances in the cross-stream direction.

3.3.1 Formulation of the Streamwise Number SW

As stated before, the streamwise analysis helps capture the effect of the ventilation source's streamwise location on the influence of the mainstream flow on the system. The inputs for the formulation of the streamwise number are the coordinates of the system's bounds in the streamwise direction x_{sys-in} and $x_{sys-out}$ from Eq. (8) and (9), and the coordinates of the inlet and outlet openings x_{in-sys} and $x_{out-sys}$ Eq. (10) and (11). Using these inputs, the streamwise numbers (SW_{in} , SW_{out}) are defined in equations Eq. (14) and (19). For example, when a system is closer to the inlet, SW_{in} is closer to zero and vice versa. Similar is the case for an outlet (SW_{out}). The SW numbers thus are used:

- To predict whether a system will lie closer or farther from a particular ventilation source (inlet or outlet).
- To rank the systems according to their closeness to a ventilation source (inlet or outlet) in the streamwise direction, which is particularly important for equipment bays packed with multiple systems.

$$SW_{in} = \left| 1 - \frac{x_{sys-in}}{x_{in-sys}} \right| \quad (18)$$

$$SW_{out} = \left| 1 - \frac{x_{sys-out}}{x_{out-sys}} \right| \quad (19)$$

3.3.2 Formulation of the Cross-Stream Number CS

The formulation of the cross-stream CS number is based on the nearest cross-stream distances from the system to the inlet and outlet. The nearest cross-stream distances (NCD) are numerous as

the system can be both above and below the inlet/outlet. In the case of cross-stream analysis, the distance of the system's top bound from inlet/outlet's top bound ($NCD_{1,in}$ and $NCD_{1,out}$) and the system's bottom bound from inlet/outlet's bottom bound ($NCD_{2,in}$, $NCD_{2,out}$) are considered. Eq. (20) to (23) define these distances for the configuration described in Figure 28.

$$NCD_{1,in} = y_{sys,u} - y_{in,u} \quad (20)$$

$$NCD_{2,in} = y_{sys,l} - y_{in,l} \quad (21)$$

$$NCD_{1,out} = y_{sys,u} - y_{out,u} \quad (22)$$

$$NCD_{2,out} = y_{sys,u} - y_{out,l} \quad (23)$$

The expressions for the CS numbers for the inlet and the outlet are defined in Eq. (24) and (25) using the nearest cross-stream distances. These numbers determine the potential influence of the mainstream flow in the cross-stream directions on the system, whether significant or weak. The influence ranges from the mainstream flow engulfing the system ($CS_{in, out} \leq 0$) to only partially impacting the system ($CS_{in, out} \leq 10$) and not at all influencing the system ($CS_{in, out} > 10$).

$$CS_{in} = \frac{NCD_{1,in} * NCD_{2,in}}{H_{sys} * H_{in}} \quad (24)$$

$$CS_{out} = \frac{NCD_{1,out} * NCD_{2,out}}{H_{sys} * H_{out}} \quad (25)$$

Figure 29 illustrates an example of how CS represents the mainstream flow influence. Case 1 shows a system that is far away from the mainstream ($CS_{in} > 10$) and is not under its influence. In case 2, the system is under the partial influence of the mainstream ($CS_{in} \leq 10$) and receives a portion of the mainstream flow. Case 3 represents a system fully engulfed by the mainstream flow. ($CS_{in} \leq 0$). Cases 4, 5, and 6 are like 1, 2, and 3, but from the outlet's perspective.

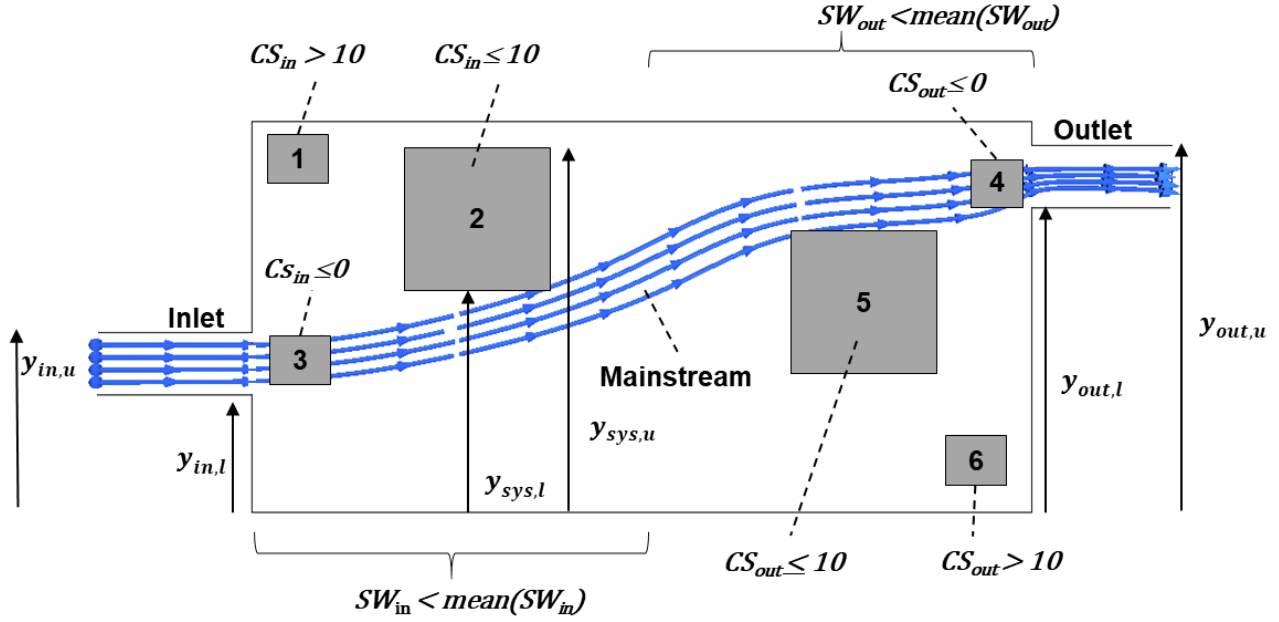


Figure 29: Definition of the CS number for six cases: 1-System close to the inlet, not influenced by the mainstream, 2-System close to the inlet, partially influenced by the mainstream, 3-System close to the inlet, engulfed by the mainstream, 4-System close to the outlet, engulfed by the mainstream, 5-System close to the outlet, partially influenced by the mainstream, 6-System close to the outlet, not influenced by the mainstream.

To summarize, the mainstream numbers SW and CS are proposed using streamwise and cross-stream evaluations. The numbers CS and SW are based on the bay's geometric configuration only, to be suitable for conceptual design, derivable from a conceptual 3D aircraft model. Thus, these new numbers will ease the connection of the thermal risk assessment methodology with a conceptual 3D aircraft model [59].

3.3.3 Mainstream Flow Analysis Using Cross-Stream and Streamwise numbers.

This section introduces a graphical representation for the mainstream analysis using the CS and SW numbers. Figure 30 shows the mapping of CS vs. SW , where the vertical axis represents CS and the horizontal axis SW . The range of CS starts from when the system is on the mainstream ($CS \leq 0$) to when system is not influenced by the mainstream ($CS > 10$). In between, the system receives some airflow and is therefore partially influenced by the mainstream ($0 < CS \leq 10$). For the streamwise analysis, the range starts from $min(SW)$, which represents the closest distance from the system to either inlet or outlet to $max(SW)$, which is the maximum possible distance.

The mapping in Figure 30 is divided into three regions vertically: not influenced by the mainstream ($CS > 10$), influenced by the mainstem ($0 < CS \leq 10$) and on the mainstream ($CS \leq 0$). The last region is further divided into two regions horizontally based on the $mean(SW)$ number. In cases where $CS \leq 10$, the SW categorizes the systems according to their closeness to either inlet or outlet in the streamwise direction. In this way, SW helps to understand the mainstream's influence better. When $SW > mean(SW)$, the system is far away either from inlet or outlet, and the system is less influenced by the mainstream, even though it is predicted to lie on the mainstream by the CS number ($CS \leq 10$). When $SW \leq mean(SW)$ the system lies closer to the inlet or outlet and has a

higher chance of being influenced by the mainstream. Also, when $SW = \min(SW)$ the considered system is the closest to the inlet or outlet and will be significantly influenced by the mainstream.

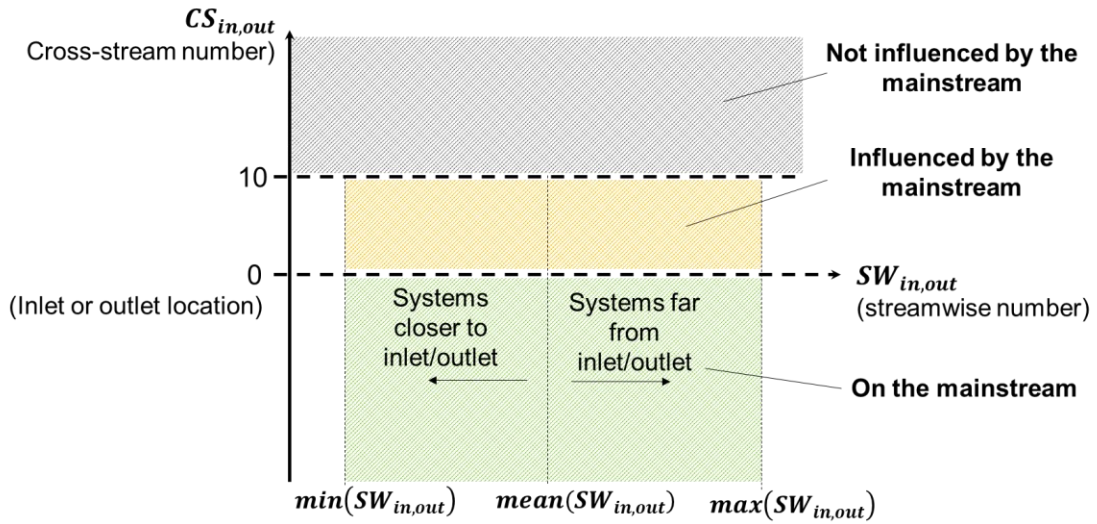


Figure 30: 2D graphical representation of the mainstream flow analysis

3.3.4 Examples of Mainstream Flow Prediction Using the Mainstream Numbers.

This section shows an example of the graphical representation of the mainstream analysis using CS and SW numbers. A simplified 2D case study (Figure 31, Table 6) is used to discuss several configurations with different mainstream flows. While still in 2D, this case involves using multiple systems of different shapes and sizes to further demonstrate the scope of the mainstream flow analysis concept, as seen in Table 3. Unlike the earlier case study, the dimensions and flow parameters of this 2D model are derived from existing standards [43]. Thus, this is closer to the real-world case. The goals of performing this case study are listed below:

- Validate the mainstream flow concept using parameters that are close to the real world
- Perform the mainstream flow analysis for multiple systems
- Investigate the effects of changing the location of the ventilation sources on the mainstream flow
- Derive CS and SW numbers for a system and compare them with the others

CFD simulations are again used to validate the MS number predictions. They are used to:

- Validate the CS and SW numbers predicted by the mainstream flow analysis
- Visualize the effects of changing location on the mainstream flow
- Illustrate the effects of the mainstream on the temperature of the equipment bay

This 2D model corresponds to a simplified configuration of an equipment bay given in [43]. These equipment bays are usually tightly packed with heat-generating equipment, such as electronic, electrical, hydraulic, pneumatic, and air conditioning components.

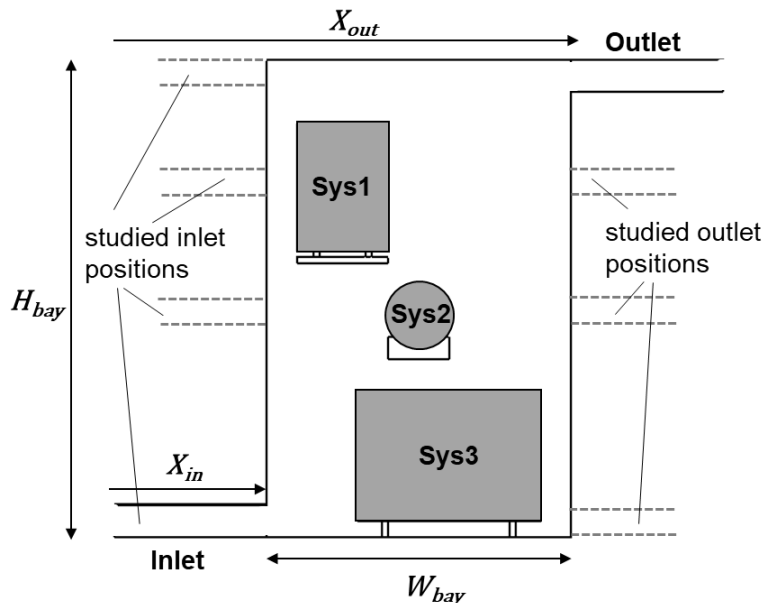


Figure 31: Geometrical description of the 2D case study with different inlet and outlet positions.

Figure 31 shows the geometrical configuration of the case study that contains three systems (System 1, System 2, and System 3). System 1 and System 3 are representative of closely packed

Modular Concept Units (MCUs), while System 2 represents a cylindrical-shaped system, such as an electric motor or a hydraulic pump. These components dissipate heat and are supported in the plane perpendicular to the viewer. The inlet length ($X_{in} = 0.5\text{m}$) is prolonged to replicate a fully established flow from the pneumatic lines. Manufacturer datasheets, such as in [60], provide the dimensions and the heat loads of the MCUs. The different configurations considered are seen in dashed lines in Figure 31.

In most cases, cabin exhaust air ventilates the equipment bays. More tightly packed bays would require an efficient ducting system for more effective cooling. In some cases, an exhaust fan is in the outlet duct to extract the hot air. This hot air is recirculated back to the air-conditioning system, typically used for cooling in most aircraft. Inefficient ducting may result in local high-temperature zones, so-called hotspots. These hotspots can cause the skin temperature of a given system to exceed operating temperatures, resulting in reduced reliability or even failure of a system [43].

This case study aims to investigate the locations of the inlet and outlet on the thermal environment of the systems and how they affect the mainstream flow. The CFD simulation uses assumptions listed in 3.1.2. The 2D mesh contains around 7320 cells and uses polygonal elements. Figure 32 shows the mesh used in one of the configurations.

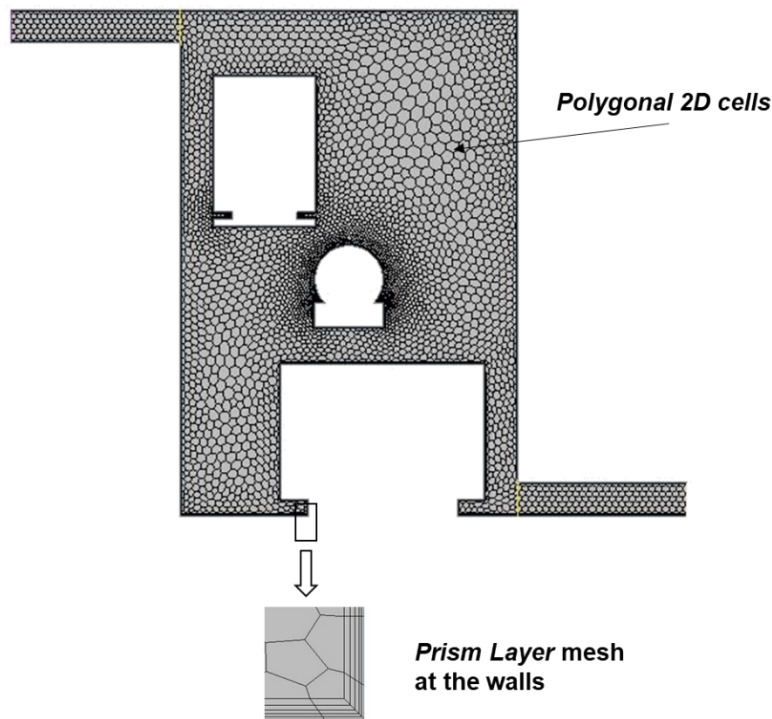


Figure 32: 2D mesh shown with prism layers at the walls for the case study, only applied to the fluid region.

For a standard day condition, in a pressurized bay ventilated by the cabin exhaust, the inlet temperature can be assumed to be equal to 25°C . In this case study, the acceptable temperature limit of the system ambient air is equal to 70°C , which in turn requires a minimum flow of up to 0.035 kg/s per kilowatt of generated heat. In this case study, a mass flow of 0.05 kg/s is assumed, thus satisfying conditions set by DO-160 [9]. The sidewalls of the compartment are assumed

adiabatic; the top and bottom walls have a temperature gradient ΔT . The top wall temperature is assumed at 50° C, while the bottom wall temperature is at 30° C, thus maintaining a constant ΔT of 20° C. This temperature gradient is representative of the reality, i.e., for an aircraft parked on the ground in normal sunny day conditions, the top wall temperatures heat due to exposure to the sun, while the bottom wall is relatively cooler. All three systems have heat loads associated derived from manufacturer data [61].

Table 6: 2D case study with multiple systems: Geometrical parameters, and boundary conditions.

Geometrical Parameters	System 1	System 2	System 3	Inlet	Outlet	Bay
$X (m)$	0.75	1	1.1	0.25	1.75	-
$Y (m)$	1.1	0.7	0.25	0.05	1.45	-
$H (m)$	0.4	0.2	0.4	0.1	0.1	1.5
$L (m)$	0.3	0.2	0.6	0.5	0.5	1
$T (^\circ C)$	$T_{lim} = 70$	$T_{lim} = 70$	$T_{lim} = 70$	$T_{in} = 25$	-	$T_{env} = 50$ $T_{bw} = 30$ $T_{tw} = 50$
$Q_{sys} (W)$	250	100	1000	-	-	1350 (Total)
$M (kg/s)$	-	-	-	0.05	0.05	-

This case study covers various inlet and outlet positions, including the highest and lowest. Table 7 summarizes the geometrical parameters required to compute CS and SW numbers.

Table 7: Inlet and outlet locations for the 2D case study.

Case	1	2	3	4	5	6	7	8	9	10	11	12
$X_{in} (m)$	0.25	0.25	0.25	0.25	0.25	0.25	0.25	0.25	0.25	0.25	0.25	0.25
$Y_{in} (m)$	0.05	1.45	0.05	1.45	0.25	0.7	1.1	0.25	0.7	1.1	1.45	0.05
$X_{out} (m)$	1.75	1.75	1.75	1.75	1.75	1.75	1.75	1.75	1.75	1.75	1.75	1.75
$Y_{out} (m)$	1.45	0.05	0.05	1.45	1.45	1.45	1.45	0.05	0.05	0.05	1.1	0.7

Figure 33 illustrates a 2D mapping of the resulting CS and SW numbers. The ranges of SW depend on the inlet and outlet locations and thus will not always be the same. The following observations can be made:

- System 1 is closest to the inlet and lies at $\min(SW_{in})$, implying that it would be under the considerable influence of the mainstream flow when its corresponding CS is less than or equal to 10 ($CS_{in} \leq 10$).
- System 3 lies at $SW_{in} > \text{mean}(SW_{in})$, and System 2 lies at $\max(SW_{in})$.
- In the CS_{out} vs. SW_{out} mapping, the opposite condition occurs, where System 3 lies on the $\min(SW_{out})$ line.
- System 2 lies at $SW_{out} > \text{mean}(SW_{out})$, and System 1 lies at $\max(SW_{out})$.

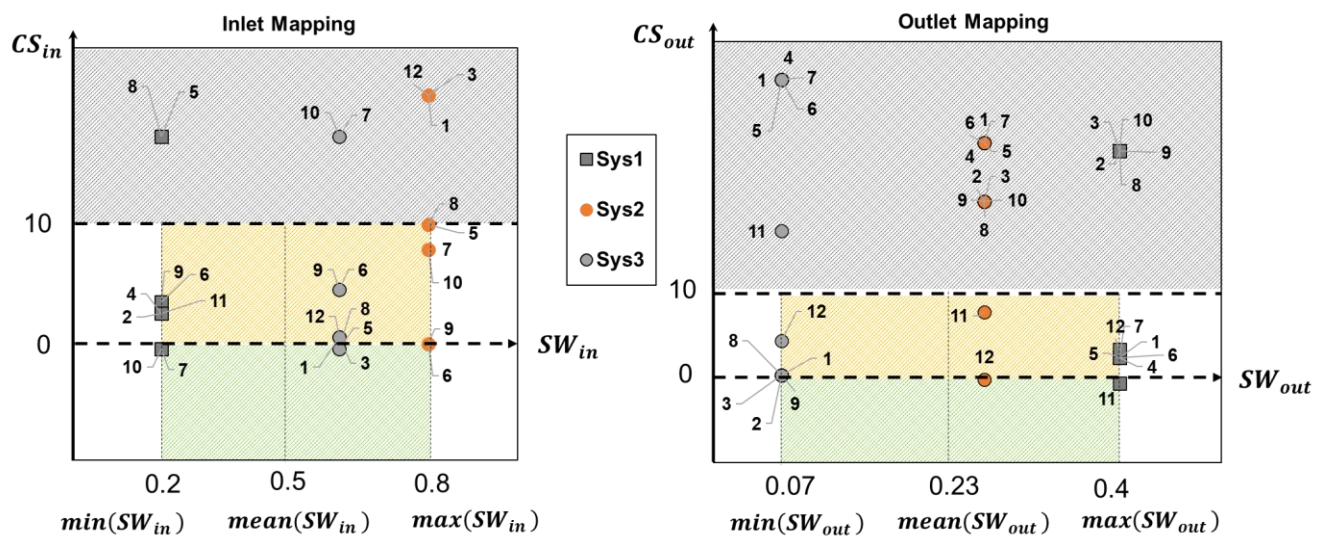


Figure 33: Mainstream numbers for the 2D case study for Cases 1-12: the grey shaded area is not under the mainstream influence, the area under the partial influence is yellow, and the area where the mainstream has a considerable influence is green.

Figure 34 and Figure 35 show the velocity and temperature fields of all the configurations. The velocity contour indicates the region with the highest velocity in the bay area (red color), nearing 0.5m/s. This region of high velocity coincides with the mainstream region definition discussed before.

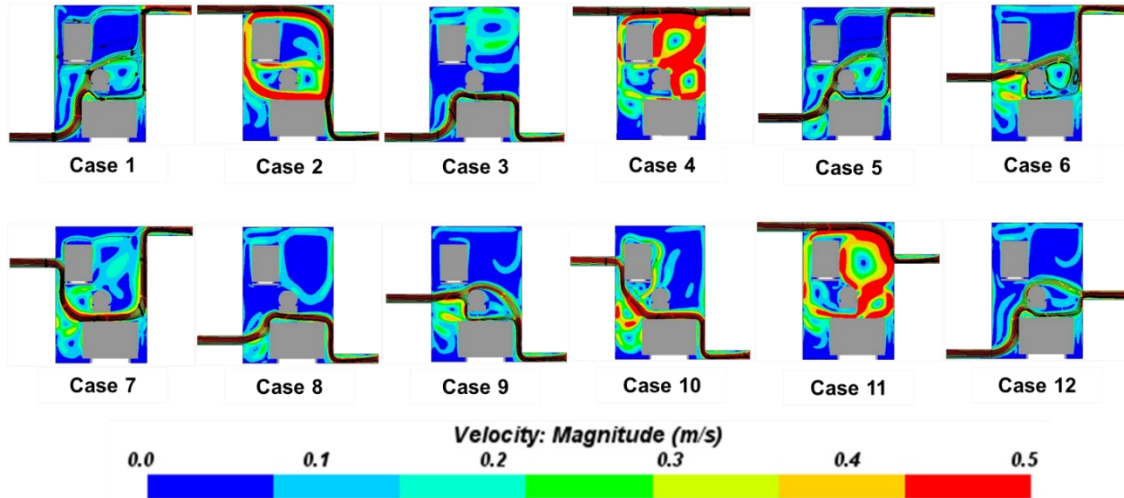


Figure 34: Velocity fields obtained from the CFD simulations of Cases 1-12 for the 2D multi-systems case study; the black streamlines indicate the mainstream flow.

The following observations can be made:

- In Case 1, System 3 is influenced by the mainstream as predicted ($CS_{in} = 0.44$) and redirects some of the flow towards System 2. System 1 receives the smallest portion of flow as predicted by its CS_{in} number (27).
- Case 3 involves a different outlet location than Case 1.
- In Case 1, the mainstream flow crosses the bay from the bottom left to the top right part, while in Case 3, the upper region of the bay is mostly unaffected, as seen by the high temperature in the zone (Figure 35). This validates the mainstream prediction for System 1 that is far away from the mainstream flow with regards to the outlet ($SW_{out} > mean(SW_{out})$ and $CS_{out} = 27$), thus is predicted to be under no influence of mainstream.
- The temperature field reveals that changing the outlet location results in a completely different thermal environment.
- In Case 2, both Systems 1 ($CS_{in} = 2.5$) and 3 ($CS_{out} = 0.44$) are predicted to be influenced by the mainstream. It can be seen from Figure 34 that indeed the mainstream flow indeed interacts with both the systems.
- In Case 4, with the inlet and outlet at the top of the bay, the mainstream flow exits straight through the outlet and generates recirculation flows downstream to System 1 and System 2 (Figure 34). Only System 1 is influenced by the mainstream flow as predicted ($CS_{in} = 2.5$), while System 2 and System 3 are far from the mainstream, as predicted ($CS_{in} = 35.44$ and $CS_{in} = 28$ respectively).

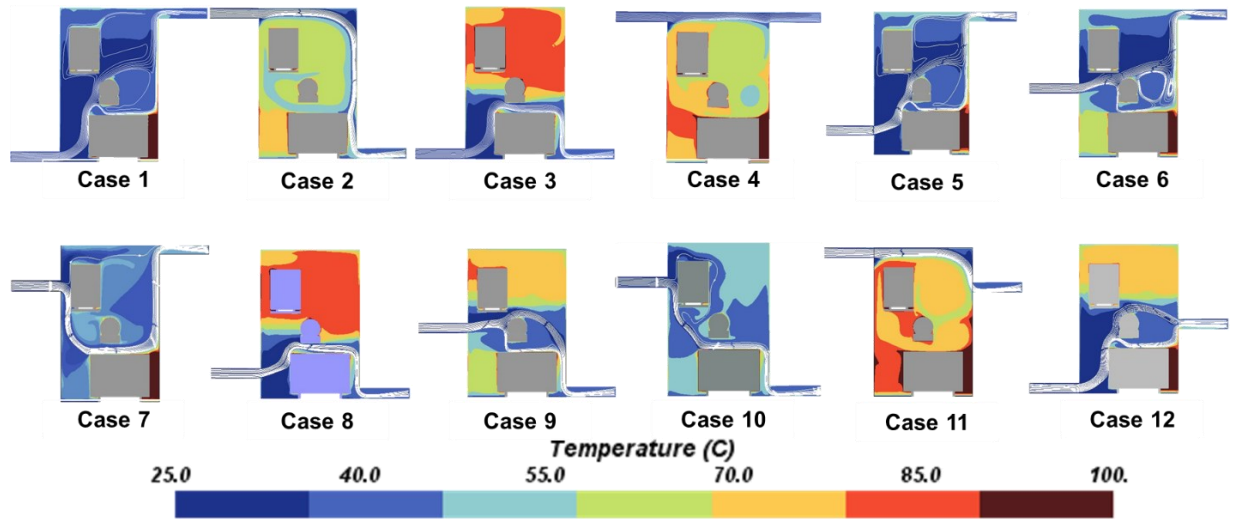


Figure 35: Temperature plots obtained from the CFD simulations of Cases 1-12 for the 2D multi-systems case study; the white streamlines indicate the mainstream flow.

- The temperature field confirms the mainstream predictions as the bottom part of the bay is hotter than the top part (Figure 35).
- Two configurations (Case 7 and 10) show situations where a system (System 1 here) obstructs the inlet opening and disturbs the mainstream flow from the inlet opening. The mainstream numbers relative to the inlet predict well this configuration for System 1 as it is on the mainstream ($SW_{in} = \min(SW_{in})$ and $CS_{in} = -0.56$).
- In addition, the mainstream numbers relative to the inlet predict that System 2 is influenced by the mainstream ($SW_{in} = \text{mean}(SW_{in})$ and $CS_{in} = 7.88$), which is confirmed by Figure 34 for the two cases.
- Moreover, the mainstream numbers can capture well the differences between Cases 7 and 10, which remain in the outlet location. Here, the mainstream numbers relative to the outlet predict that System 3 is influenced by the mainstream flow for Case 10 ($SW_{out} = \min(SW_{out})$ and $CS_{out} = 0.44$), while it is not influenced for the Case 7 ($SW_{out} = \min(SW_{out})$ and $CS_{out} = 35.44$).
- In addition, the temperature field shows a hot spot close to System 3 for Case 7 and not for Case 10. In Case 11, System 1 is predicted to be under the influence of mainstream ($CS_{in} = 2.5$, $CS_{out} = -0.56$).
- The two other systems are not influenced by the flow, with System 3 being the furthest away from receiving any airflow ($CS_{in} = 28$). Thus, as seen in Figure 35, there is a hotspot near System 3.

3.3.5 Conclusion

In summary, Section 3.3 introduced the mainstream flow analysis to investigate ventilation aspects at the system level. New DN are explored to represent the mainstream effect. A preliminary set of DN, S_I , and S_2 was introduced. They were not suitable for ranking multiple systems. Also, they could not predict if the bounds of a system are located in the mainstream flow. Hence, the new CS and SW numbers were defined. These numbers were plotted against each other to map the area under the mainstream influence. A case study using multiple systems in a 2D aircraft bay was performed to demonstrate the mainstream flow prediction using these numbers. Finally, the velocity and temperature plots from the CFD results were used to validate these MS numbers.

Section 3.4 discusses how the existing TRA is updated with the mainstream flow analysis. Other system-level analyses are also discussed. The enhanced thermal risk scoring using these system-level analyses is presented at the end.

3.4 Updated Thermal Risk Assessment

This section discusses how the TRA, previously shown in Figure 4, in Section 2.3.1 and 2.4, is improved by the integration of the mainstream flow analysis. The scoring was developed in collaboration with Dr. Florian Sanchez. As a reminder, the TRA uses an approach based on penalty points. High scores correspond to unfavorable configurations (higher thermal risk) and, lower scores correspond to favorable configurations (lower thermal risk). The thermal risk scoring workflow is discussed next.

3.4.1 Thermal Risk Scoring Workflow with Mainstream Flow Analysis

Thermal risk scoring is a conditional multiplicative process. Therefore, some analyses are only required depending on the results of prior analyses. In case one analysis step is skipped, its score is equal to one ($TR_{\text{skipped}} = 1$). The scoring begins with the ventilation analysis (TR_1). If forced or mixed ventilation is identified, mainstream flow analysis is considered (TR_3). The mainstream scoring procedure is followed as explained in 3.2.3. After the mainstream flow analysis, if a system is closest to the inlet, its temperature limit is compared to the inlet temperature and the environment ($TR_{4.1}$ and $TR_{4.3}$). In other cases, the system's limit temperature is compared to the bay walls and the environment ($TR_{4.2}$ and $TR_{4.3}$). The next steps involve the system integration scoring (TR_5) and the heat removal potential scoring (TR_6). Finally, the system's radiation heat transfer to the walls is checked if only the walls exceed the system's temperature limit (TR_7).

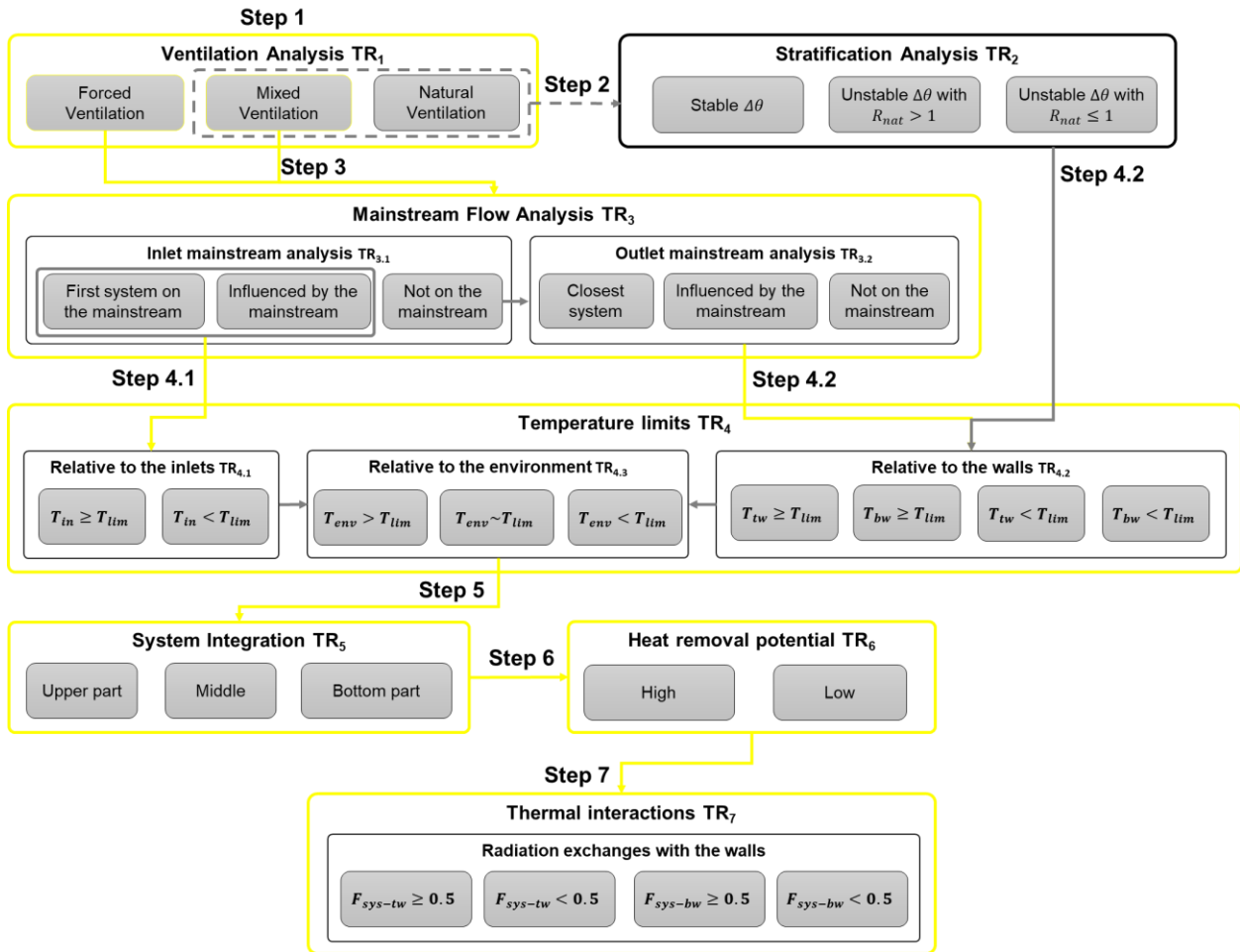


Figure 36: Flowchart for the thermal risk scoring with mainstream flow analysis; the steps to be followed are highlighted in yellow.

The final thermal risk score combines the scores from each of these individual analyses listed in Table 8. The scoring starts with assessing the ventilation state of the aircraft bay discussed in the following section

Table 8: Thermal risk scores for all modules.

Thermal risk assessment parameter	Score	Thermal risk assessment parameter	Score
Ventilation analysis	TR₁	Temperature stratification analysis	TR₂
Natural convection: $Ri_\varphi \gg 1$	3	Unstable thermal gradient: $R_{nat} \leq 1$	3
Mixed convection: $Ri_\varphi \sim 1$	2	Unstable thermal gradient: $R_{nat} > 1$	2
Forced convection: $Ri_\varphi \ll 1$	1	Stable thermal gradient	1
Mainstream flow analysis		TR₃	
Mainstream analysis relative to an inlet	TR_{3.1}	Mainstream analysis relative to an outlet	TR_{3.2}
Cross-stream Far from the mainstream: $CS_{in} > 10$	3	Cross-stream Far from the mainstream: $CS_{out} > 10$	3
Close to the mainstream: $CS_{in} \leq 10$	1.5	Close to the mainstream: $CS_{out} \leq 10$	2
On the mainstream: $CS_{in} \leq 0$	1	On the mainstream: $CS_{out} \leq 0$	1.5
Streamwise Farthest systems: $SW_{in} > \text{mean} SW_{in} $	2	Streamwise Farthest systems: $SW_{out} > \text{mean} SW_{out} $	2.5
Closest systems: $SW_{in} \leq \text{mean} SW_{in} $	1.5	Closest systems: $SW_{out} \leq \text{mean} SW_{out} $	2
First system: $SW_{in} = \text{min} SW_{in} $	1	First system: $SW_{out} = \text{min} SW_{out} $	1.5
System integration	TR₅	Temperature limits	TR₄
Top of the bay: $Y_{sys}/H_b \sim 1$	3	Relative to an inlet	TR_{4.1}
Middle of the bay: $Y_{sys}/H_b \sim 0.5$	2	Hot inlet: $T_{in}/T_{lim} \geq 1$	2
Bottom of the bay: $Y_{sys}/H_b \ll 1$	1	Cold inlet: $T_{in}/T_{lim} < 1$	1
Heat removal potential	TR₆	Relative to the bay	TR_{4.2}
High: $HR < 1$	HR	Hot bottom wall: $T_{bw}/T_{lim} > 1$	2
Low: $HR \geq 1$	1	Hot top wall: $T_{tw}/T_{lim} > 1$	
Thermal interactions	TR₇	Cold bottom wall: $T_{bw}/T_{lim} < 1$	1
Wall to system radiations (only if $TR_{4.2} > 1$)		Cold top wall: $T_{tw}/T_{lim} < 1$	
$F_{sys-tw} \geq 0.5$		Relative to the environment	TR_{4.3}
$F_{sys-bw} \geq 0.5$	2	Hot environment: $T_{env}/T_{lim} > 1$	3
$F_{sys-tw} < 0.5$		Warm environment: $T_{env}/T_{lim} \sim 1$	2
$F_{sys-bw} < 0.5$	1	Cold environment: $T_{env}/T_{lim} < 1$	1
Total thermal risk score		$TR_{tot} = f(TR_1, TR_2, TR_3, TR_4, TR_5, TR_6, TR_7)$	
Low risk		$TR_{tot} < 5$	
Medium risk		$5 \leq TR_{tot} \leq 9$	
High risk		$TR_{tot} > 9$	

3.4.2 Ventilation Analysis Scoring (TR₁)

A forced ventilation condition is favorable for cooling of the bay compared to natural ventilation conditions. The scoring for this analysis is listed in Table 8 (TR₁).

The lowest score (most favorable) is attached to a forced ventilation condition. The flow is strong, and thus, the rate of heat transfer is higher when compared to mixed/natural ventilation. The highest score (least favorable) is thus assigned to the natural ventilation condition. With a flow that is weak, the rate of heat transfer is lower.

The next step is the temperature stratification analysis. In cases of forced ventilation ($Ri \ll 1$), this step is skipped (TR_{skipped} = 1). Temperature stratification is analyzed only in the cases of mixed or natural ventilation.

3.4.3 Temperature Stratification Analysis Scoring (TR₂)

Temperature stratification analysis is the next step of thermal risk assessment. From Table 8, the least desirable condition is when there is an unstable thermal gradient which is driven by heat loads. As seen in 2.3.1, this may result in the formation of a potential hot zone with little flow reaching it. The most desirable condition is when the thermal gradient is stable and thus allows for better mixing of the flow in the bay.

This analysis is done in cases of mixed/natural ventilation only. In cases of forced convection, the strong flow of cooling air would dominate the thermal gradient formed in the bay. In cases of natural/mixed ventilation, the heat loads and/or the temperature difference between the walls influence this phenomenon.

System-level analyses are performed after this step, starting with the mainstream flow analysis.

3.4.4 Mainstream Flow Analysis Scoring (TR₃)

Mainstream flow analysis is a system-level analysis performed to assess the influence of the mainstream flow on a system. This step is the third step in the thermal risk scoring process. Mainstream flow analysis is only done in the cases of forced or mixed ventilation, as discussed in 2.4.1. The analysis results in *MS* numbers, specifically the cross-stream (*CS*) and the streamwise (*SW*) number. The mainstream scores are calculated using the values of these numbers. *MS* numbers depend on whether the ventilation source is an inlet or an outlet. Thus, that is considered while deriving the scores for this analysis.

The idea behind each individual score is to penalize unfavorable situations. The score must also fit with the grand scheme of thermal risk assessment. Thus, the most favorable situation will have the least score. In the case of mainstream flow analysis, the least score possible is 1, with each number (*CS* and *SW*) being given its own weightage. Straying from this perfect scenario results in doubling, tripling of the *MS* scores. This makes the *MS* scoring and the overall conservative. This tightens the constraints and thus allows for a much safer system-bay configuration from a thermal risk point. Table 8 shows the *MS* scoring module. It also lists scores of each individual *MS* number.

Mainstream scoring follows the logic shown in Figure 37.

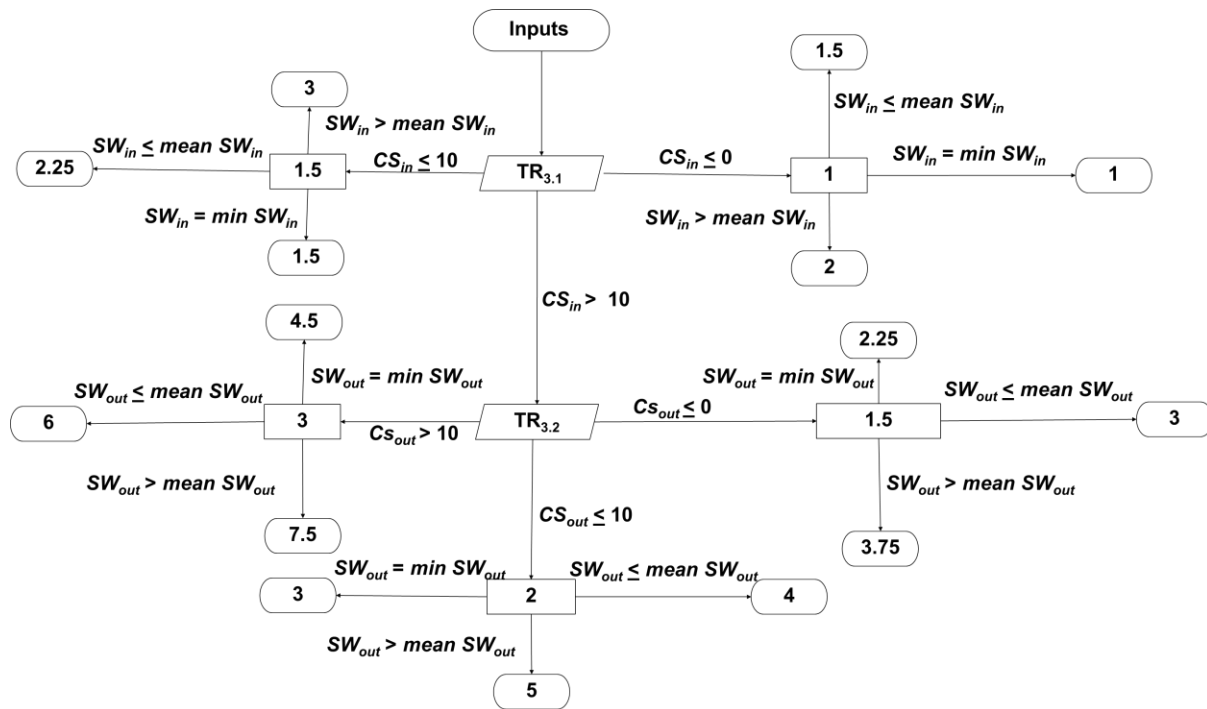


Figure 37: The MS scoring flowchart. The logic of scoring is shown along with each possible score.

For each system, the following steps are followed:

1. Calculation of the CS and SW numbers with the inlet(s). Each number has its own scoring ($TR_{3,1}$). The final MS score involves multiplying these scores if the following conditions are met.
2. If CS_{in} in all the dimensions ($CS_{in(x)}$, $CS_{in(y)}$, and $CS_{in(z)}$) is less than 10, meaning that the system is under the partial influence of the mainstream, the following steps are taken:
 - a. If $CS_{in} \leq 0$, this means the system is under a strong influence of the mainstream and thus is initially given the lowest score (1).
 - b. If $0 < CS_{in} \leq 10$, this means the system is under a weak or a partial influence of the mainstream and is given the second-lowest score (1.5). This value is multiplied by the corresponding SW scores. The result is the final MS score.
 - c. If $CS_{in} > 10$, this means the system is not influenced by the inlet, and thus CS numbers from the outlet ($TR_{3,2}$) are used for its MS scores.
3. SW_{in} scores depend on the SW_{in} numbers.
 - a. If the system is nearest to the inlet ($SW_{in} = minSW_{in}$), it is given the least score (1). This value is multiplied by the corresponding CS_{in} scores. The result is the final MS score.

- b. If the system is far away from the inlet ($SW_{in} > meanSW_{in}$), it is given the highest score (2). This value is multiplied by the corresponding CS_{in} scores. The result is the final MS score.
- c. If the system lies somewhere in between ($SW_{in} \leq meanSW_{in}$), it is given the median score (1.5). This value is multiplied by the corresponding CS_{in} scores. The result is the final MS score.

The same procedure is used for scoring MS scoring with respect to the outlet. (TR3_{3.2}). However, the scores assigned to the outlet are different and higher than for the inlet. This is because the fresher cold air coming from the inlet makes it a favorable ventilation source from a thermal risk point of view.

If multiple ventilation sources are present in a bay, then the source that results in the least MS score is the one selected for MS scoring. After the mainstream flow analysis scoring, system temperature limits scoring is done. The next section discusses this in detail.

3.4.5 Temperature Limits Scoring (TR4)

The temperature limits analysis compares the temperatures of the inlet (T_{in}), the bay walls (T_{top} , T_{bot}), and the ambient environment (T_{env}) to the system limit temperature (T_{lim}). The scoring for this module depends on the temperature ratios.

This step is used to check whether a particular temperature (inlet, walls, environment) exceeds the maximum admissible system temperatures (temperature limit). If yes, this adds to the overall thermal risk. The temperature limit scoring is shown in Table 8. If the system is closest to the inlet, then its limit temperature (T_{lim}) is compared to the inlet temperature (T_{in}) and the ambient environment temperature (T_{env}) shown by steps TR4.1 and TR4.3. In other cases, its limit temperature (T_{lim}) is compared to the bay walls temperatures (T_{bot} , T_{top}) and the ambient environment temperature (T_{env}) shown by steps TR4.2 and TR4.3. Temperatures lower than the system limit temperature are desired and thus given a score of 1.

The next step discussed is to score the system on its vertical location in the bay.

3.4.6 System Integration Scoring (TR5).

The system integration scoring follows from the system integration analysis discussed in state-of-the-art. The vertical location of the system (Y_{sys}) is compared to the height of the aircraft bay (H_{bay}). The system at the top ($Y_{sys} / H_{bay} \approx 1$) receives hotter lower density air arising from the bottom and thus is penalized and given a higher risk score. Table 8 shows the system integration scoring. The next section discusses the heat removal potential scoring.

3.4.7 Heat Removal Potential Scoring (TR6).

As discussed in 2.4.2, heat removal potential discusses the performance of a ventilation source with respect to a system. A lower HR means a higher heat removal potential. Table 8 shows the heat removal potential scoring in TR6.

The score depends on the HR number and is split into two conditions, recall Eq. (7);

1. When $HR < 1$, the advection capacity is greater than the combined heat loads of the systems ventilated, this is a desirable outcome. Thus, the score is the HR number itself.
2. When $HR \geq 1$, the advection capacity is lower than the combined heat loads of the systems ventilated. Thus, the score given is 1.

The final step of the enhanced risk scoring is the thermal interactions scoring, which is discussed next.

3.4.8 Thermal Interaction Scoring (TR₇)

The system to wall radiations has already been discussed in 2.3.1. When the view factor (V.F) between a system and the bay wall is high ($F_{sys-tw}, F_{sys-bw} \geq 0.5$), radiation heat transfer between them is significant. This step of the scoring is used only if the temperature of these walls is greater than the system limit temperature ($TR_{4.2} = 2$). Thus, if V.F between the systems and the walls is high, it is scored higher on the risk scale, as shown in. This step concludes all the risk scoring steps of the enhanced thermal risk scoring.

In the end, all the individual scores discussed above are multiplied ($TR_1 * TR_3 * TR_4 * \dots$). The final thermal risk score is compared to the thermal risk scale given in Table 8. A total thermal risk score of less than 5 indicates low thermal risk. Medium thermal risk includes risk scores between 5 and 9. A score higher than 9 indicates a high thermal risk.

Thus, an enhanced thermal risk scoring method is presented. It includes all the analyses previously considered and includes mainstream flow and heat removal potential analyses.

3.5 Conclusion

The updated thermal risk assessment was introduced. Thus, using limited inputs at the conceptual design stage and with the help of dimensionless numbers, the thermal risk of an aircraft system can be predicted.

Now, this updated TRA is applied on real-world aircraft bays. These bays form the 3rd and the last level of complexity discussed in Section 3.1.1. The aircraft bays are in 3D with multiple systems and multiple ventilation sources. Thermal risk is predicted for each system in these bays and compared with the CFD results. Results are discussed and conclusions drawn from them.

4 Application of the Updated Thermal Risk Assessment on Aircraft Equipment Bays

This chapter discusses the application of the updated thermal risk assessment (TRA) in two case studies for complex aircraft equipment bays, further validating the improved TRA, as introduced in Chapter 3. Figure 38 shows the configurations of the studied avionics bays and their potential locations inside an aircraft.

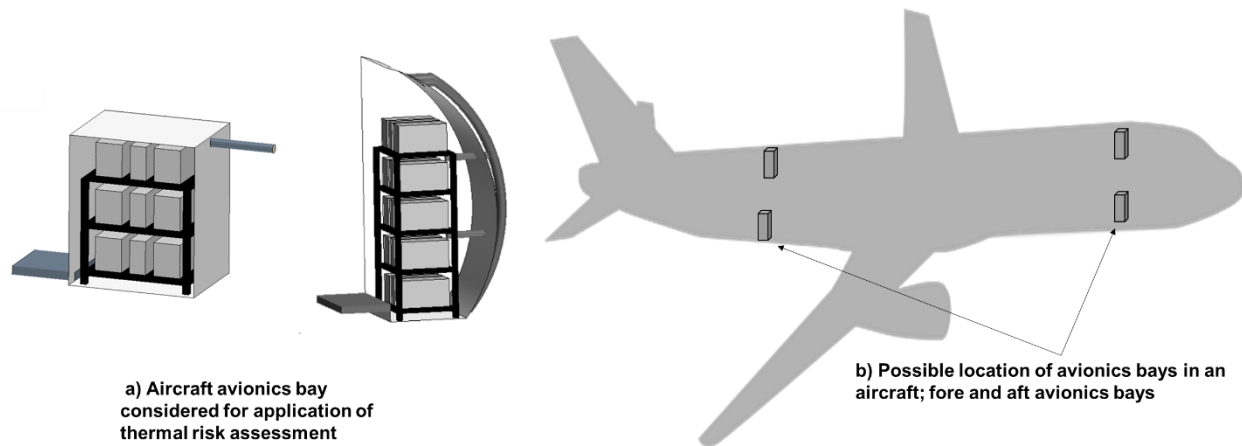


Figure 38: Configurations of the aircraft equipment bays considered and their possible locations inside an aircraft seen from a side view.

Section 4.1 provides background on aircraft avionics and their thermal constraints. Section 4.2 applies the updated TRA on a 3D avionics bay with multiple systems and a single outlet, and section 4.3 covers the most complex case study, an avionics bay with multiple systems and multiple outlets.

The two avionics rack configurations covered in this section represent real aircraft equipment bays, as defined in the SAE AIR [43]. The mainstream flow influence is analyzed for each system in the racks. The case studies also act as validation; the thermal risk assessed by the approach is validated against the CFD results of these studies.

The validation compares the thermal risk (low, medium, and high) predicted from the TRA with an equivalent risk from the CFD results. This equivalent risk is derived by extracting the average ambient temperature of each system from the CFD results. The ambient zone represents the zone where a temperature probe is inserted to record the system temperature [9]. Figure 39 is a schematic illustrating the ambient zone in which the temperature probe is inserted for recording the temperature.

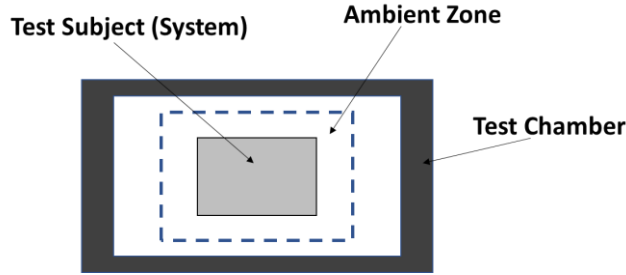


Figure 39: Schematic of a test chamber for thermal testing for aircraft systems; the temperature probes are inserted in the ambient zone.

The ambient temperatures of the system are compared to the system limit temperatures (in this chapter, the highest temperatures at which a system can operate [9]). This comparison leads to the following proposal for the classification of the thermal risk:

- Low risk: $T_{sys} < 0.95 T_{lim}$;
- Medium risk: $0.95 T_{lim} \lesssim T_{sys} \lesssim 1.05 T_{lim}$;
- High risk: $T_{sys} > 1.05 T_{lim}$

A medium-risk within 5% of the temperature limit of the system is defined. Usually, a much more detailed analysis is required in the cases of medium thermal risk.

The systems used in this chapter are aircraft avionics. The next section details how the characteristics of avionics systems with respect to their thermal requirements.

4.1 Aircraft Avionics and Their Thermal Management

Aircraft avionics have been around since World War II. Initially developed for the military, early uses of avionics were in the field of navigation (radar). The introduction of transistors in the 1950s and 60s saw a step towards the digitalization of other aircraft systems, starting with engine and flight controls. Digital aircraft systems would then come into existence in the 1970s primarily for military uses (navigation, attack systems). With the advent of Full Authority Digital Engine Control (FADEC), engine control would be fully digitized in the 70s. Since 1980 digital avionics technology has been increasingly used, replacing both electrical/mechanical control. Modern aircraft like Boeing 777 and Airbus A380 use fully digital flight control with electrical backups. In modern times avionics are widely used in the control of all aircraft systems, such as fuel, electrical, landing gear, environmental, or flight control systems[62]. Therefore, the amount of individual avionics boxes, so-called Line Replaceable Units (LRU), has increased significantly. Their dimensions are standardized according to the Modular Concept Unit (MCU) [62,63].

The MCUs have various environmental constraints to consider, such as electromagnetic interference, temperature fluctuations, humidity, pressure, and vibration. The thermal characteristics of these systems, such as ventilation conditions and system heat loads, are derived from the requirements set by avionics installation standards [64] and from the manufacturer datasheets [61].

In the absence of specification, a system's maximum allowable heat load can be attributed directly to its size [64]. Table 9 shows the maximum permissible heat dissipation with and without a forced

ventilation system. The system heat loads and dimensions considered for these case studies are derived from the manufacturer datasheets [61].

Table 9: The maximum allowed heat dissipation with and without cooling air for a given size of the avionics system [64].

LRU size (MCU)	Maximum LRU heat load (Watts)	
	With cooling air	Without cooling air
2	250	10
3	375	12
4	500	15
5	625	17
6	750	20
7	875	22
8	1000	25
9	1125	27
10	1250	30
11	1375	32
12	1500	35

The DO-160 [9] provides the methods on how to test for system compliance. It includes testing for both survival and operating temperatures. Multiple tests are designed for different types of equipment, ranging from pressurized systems, unpressurized systems, systems under partial temperature control, and systems under full temperature control. The tests replicate the ventilation configurations used for these avionics racks [9]. Avionics installation standards also define the cooling air characteristics required for forced cooling of these racks. The mass flow rate of inlet air is required to be at least 3 lbs/min for every kilowatt (kW) of heat dissipated by all the systems combined. The maximum coolant temperature is also outlined [64]. Thus, designers should stick to these ranges when opting for a forced cooled strategy for their avionics racks.

Using the ventilation conditions discussed above, the updated TRA is applied to the first aircraft equipment bay in the next section.

4.2 Aircraft Avionics Bay with Multiple Systems and a Single Inlet/Outlet Configuration

In this section, a 3D model of an aircraft equipment bay with multiple systems is used for the application of the updated TRA. There is a further increase in complexity (see Table 3) from earlier case studies, with the mainstream flow being analyzed in all dimensions. The equipment bay, supporting racks, and the systems are all derived from a real-world equipment bay [43]. Their dimensions and flow parameters are yet again derived from the standards [43,61,64]. The goals of this case study are:

- Mainstream flow analysis in 3D
- *MS* numbers in 3D and their comparisons among the different systems

- Application of the updated TRA on a real-world aircraft equipment bay
- Predicting thermal risk for each system and ranking them from low to high risk

The CFD simulation of this real-world model is used as a validation for both the mainstream flow analysis and the thermal risk predictions by the updated TRA. It is used for the following:

- Visualization of the mainstream in 3D
- Validation of the *CS* and *SW* predictions
- Validation of the thermal risk predictions

4.2.1 Description of the Configuration

The avionics rack consists of nine avionic boxes (called System 1-9). The size of these systems is based on the sizing standards set by ARINC [62]. The characteristics of these systems are defined based on an avionics manufacturer’s datasheet [61]. Their sizes are the so-called 3 MCU and 5 MCU. Figure 40 shows the dimensions and their heat loads derived from the same datasheet [61].

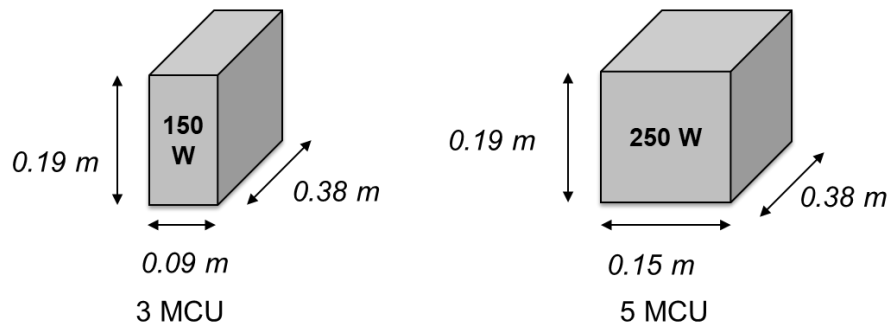


Figure 40: MCUs and their dimensions.

These systems are mounted on a supporting rack and are connected via ARINC 600 connectors [61]. Generally, in conceptual design, the connectors and the wiring are not considered. Thus, they are not modeled in the case studies. The supporting racks have holes that act as individual air inlets for each system (Figure 41).

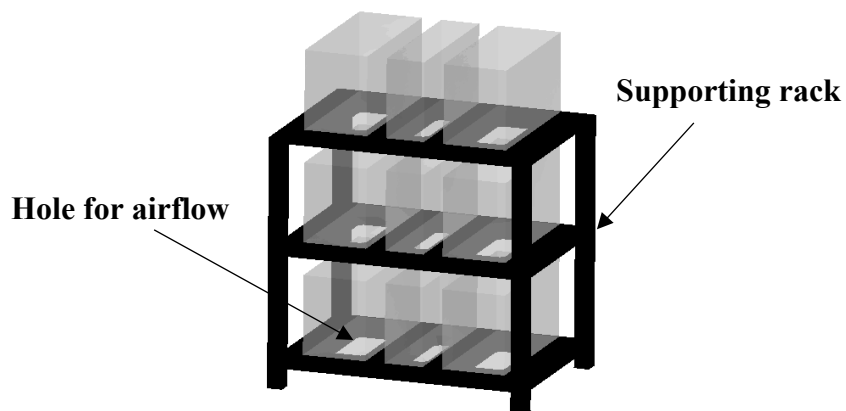


Figure 41: Supporting rack modeled for supporting the systems (translucent).

The bay that houses the avionics rack has an inlet at the bottom and an outlet at the top. The inlet is rectangular and provides airflow from the cabin exhaust. The suction created by the fan in the outlet drives the ventilation system. The exhaust from the outlet is then recirculated back to the air-conditioning system of the aircraft. Figure 42 shows the 3D geometrical configuration of the CFD model.

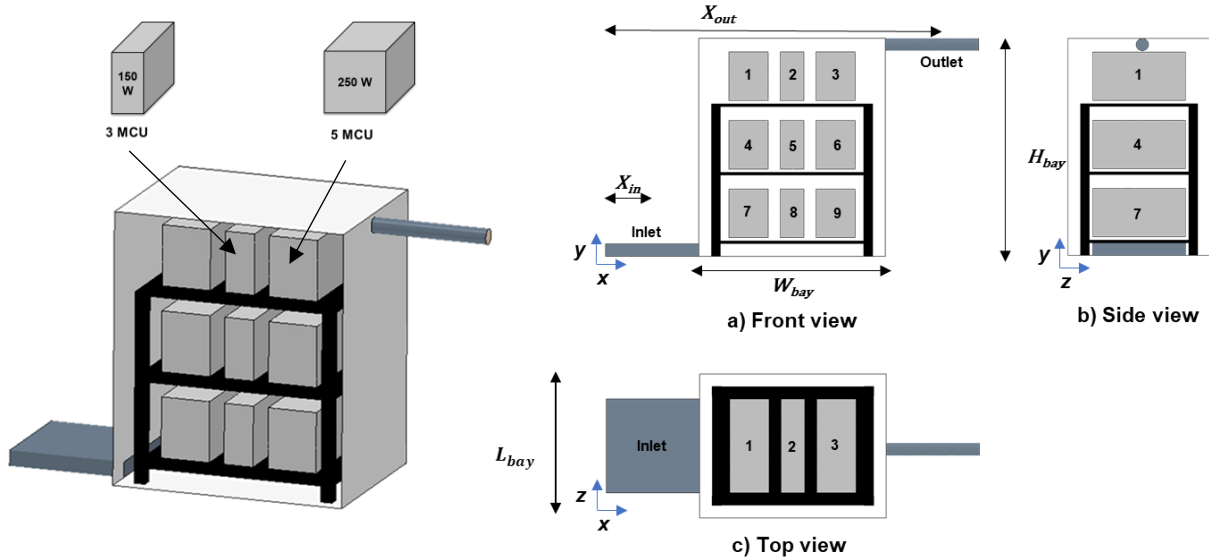


Figure 42: 3D Model of the avionics bay and the three-view representation with the associated geometrical parameters shown.

As in Chapter 3, the 3D model of the rack with the systems and the bay is constructed in STAR-CCM+. A steady-state CFD simulation is performed for the validation of both mainstream flow analysis and the overall thermal risk. Again, STARCCM+ is used as the CFD software. The simulation assumes the following:

- Two regions used; fluid (bay, system surfaces, inlet, and outlet) and solid (supporting rack)
- Air modeled as an incompressible and ideal gas
- Gravity present and acting in the negative Y-axis
- Radiation heat transfer considered
- Stagnation inlet boundary at the inlet opening
- Negative mass flow inlet boundary at the outlet

The mesh contains around 1,000,000 cells and uses polyhedral elements. The software uses *Prism Layer* cells (same as in Chapter 3) for solving the boundary layer flow. Figure 43 shows the mesh in the XY plane. *Prism Layer* cells can be seen near the wall boundaries.

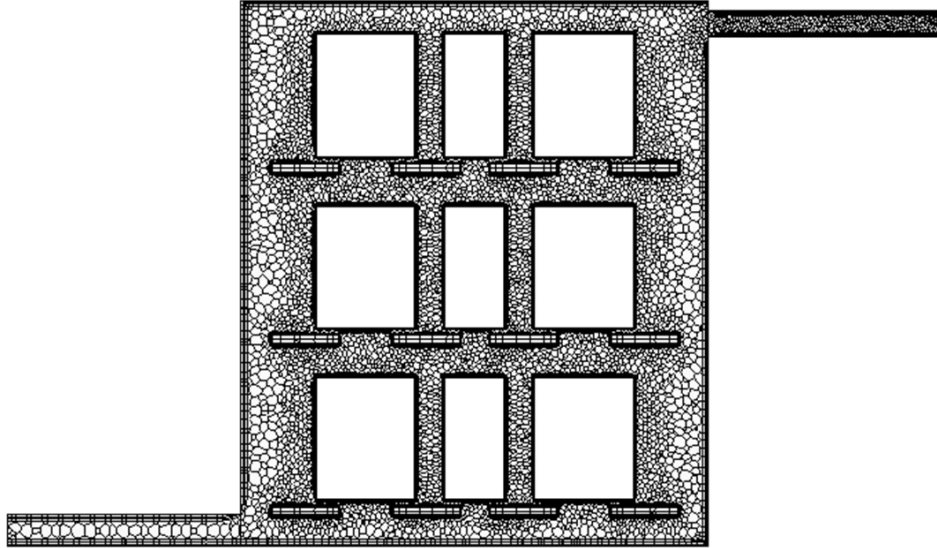


Figure 43: Mesh plane of the avionics bay in the front view, prism layers seen near the walls.

The boundary conditions for both the prediction and the CFD study are derived from the most critical operating case on the ground:

- The highest Outside Air Temperature (OAT) an aircraft may experience could go up to 55°C [3]. An aircraft parked on the runway during a hot day in areas like Dubai would experience this condition.
- The top wall temperature ($T_{top} = 50^{\circ}\text{C}$) of the bay is set close to this OAT, assuming insulation between the fuselage skin and the bay.
- The bottom wall temperature ($T_{bot} = 30^{\circ}\text{C}$) is much lower and set close to the inlet temperature. Other walls of the bay are considered adiabatic. The avionics bay is located within the aircraft. Thus, the wall temperatures would not be as high as the OAT.
- The temperature of the air-inlet ($T_{in} = 27^{\circ}\text{C}$) is derived from the avionics installation standards. In case of forced cooling, cabin exhaust acts as the inlet air [64].
- The mass-flow rate for the air-inlet is derived from SAE-AIR [43].

These boundary conditions and other geometrical parameters are listed in Table II in the Appendix. A segregated flow-energy solver with SST $k-\omega$ turbulence model is selected [65]. The solution achieves convergence within 5000 iterations.

The next section describes and discusses the mainstream flow analysis conducted on this case study.

4.2.2 Mainstream Flow Analysis

This section discusses the mainstream flow prediction using mainstream numbers and comparison with the CFD results. In the mainstream flow prediction, Cross-stream (CS) and streamwise (SW)

numbers are listed for each system. A mainstream mapping illustrates whether a system lies on the mainstream. The next part discusses the CFD results. The mainstream is visualized using the CFD results, allowing comparison of the prediction.

The geometrical parameters of the avionics bay are listed in Table II. Using the mainstream scoring method presented in 3.4.4, a mainstream score is assigned to each system in the rack. The mainstream scores are listed in Table 10 below, along with the CS and SW numbers of each system. The avionics rack is symmetrical in the Z -axis (lengthwise). Thus, the MS numbers in the Z -axis are neglected.

Table 10: Mainstream numbers for each system with respect to the inlet and outlet.

System	Mainstream Score	Inlet		Outlet	
		CS_{in} (y)	SW_{in} (x)	CS_{out} (y)	SW_{out} (x)
System 1	5	46.94	0.31	1.14	0.42
System 2	5	46.94	0.86	1.14	0.29
System 3	3	46.94	1.26	1.14	0.10
System 4	7.5	16.37	0.31	16.07	0.42
System 5	7.5	16.37	0.86	16.07	0.29
System 6	4.5	16.37	1.26	16.07	0.10
System 7	1.5	1.24	0.31	46.43	0.42
System 8	3	1.24	0.86	46.43	0.29
System 9	3	1.24	1.26	46.43	0.10

The mainstream mapping is shown in Figure 44, illustrating the mainstream influences of the inlet and outlet. The following observations can be made:

- System 7 has the lowest mainstream score ($MS = 1.5$) of all the systems. It has the lowest cross-stream ($CS_{in} = 1.24$) and streamwise ($SW_{in} = 0.31$) numbers with regards to the inlet. Thus, it lies closest to the inlet.
- Systems 3, 6, and 9 have the next lowest mainstream scores ($MS = 3$). System 3 lies closest to the outlet. Thus, it has the lowest cross-stream ($CS_{out} = 1.14$) and streamwise ($SW_{out} = 0.1$) numbers concerning the outlet.
- The precedence of inlet over outlet can be seen in the MS scores of Systems 7 and 3. Although both systems are closest to the inlet and outlet, the system closer to the inlet has a favorable scoring on the MS scale.
- Systems 8 and 9 have the lowest cross-stream numbers ($CS_{in} = 1.24$). Thus, they are closest to the inlet vertically (cross-stream). As seen in the mapping, both systems are farther from the inlet in the stream-wise direction ($SW_{in} > meanSW_{in}$). This is the reason both have an equal MS score.
- Similar conclusions can be drawn for Systems 1 and 2, respectively, but from the outlet's perspective.

- Systems 4 and 5 have the highest MS score. Both systems are neither under the influence of the inlet ($CS_{in} > 10$) nor the outlet ($CS_{out} > 10$). System 6 ($MS = 4.5$) is closest to the outlet in stream-wise direction ($SW_{out} = 0.1$).

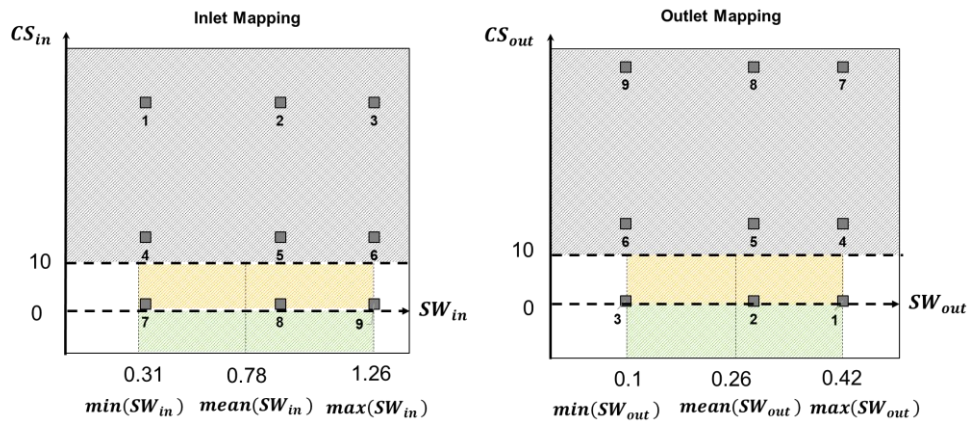


Figure 44: Mainstream numbers mapping for Systems 1 to 9: the grey shaded area is not under the mainstream influence, the area under the partial influence is yellow, and the area with considerable mainstream influence is in green.

The MS scores concerning the inlet are lower than the scores concerning the outlet. This is because there is a bigger chance to be cooled by the inlet compared to the outlet.

Streamlines are used to visually represent the mainstream for the avionics bay. The closeness of the systems to this mainstream can be compared and cross-checked with the various mainstream numbers assigned to each.

Figure 45 shows the mainstream in the form of streamlines evolving from the inlet and exiting towards the outlet. The velocity of the mainstream is normalized with the inlet flow velocity ($V_{in} = 2.2 \text{ m/s}$). Most of the flow moves along the avionics bay's bottom wall and then along the wall towards the outlet side before exiting through the outlet. Systems far away from the mainstream have very low-speed flow around them ($V < 0.5 \text{ m/s}$).

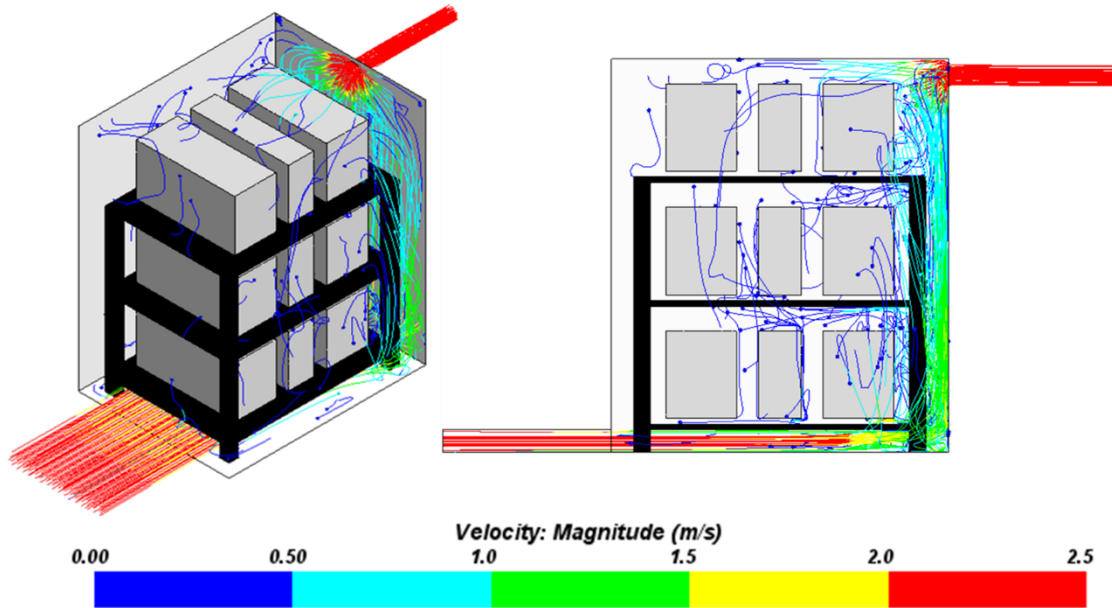


Figure 45: Velocity streamlines normalized with inlet flow speed. The mainstream flow moves along the bottom and right walls towards the outlet.

Figure 46 shows the velocity field in front and top views. The following observations are made:

- Systems 1, 2, and 3 are indeed farthest ($CS_{in} = 46.94$) from the inlet mainstream in a cross-stream direction.
- Systems 7, 8, and 9, as predicted, are closest to the mainstream in the cross-stream direction ($CS_{in} = 1.24$).
- In the streamwise direction, indeed, Systems 3, 6, and 9 are closest to the mainstream ($SW_{out} = 0.1$) with regards to the outlet, as shown in the top view of Figure 46; they are influenced by the flow near the outlet wall.
- System 2 ($CS_{out} = 1.14$) receives some mainstream flow as it exits through the outlet.
- System 3 is, as predicted, influenced in both the streamwise and cross-stream directions as the flow exits.
- The flow from the inlet first influences System 7 ($SW_{in} = \min SW_{in}$), then slows down as it reaches System 9 ($SW_{in} = \max SW_{in}$).
- Systems 4 and 5 have the highest MS scores ($MS = 7.5$). These systems, along with System 1 ($MS = 5$), have the lowest flow circulation around them.
- System 7 ($MS = 1.5$), as predicted, is the first system impacted by the flow, being closest to the inlet.
- Systems 3, 8, and 9 have the same mainstream scoring ($MS = 3$). Although System 3 lies much closer to the mainstream than Systems 8 and 9, it being near the outlet (receiving hotter flow) puts it on par with the latter systems on the mainstream scoring.

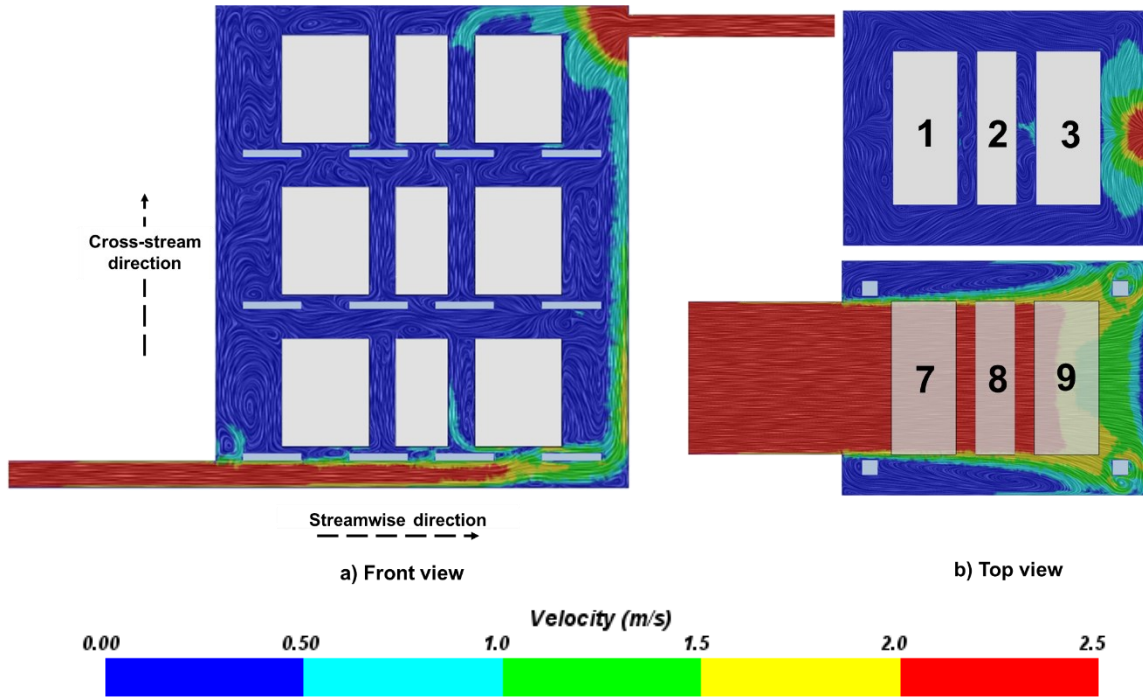


Figure 46: Velocity plots along different section planes in the front and top views; Systems far away from the mainstream experience very little flow.

The next step involves combining these *MS* scores with the rest of the scores from the enhanced risk scoring to give an overall thermal risk score. Predicting this thermal risk and then validation using CFD results is carried out in the next section.

4.2.3 Thermal Risk Prediction and Comparison with CFD

This section discusses the thermal risk scoring for the case study. The enhanced thermal risk scoring is given in Chapter 3, which details the workflow of thermal risk scoring with the mainstream flow analysis. Table 11 lists the thermal risk for each system. Scores for individual analyses are also listed. Using the Richardson number ($Ri < 1$), the ventilation scores of each system are given ($TR_1 = 1$). The stratification scores ($TR_2 = 1$) also follow the reasoning above. Systems 1, 2, and 3 lie in the top half of the bay, and thus their system integration scores ($TR_4 = 3$) are the highest. On the contrary, Systems 7, 8, and 9 have the lowest system integration scores ($TR_4 = 1$). The walls and the inlet are under the set temperature limit ($T_{lim} = 70^\circ \text{C}$); thus, the temperature limits score is unity for all systems ($TR_5 = 1$)

Table 11: Thermal risk assessment for Systems 1 to 9; scores listed for all the conducted analyses.

System	Ventilation TR ₁	Stratification TR ₂	Mainstream TR ₃	System Integration TR ₄	Temperature Limits TR ₅	Heat Removal Potential TR ₆	Thermal Risk Score	Thermal Risk
System 1	1	1	5	3	1	1	15	High
System 2	1	1	5	3	1	1	15	High
System 3	1	1	3	3	1	1	9	Medium
System 4	1	1	7.5	2	1	0.24	3.6	Low
System 5	1	1	7.5	2	1	1	15	High
System 6	1	1	4.5	2	1	1	9	Medium
System 7	1	1	1.5	1	1	0.24	0.4	Low
System 8	1	1	3	1	1	0.24	0.7	Low
System 9	1	1	3	1	1	1	3	Low

From Table 11, the following observations can be made:

- Systems 1, 2, and 5 are at high risk.
 - Systems 1 and 2 are at the top of the bay (TR₄ = 3), which puts them at high thermal risk.
 - System 5, being in the middle and not being influenced by either inlet/outlet, is predicted to be also at high thermal risk.
- Systems 3 and 6 are predicted to carry a medium thermal risk.
 - System 3 is nearest to the outlet, and even though it has a higher system integration score (3), its *MS* score is lower. Thus it is at medium risk.
 - System 6 lies close to the outlet in the streamwise direction, and its system integration score is neither high nor low, thus placing it in the medium thermal risk.
- Low thermal risk is attached to Systems 4, 7, 8, and 9.
 - Mainstream scores for Systems 7, 8, and 9 are the lowest, meaning they are under the strongest influence of the inlet flow.
 - Although System 4 has a higher *MS* score, it is predicted to be at a lower risk as its heat removal potential is high (TR₆ = 0.24). This means that System 4 is grouped with the inlet flow and has a higher potential for heat removal.

Figure 47 shows the temperature plots of the CFD study. The following observations can be made:

- System surfaces closer to the mainstream (Systems 3, 6, 7, 8, and 9) are at a lower temperature
- Systems away from either inlet or outlet are higher in temperature (System 1)
- Systems closer to either the inlet (System 7) or the outlet (System 3) are cooler as they receive most of the airflow, either entering or exiting the bay

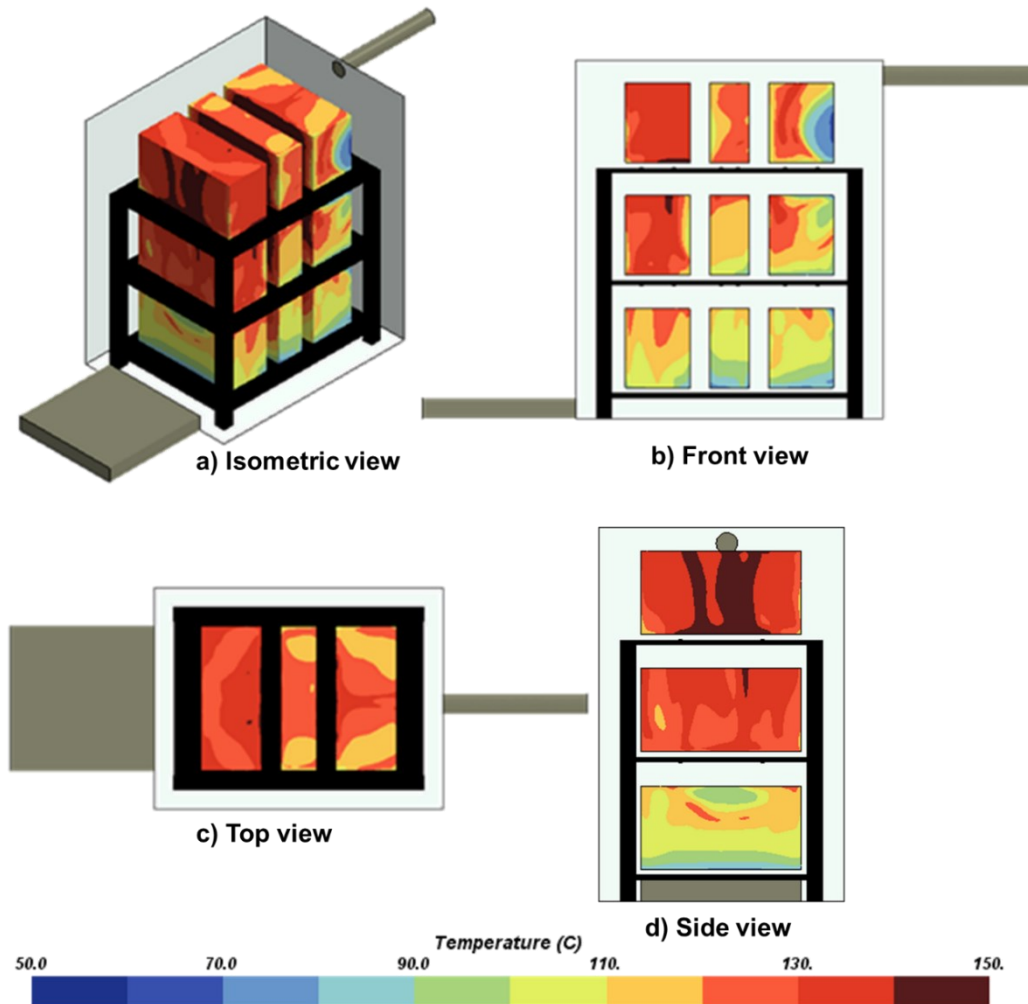


Figure 47 Temperatures of the systems from the CFD results in different views; surfaces of the systems closer to the mainstream are at lower temperatures.

Table 12 compares the thermal risk prediction and the CFD results for each system. The ambient zone temperatures of each system are also listed. The TRA correctly predicts the risk of Systems 1, 2, 5, 7, 8, and 9. However, the following deviations from the expected results can be observed:

- For System 6, the predicted risk is medium, whereas the CFD simulation indicates it to be at a lower risk. Figure 48 gives the temperature distribution of the bay in the front view. The region around System 6 is cooler than predicted as it experiences a large flow moving towards the exit. This occurs as the flow first moves quickly towards the wall opposite the inlet unhindered. When it reaches the wall, recirculation occurs (Figure 45), generating effective cooling for systems nearby (6 and 9). This flow effect cannot be accurately predicted as it is three-dimensional in nature.
- System 3 is predicted to be at a medium risk but is observed to be at high risk from the CFD. It is because the flow heats up as it approaches the system. Also, only the surfaces of the system close to the mainstream are cooler. The ambient temperatures which are

extracted from each system are averaged over the whole volume surrounding it and thus puts the system at a higher risk.

- In the case of System 4, although it is correctly predicted not to lie on the mainstream, the heat removal score it receives ($TR_6 = 0.27$) predicts it to be cooled by the inlet flow. The inlet flow does not interact with this system and thus puts it at high risk. The supporting rack does not allow for a strong flow to develop near System 4. Again, although its surfaces close to the inlet ($SW_{in} = \min SW_{in}$) are cooled by some flow, the surfaces away from the flow are much hotter, resulting in higher ambient temperatures (Figure 48).

Table 12: Comparison of thermal risk predictions and CFD results.

System	Thermal risk prediction		Thermal risk derived from CFD results	
	Thermal risk score	Thermal risk predicted	$T_{sys,env}$ ($^{\circ}C$)	Thermal risk derived from CFD
System 1	15	High	101	High
System 2	15	High	98	High
System 3	9	Medium	83	High
System 4	3.6	Low	84	High
System 5	15	High	78	High
System 6	9	Medium	64	Low
System 7	0.4	Low	64	Low
System 8	0.7	Low	59	Low
System 9	3	Low	53	Low

In summary, the TRA correctly predicts the risk of most of the systems. For Systems 3 and 6, a much-detailed analysis for medium thermal risk could result in a much more accurate prediction. System radiation effects are not yet investigated and are not part of this thesis. They may also play an effect in confined spaces with heat-generating bodies close to each other. The supporting rack of the avionics bay is not a part of the TRA. This means that the flow obstructions caused by it are not accounted for in the prediction.

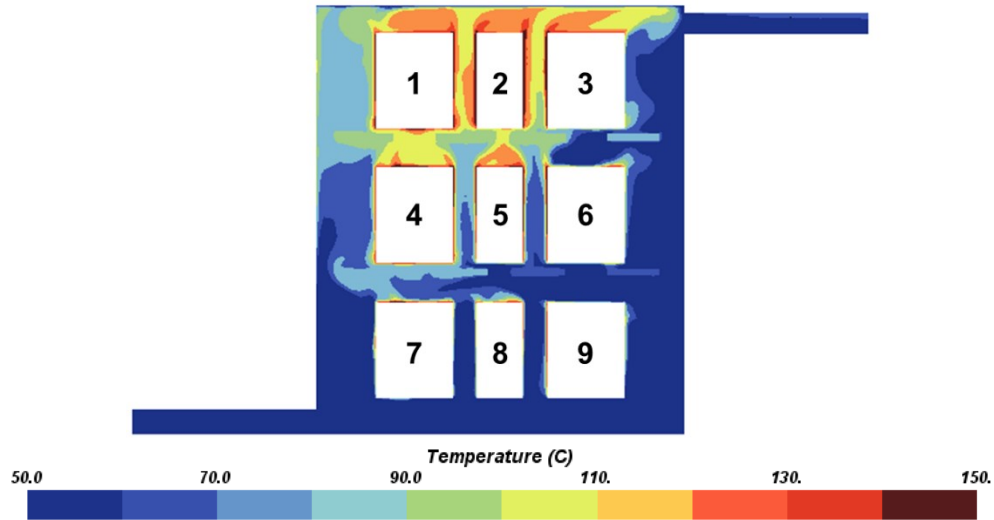


Figure 48: Temperature plot of the bay section in the front view; the regions close to the mainstream are shown cooler. Hotspots can be seen around System 4.

To conclude, this case study applied the updated TRA on a single inlet/outlet avionics bay with nine systems. The mainstream numbers *CS* and *SW* are predicted for each system, and the mainstream flow is visualized using the CFD. *CS* and *SW* predictions are validated with the velocity fields and streamlines. The CFD results agree with the predictions as they correctly predict the distance to the mainstream from each system. Overall, most of the system's thermal risks are predicted correctly by the method.

In the next case study, an even more complex avionics bay is investigated to demonstrate the capability to investigate various ventilation concepts. This avionics bay consists of multiple outlets. Updated TRA is applied on four different outlet configurations, and results are discussed.

4.3 Aircraft Avionics Rack with Multiple Systems and Multiple Outlets

The goals of this case study include:

- Investigation of the effects of multiple outlets on the mainstream flow
- Application of TRA on a complex shaped bay with multiple ventilation sources
- Comparison of different outlet configurations
 - The best ventilation configuration to be chosen among all

Thus, when *MS* numbers are predicted for each system, they are not only compared among each other but also with other design configurations. The CFD simulation is used for validation of the following aspects:

- Mainstream flow predictions with respect to multiple ventilation sources
- Thermal risk prediction for each system
- Capability to compare between different ventilation design configurations

4.3.1 Description of the Cases

The avionics bay used in this case study is illustrated in Figure 49 below and is typical for an avionic rack in smaller commercial or business aircraft. It consists of a rack with fifteen systems, one inlet, and three outlets. A suction fan is attached at the end of the main outlet pipe near the bottom of the bay. The aircraft's air-conditioning system recirculates the exhaust air. The inlet is shaped rectangular to represent a large opening for the cold air. Outlets are circular in cross-section. The inlet and outlets are based on the description provided in SAE-AIR [43]. The avionics bay, in this case, is curved in keeping with the fuselage shape [27,30]. Its dimensions are derived using the cabin dimensions of a Bombardier Global 7500 business jet [30,66]. The curved section is the bay top wall in this case study. All the other aspects of the avionics bay (supporting rack and systems.) are like the configuration in Section 4.2.

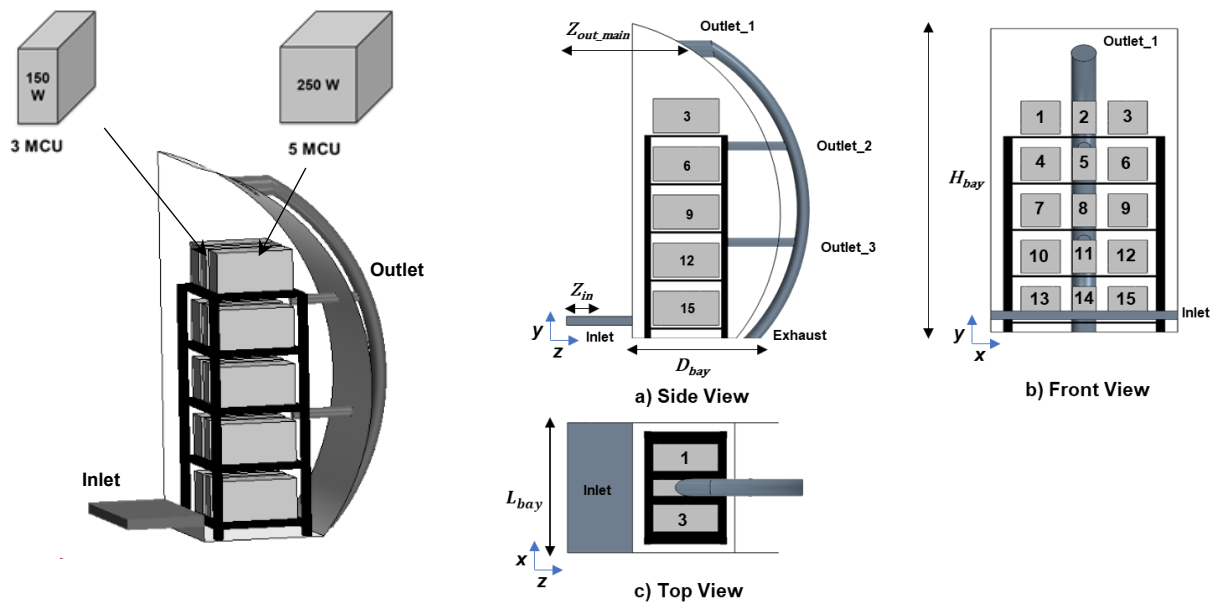


Figure 49: 3D Model of the aircraft avionics rack with multiple outlets and three-view representation with the geometrical parameters.

Four different cases can be derived from the original avionics bay. Each case has a different outlet configuration. A comparative study is done between these cases, discussing the mainstream flow analyses and the thermal risk for the systems in each case. Figure 50 gives the cases as seen in the side view.

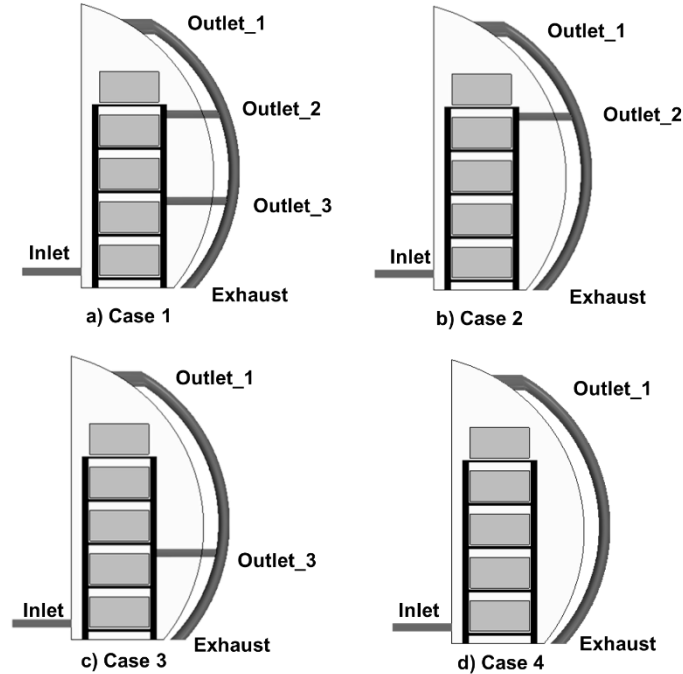


Figure 50: The different cases for which the TRA is applied are shown in the side view.

Similar to section 4.2, the 3D model of the rack with the systems and the bay is constructed in STAR-CCM+. A steady-state CFD simulation is performed for the validation of both mainstream flow analysis and the overall thermal risk. The simulation assumes the following:

- Two regions used; fluid (bay, system surfaces, inlet, and outlet) and solid (supporting rack)
- Air modeled as an incompressible and ideal gas
- Gravity present and acting in the negative Y-axis
- Radiation heat transfer considered
- Stagnation inlet boundary at the inlet opening
- Negative mass flow inlet boundary at the exhaust

The number of elements in each mesh for all four cases is given in Table 13. As in 4.2, polyhedral elements are used.

Table 13: Mesh cells generated for CFD model of each configuration.

Configuration	Case 1	Case 2	Case 3	Case 4
No. of mesh cells	771,726	751,716	757,426	732,697

The boundary conditions for this CFD study are the same as for Section 4.2.

- The aircraft is assumed to be parked on a runway on a very hot day. The bay top wall (curved section), the bottom wall, inlet, and ambient temperatures are the same as in Section 4.2.
- The mass flow rate of the air inlet is derived using SAE-AIR [43].

All the cases use the same boundary conditions. These boundary conditions are listed in detail in the Appendix (Table III). The solver and the turbulence model selected are the same as in Section 4.2 (segregated, SST k-w turbulence). For all the cases, the solution achieves convergence under 5000 iterations.

The results of this CFD study are used as validation to discuss the mainstream flow analysis and the TRA. The next sections discuss both, starting with the mainstream flow analysis.

4.3.2 Mainstream Flow Analysis

The mainstream mapping related to each ventilation source is given in Figure 51. The *CS* and *SW* numbers concerning each ventilation source are listed in Table IV in the Appendix. While the table lists all the ventilation sources and the associated numbers, the cases without a particular ventilation source would not be associated with the mainstream numbers of said source. For example, the *CS* and *SW* numbers for *Case 2* (no bottom outlet) would only use the numbers w.r.t *Outlet_1* and *Outlet_2*, respectively. The case with all the outlets available (*Case 1*) uses all the numbers listed. Unlike section 4.2, the avionics bay is not symmetric in the *Z*-axis. Thus, *CS* and *SW* numbers are considered in all three axes. *MS* scores are derived using the mainstream scoring (TR_3). The *MS* scores are listed for each case in Table 14.

Table 14: *MS* scores for all the systems in four cases.

System	<i>MS</i> scores			
	Case 1	Case 2	Case 3	Case 4
System 1	3	3	3	3
System 2	2.25	2.25	2.25	2.25
System 3	3	3	3	3
System 4	3	3	4	4
System 5	3	3	3	3
System 6	3	3	4	4
System 7	3	4	3	4
System 8	3	3	3	3
System 9	3	4	3	4
System 10	3	4.5	3	5
System 11	3	3.75	3	3.75
System 12	3	4.5	3	5
System 13	1	1	1	1
System 14	1	1	1	1
System 15	1	1	1	1

- In all four cases, Systems 13, 14, and 15 have the lowest MS scores ($MS = 1$). These systems have the lowest CS value with regards to Y -axis ($CS_{in}(y) = -0.21$).
 - System 14 has the lowest CS value with respect to X -axis ($CS_{in}(x) = -1.39$). Thus, System 14 lies closest to the inlet, followed by Systems 13 and 15.
 - As the inlet remains unchanged, their MS scores are constant in each case.
- The MS scores of Systems 10, 11, and 12 are equal ($MS = 3$) in the cases where the bottom outlet ($Outlet_3$) is considered; *Case 1* and *Case 3*. Their lowest CS number ($CS_{out}(y) = 1.28$) is with regards to $Outlet_3$, meaning they are closest to it.
 - In the absence of $Outlet_3$, the MS scores of Systems 10 and 12 get influenced by either the top outlet ($Outlet_2$) or the main outlet ($Outlet_1$).
 - For System 11, in the absence of $Outlet_3$, its CS and SW numbers are lowest with regards to $Outlet_1$.
 - As seen in Table 14, deleting $Outlet_3$ increases the MS scores.
- The MS scores for Systems 7, 8, and 9 display the same behavior as above, increase when $Outlet_3$ is deleted. But in their case, they are closer to both $Outlet_2$ and $Outlet_1$. This gives them a lower MS score compared to Systems 10, 11, and 12 in the absence of $Outlet_3$.
- The MS scores for Systems 4, 5, and 6 are equal ($MS = 3$) in the cases where $Outlet_2$ is present; *Case 1* and *Case 2*. Like the systems near $Outlet_3$, their scores increase when $Outlet_2$ is deleted. In that case, their CS and SW numbers are derived with regards to $Outlet_1$.
- Systems 1, 2, and 3 have the same MS scores in all four cases. Their scores are derived from CS and SW numbers with respect to $Outlet_1$.
 - System 2 is closest to $Outlet_1$ in X axis ($CS_{out}(x) = -0.13$), thus it has the lowest MS score ($MS = 2.25$) among these systems.

To conclude, changing the outlet configuration changes the MS scores of some systems. The systems close to either *Inlet* or $Outlet_1$ do not see any changes in their MS scores.

As the number of ventilation sources decreases, the systems' relative distances to the ventilation sources increases. Thus, combining the scores for all the systems, the least average MS score is attributed to *Case 1*, while the highest average MS score is for *Case 2*.

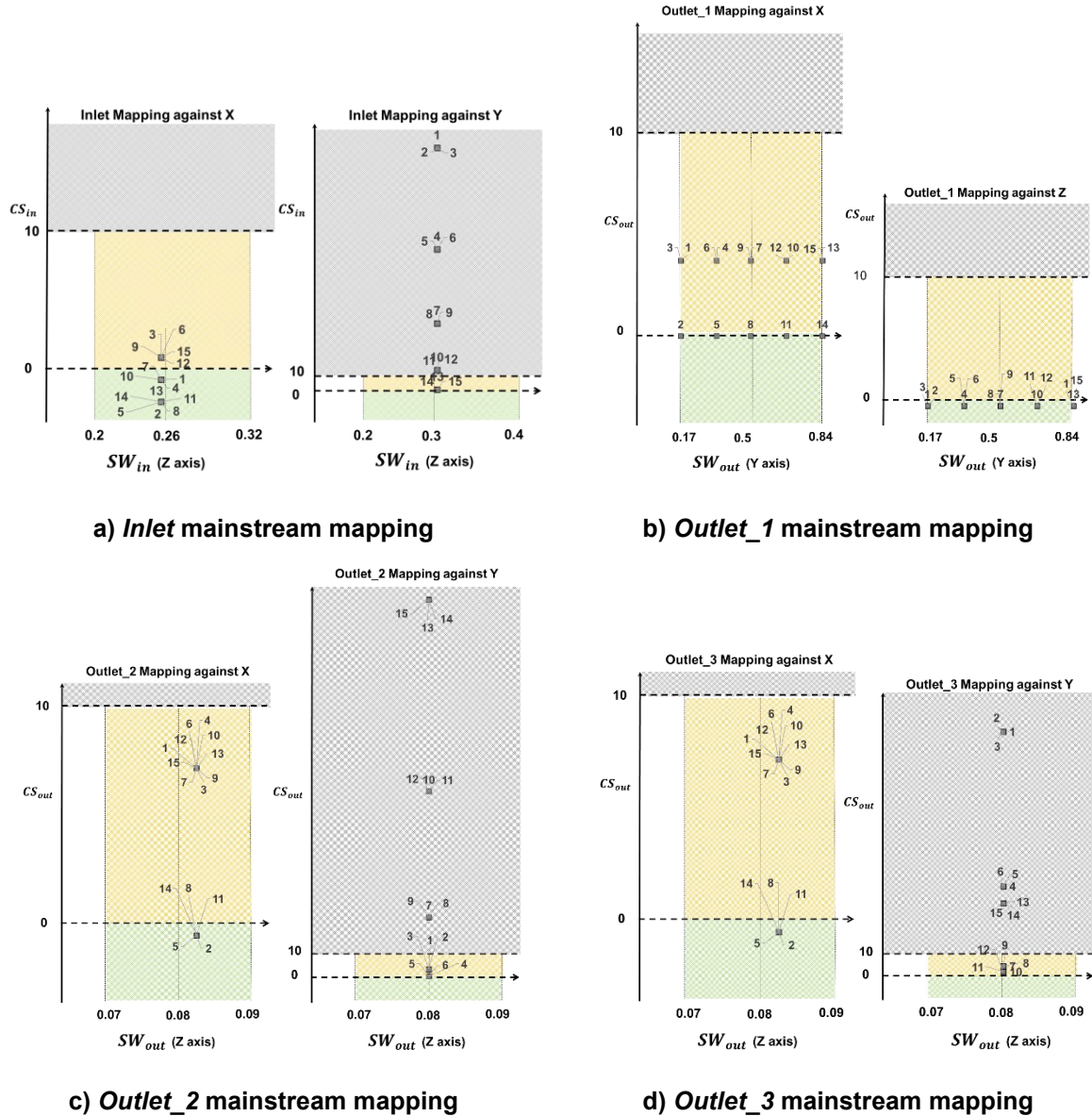


Figure 51: Mapping of the CS and SW numbers for different ventilation sources; green region indicates a strong mainstream influence. Orange indicates that the mainstream influence is weak. In the grey region, the mainstream influence is negligible.

Figure 52 below shows the streamlines plot for *Case 1*. The mainstream can be seen moving from the inlet, interacting with the systems at the bottom, then rushing along the curved wall towards the top, where it exits through *Outlet_1*. The systems in the middle, near *Outlet_2* and *Outlet_3*, receive the remaining flow, recirculated from the top. The flow interacts with these systems and exits through *Outlet_2* and *Outlet_3*, respectively.

In Figure 52 b)-d), the regions near the mainstream can be identified clearly. The following observations can be made:

- Systems at the bottom (13, 14, and 15) lie directly in the mainstream

- Systems 5 and 11, which are the nearest to *Outlet_2* and *Outlet_3*, are under the mainstream influence, as predicted by their respective *CS* numbers.
- Systems 1, 2, and 3 are in the mainstream, as most of the flow rushes towards the exit from *Outlet_1*

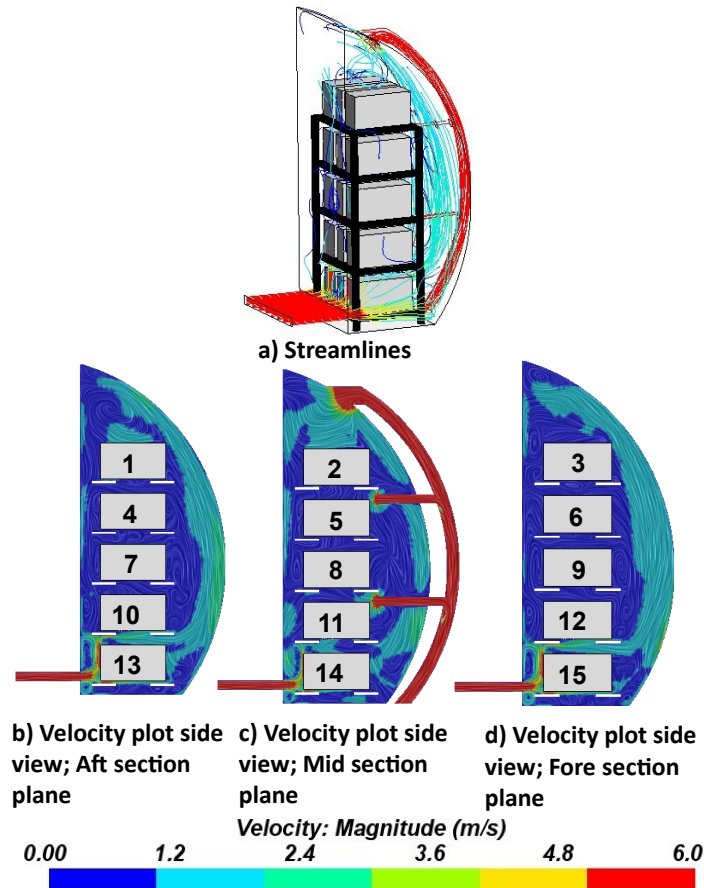


Figure 52: Velocity streamlines and velocity plots in the side view for Case 1 containing all outlets; a) Streamlines show originating from the inlet and moving across the curved wall of the bay Velocity plots for the b) aft section, c) mid-section, and d) fore section of the bay are also seen.

In cases without *Outlet_2* and *Outlet_3* (Case 2, 3, and 4), systems close to the missing outlets see a change in their *MS* number. Figure 53 shows the following:

- The *MS* of System 11 increases (from 3 to 3.75) as the bottom outlet (*Outlet_3*) gets deleted (Figure 53-c, Figure 53-d)
- There is no change in *MS* number (3) for either Systems 5 or 8.
 - These systems are categorized as being influenced by the mainstream with regards to *Outlet_1* as shown on the *Outlet_1* mainstream mapping in Figure 51.
 - The flow fields in Figure 53 show that these systems (Systems 5 and 8) are away from the mainstream flow (not influenced by the mainstream) in the absence of *Outlet_2* (Figure 54-g, Figure 54-h) and *Outlet_3* (Figure 54-c, Figure 54-d), respectively.

- This is different than what is predicted. It occurs as the flow in the CFD does not go directly from the inlet towards the *Outlet_1*. It travels along the curved section of the bay, thus not influencing these systems.
- As this flow pattern is 3D in nature, this cannot be predicted accurately by the mainstream flow analysis.

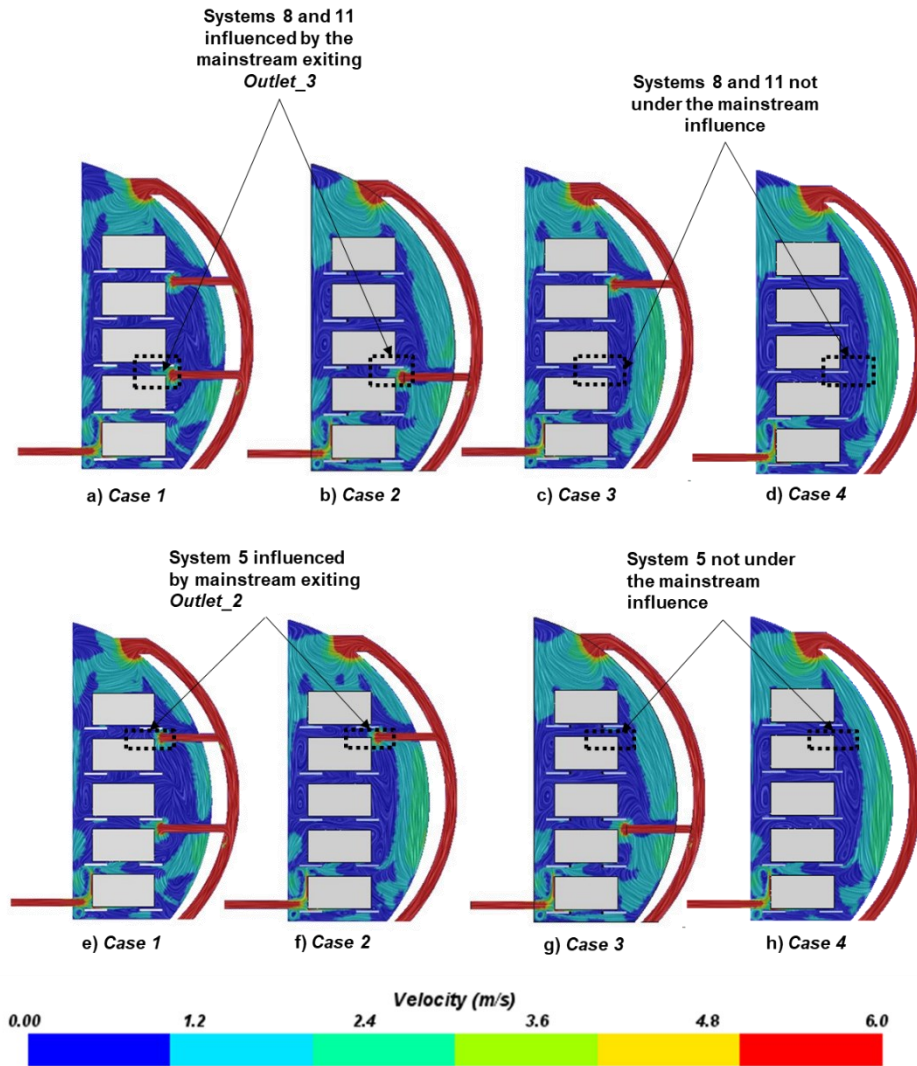


Figure 53: Side views of the velocity plots shown; changes in ventilation configuration change the mainstream flow. Systems 5, 8, and 11 are discussed.

- Systems 1, 2, 3, 13, 14, and 15, as predicted by their *MS* scores, lie on the mainstream for all cases.

To conclude, the validation with CFD reveals that most of the systems follow the prediction, with the exception of the flow around Systems 5 and 8. This is due to the mainstream following the curved section of the bay. The mainstream flow analysis cannot accurately predict this due to the flow's three-dimensional nature. To account for these cases, mainstream flow analysis can include

irregular shapes of the zone. It can also benefit from more quantitative comparisons with CFD results.

Next, these *MS* scores are combined with other scores, and thermal risk is predicted for each system. The thermal risk is compared among all configurations and then finally compared with the CFD results.

4.3.3 Thermal Risk Prediction and Comparison with CFD

This section can be divided into two parts, thermal risk prediction, and comparison with CFD. TRA predicts the thermal risk for each system in the avionics bay, similar to sub-section 4.2.3. Thermal risk predictions are compared between all four cases. Finally, these scores are compared with CFD simulations.

1. Thermal Risk Prediction

Figure 54 illustrates the thermal risk for each system and each case. Thermal risk regions are shaded as red for high risk, orange for medium risk, and green for low risk. Table V in the Appendix provides the scores for the individual analyses. Thermal risk scoring for each module is described as follows:

- As in Section 4.2, the ventilation state of the case study is forced ($Ri < 1$). Thus the ventilation of all the systems is equal ($TR_1=1$).
- The stratification scores are also similar and equal for each system ($TR_2=1$). Systems 1, 2, and 3 are located at the top of the bay and have the highest system integration scores ($TR_4=3$).
- Systems 10 to 15 are located near the bottom and have the lowest system integration scores ($TR_4=1$). Temperature limits analysis attributes a score of one to each system in all configurations ($TR_5=1$).
- The closest ventilation source according to the *HR* potential analysis is given in Table 15. In the absence of a ventilation source (*Outlet_2*, *Outlet_3*), the *HR* number is calculated using the next closest ventilation source.

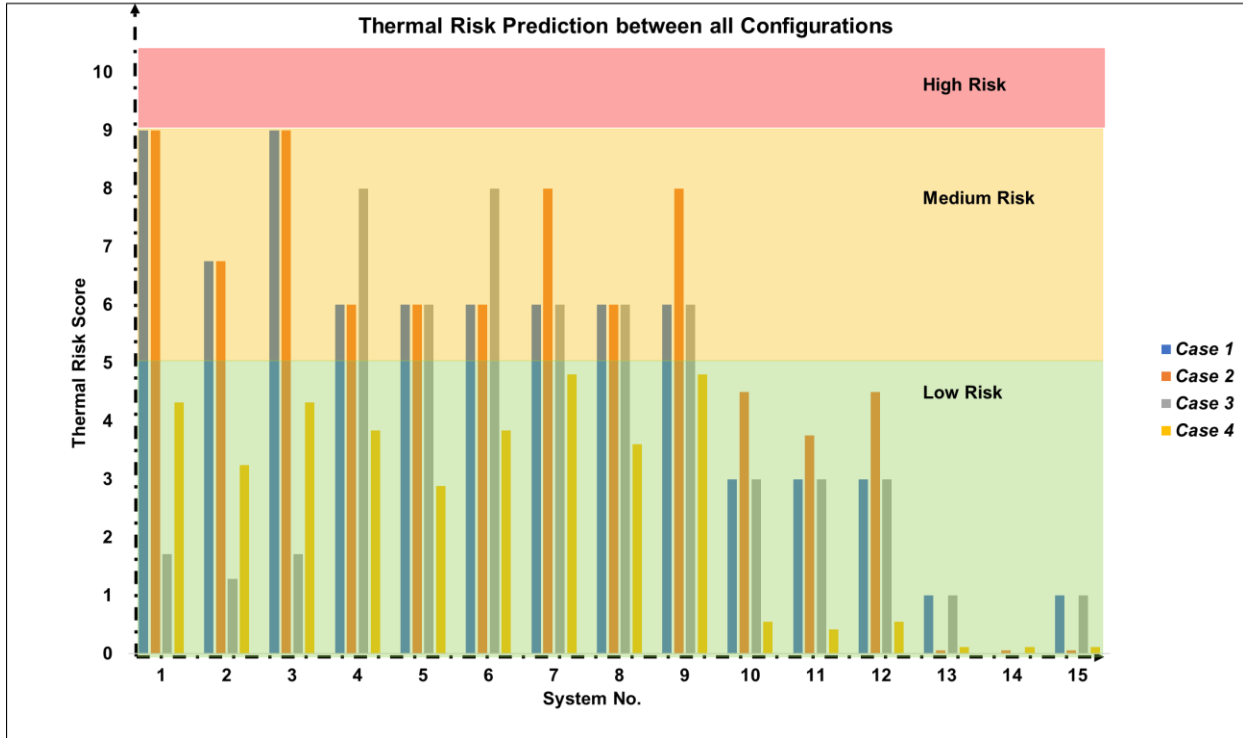


Figure 54: Comparison of thermal risk prediction for each system between all configurations

Figure 54 allows for the following conclusions:

- The thermal risk of Systems 13, 14, and 15 is the lowest ($TR_{tot} \leq 1$) in all the cases, as these systems are located directly in front of the inlet and have the lowest MS scores among all ($MS = 1$).
- The majority of the systems have a low thermal risk score ($TR_{tot} < 5$), while no system is in a high thermal risk zone ($TR_{tot} \leq 9$).
- The change in outlet configuration causes systems to change from medium thermal risk to low thermal risk and vice versa.

In Case 1,

- Systems 1 and 3 have the highest thermal risk scores ($TR_{tot} = 9$), as they are located in the top half of the avionics bay, and their system integration score is the highest ($TR_4 = 3$). Their thermal risk score is medium ($5 < TR_{tot} < 9$). Their HR potential is lowest ($TR_6 = 1$). In fact, except System 14 ($TR_6 = 0.01$), all systems are assigned the maximum HR scores ($TR_{tot} = 1$).
- The MS scores remain constant for Systems 4 to 10 ($MS = 3$). Only their system integration scores (TR_5) decrease as the inlet is now closer to the systems. Thus, to summarize, Systems 1-9 is predicted to be at medium risk, this being a combination of their HR potential scores and their system integration scores.

Table 15 lists the ventilation sources attached to a system for HR calculations.

Table 15: Systems grouped by ventilation source for HR potential calculations.

System	Ventilation Source for Heat Removal			
	Case 1	Case 2	Case 3	Case 4
System 1	Outlet_2	Outlet_2	Outlet_1	Outlet_1
System 2	Outlet_2	Outlet_2	Outlet_1	Outlet_1
System 3	Outlet_2	Outlet_2	Outlet_1	Outlet_1
System 4	Outlet_2	Outlet_2	Outlet_3	Outlet_1
System 5	Outlet_2	Outlet_2	Outlet_3	Outlet_1
System 6	Outlet_2	Outlet_2	Outlet_3	Outlet_1
System 7	Outlet_3	Outlet_2	Outlet_3	Outlet_1
System 8	Outlet_3	Outlet_2	Outlet_3	Outlet_1
System 9	Outlet_3	Outlet_2	Outlet_3	Outlet_1
System 10	Outlet_3	Outlet_2	Outlet_3	Inlet
System 11	Outlet_3	Outlet_2	Outlet_3	Inlet
System 12	Outlet_3	Outlet_2	Outlet_3	Inlet
System 13	Outlet_3	Inlet	Outlet_3	Inlet
System 14	Inlet	Inlet	Inlet	Inlet
System 15	Outlet_3	Inlet	Outlet_3	Inlet

In Case 2,

- Thermal risk scores for the top half of the bay remain the same. Systems near the bottom, where the now-deleted *Outlet_2* was located, see a change in their thermal risk scores.
- Systems 7,9, 10, 11, and 12 see an increase in their MS scores. Thus, their corresponding thermal risk scores also increase while still staying in the medium risk zone. While their ventilation source changes from *Outlet_3* to *Outlet_2*, the HR score does not change as both of their values are equal.
- Going down, the ventilation source for Systems 13, 14, and 15 changes from *Outlet_3* to the *Inlet*, and thus their HR potential increases. Thus, further decreasing their thermal risk.

Similarly, in Case 3,

- For the top half of the bay, the thermal risk scores changes. While the *MS* scores for Systems 1, 2, and 3 are constant, their ventilation source changes from *Outlet_2* to *Outlet_1*. This increases their heat removal potential and thus decreasing their overall thermal risk scores, moving from medium to low thermal risk in this case.
- On the other hand, the thermal risk scores for Systems 4, 5, and 6 increase as their *MS* score has increased.

In Case 4,

- The absence of both *Outlet_2* and *Outlet_3* divides the systems among two ventilation sources (*Outlet_1* and *Inlet*).

- Although *MS* scores for some systems increase due to the deletion of the outlets close to them, the heat removal potential also increases, thus bringing down the overall thermal risk.
- Every system has a low thermal risk in this configuration.
- Thus, from a thermal risk perspective, this is the best ventilation configuration.

To conclude, changing the ventilation configuration results in a change in *MS* scoring and the *HR* number, thus affecting the overall thermal risk score. The systems grouped with either *Outlet_1* or *Inlet* see a higher heat removal potential and thus reduction in their scores. In case the *HR* score does not change, the *MS* score is the driving force behind the overall thermal risk.

According to the prediction, the best configuration overall is the following:

1. *Case 1*, ($TR_{avg} = 2.5$, $TR_{median} = 3.2$) which is better than
2. *Case 2* ($TR_{avg} = 3.7$, $TR_{median} = 3$) which is more favorable than
3. *Case 3* ($TR_{avg} = 4.8$, $TR_{median} = 6$) and the least favorable configuration from a thermal risk point of view is
4. *Case 4* ($TR_{avg} = 5.17$, $TR_{median} = 6$).

2. Comparison with CFD

To illustrate the thermal risk and to easily compare the TRA with the CFD simulation results, each system is color-coded according to the thermal risk, as depicted in Figure 56.

Table 16 shows the ambient system temperatures and the corresponding risk from CFD simulations. The predictions are accurate for most of the systems and are conservative whenever differing from the CFD results.

In *Case 1*,

- Systems 1-9 are predicted medium thermal risk, but only System 7 and 9 are at medium thermal risk from the CFD. This is due to the curvature of the bay, which makes the systems at the top (System 1-6) closer to the flow than predicted. The mainstream sticks to the curved section wall before interacting with the systems at the top and exiting through *Outlet_1*. The updated TRA models the bay as rectangular to simplify the inputs and thus does not account for its curvature. Moreover, the mainstream flow analysis cannot predict the complex 3D nature of the flow, which in this case, moves along the curved section. This trend can be seen in *Case 2* (Systems 1-6) and *Case 3* (Systems 4-6) as well, where the systems at the top predicted to lie at medium risk are at lower risk.
- System 8 is predicted to be at medium thermal risk but is at low thermal risk from the CFD results. A much-detailed analysis is required in this case.

Case 2,

- As predicted by the thermal risk scoring, it is the least favorable case from a thermal risk perspective. This is confirmed by the CFD results.
- The configuration has the most systems at medium risk out of all four.

- Removal of *Outlet_3* increases the ambient temperatures of Systems 5 and 8, thus increasing their thermal risk when compared to *Case 1*.

Case 3 is the most favorable configuration for thermal risk from the CFD results.

- All systems, in this case, lie at low thermal risk.
- The flow extraction is optimally divided between *Outlet_3* and *Outlet_1*.
- Systems 7-9 are at low thermal risk, contrary to the prediction. The scoring predicts these systems to be grouped with *Outlet_3* for heat removal potential ($TR_{tot}=1$), whereas the heat from these systems is extracted by *Outlet_1*.

In *Case 4*:

- Thermal risk for System 7 is higher than predicted:
 - The ambient temperature of this system ($T_{sys,env} = 68^\circ\text{C}$) is 1.5°C above the low thermal risk limit.
 - The higher temperature could be due to hotspots forming near the system, as shown in Figure 55 when compared to Systems 8 and especially 9.
 - As the avionics bay is symmetrical in *X*, this would not be accounted for by the updated TRA. This is a 3D effect of the CFD simulation and cannot be predicted by it.
 - Looking into the radiation exchanges between closely packed systems might shed some light on this system's thermal risk. Also, as mentioned before, a much-detailed analysis is required to improve upon the medium risk prediction.

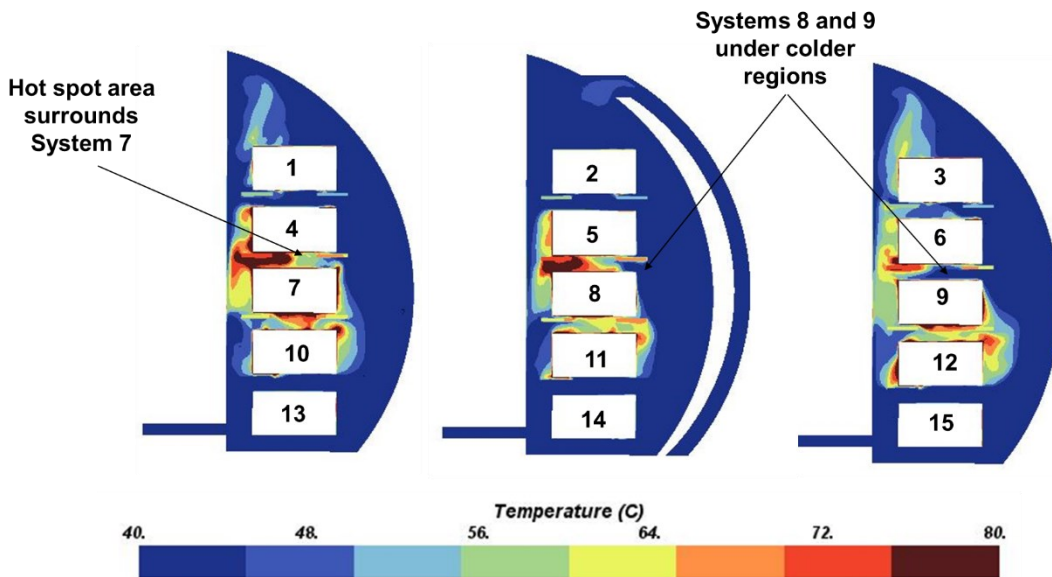


Figure 55: Temperature plot showing the hot spots formed near System 7, while Systems 8 and 9 have a cooler surrounding region.

The CFD results put *Case 3* as the best configuration from a thermal standpoint. Conversely, *Case 2* is the worst configuration from the CFD results.

To conclude, the predicted thermal risk is validated using the thermal risk derived from the CFD. The results are satisfactory, as the predictions are correct or conservative, which is good for conceptual design.

The following conclusions can be made:

- Systems 10-15 all have a low thermal risk.
- Systems at the top (Systems 1-6) are predicted to carry a medium thermal risk. The CFD results differ and, in most cases, put them at a lower thermal risk. This is due to the curvature of the bay wall along which the mainstream flows. The TRA predicts systems at the top to lie away from this flow.
- Changes in ventilation configuration affect the systems' thermal risk in CFD, moving them from medium risk to low risk and vice versa.
- System 7 in *Case 4* is at a higher risk than its prediction. This is an asymmetrical effect of the 3D CFD simulation, which is not under the scope of conceptual TRA, which is generally of low fidelity.
- There are many systems at medium thermal risk, a much-detailed analysis on the thermal conditions would define the limits better, and the prediction's accuracy would increase. One such analysis is the radiation heat transfer between two systems and between systems and the walls. Analyzing radiation in closely packed avionics bays, as presented in this section, would provide a complete picture of the system's thermal risk.
- The best configuration from a thermal standpoint was predicted to be *Case 4*. From the CFD results, one can identify *Case 3* as the best configuration. Both the thermal risk prediction and CFD results agree with *Case 2* to be the worst configuration.

Table 16: Thermal risk derived from the CFD results using ambient temperatures.

System	Case 1		Case 2		Case 3		Case 4	
	$T_{sys,env}$ (°C)	Thermal risk from CFD						
System 1	45	Low	49	Low	46	Low	45	Low
System 2	41	Low	43	Low	41	Low	43	Low
System 3	40	Low	47	Low	43	Low	47	Low
System 4	62	Low	65	Low	52	Low	56	Low
System 5	57	Low	69	Medium	47	Low	50	Low
System 6	57	Low	66	Low	51	Low	55	Low
System 7	67	Medium	69	Medium	58	Low	68	Medium
System 8	61	Low	71	Medium	52	Low	66	Low
System 9	69	Medium	69	Medium	64	Low	63	Low
System 10	54	Low	58	Low	54	Low	61	Low
System 11	49	Low	59	Low	52	Low	62	Low
System 12	54	Low	61	Low	56	Low	60	Low
System 13	32	Low	32	Low	31	Low	32	Low
System 14	31	Low	32	Low	31	Low	31	Low
System 15	31	Low	32	Low	32	Low	32	Low

Section 4.2 applied the TRA on an aircraft avionics rack with a single inlet and outlet. The Mainstream flow analysis was carried out in 4.2.2. The mainstream flow predictions were validated via streamlines and velocity plots. *MS* scores matched with the validation for almost all systems. Thermal risk predictions agreed with CFD results for 6 of the 9 systems. The differences were due to the three-dimensional nature of the flow, obstructions to the flow not modeled in the TRA, and system surfaces at different temperatures (hot spots). Radiation heat transfer analysis could shed some light on these closely packed systems.

In section 4.3, an avionics bay with a single inlet and multiple outlets was used. 4 different cases were chosen, each with a different outlet system. *MS* scores changed as the ventilation source nearest to the system was added or deleted. Validation with the CFD showed that indeed, deleting either *Outlet_2* or *Outlet_3* changed the mainstream flow and thermal risk near the systems closest to those ventilation sources. Thermal risk from CFD agreed with the predictions in most of the cases. The best and the worst cases from a thermal risk standpoint were identified.

This concludes the chapter on the application of TRA on real-world aircraft equipment bays. The next chapter concludes the thesis and discusses the challenges faced and the scope of future work in TRA at aircraft conceptual design.

5 Conclusion and Future Work

This final section of the thesis summarizes and concludes the contributions and discusses future avenues of research.

5.1 Summary of Contributions

As part of an effort to develop a thermal analysis capability for the conceptual design of future aircraft, this thesis contributes to improving the thermal risk assessment (TRA) method. This thesis makes three contributions.

The first contribution of this thesis concerns the mainstream flow analysis. The new mainstream flow analysis studies the relative locations of the systems in aircraft equipment bays and establishes a geometrical relationship between the systems and the mainstream flow. Two new dimensionless numbers are developed, the cross-stream (*CS*) number and the streamwise number (*SW*), to quantify this relationship. These DN allow the evaluation of the cross-stream and streamwise distance of each system from the mainstream flow. Based on additional information, such as the location of the inlet and outlet, one can now estimate if the mainstream flow influences a system. The desired ranges for *CS* and *SW* are established using CFD analysis for a 2D case study. In addition, this approach was validated with a more complex CFD case study.

As a second contribution, the system-level analysis has been improved in the TRA, including the associated scoring. As another system-level analysis, the heat removal potential analysis was introduced in parallel to this thesis. Both analyses, the mainstream and heat removal potential, were integrated into the TRA, and the thermal risk scoring was enhanced in collaboration with members of the Aircraft Systems lab at Concordia University. This updated TRA is validated using case studies containing two realistic aircraft avionics bays in 3D. The first avionics bay had a fixed ventilation configuration with nine systems. The 2nd avionics bay had varying outlet configurations and even more systems than the 1st. The thermal risk is predicted for each system in both the avionics bays. Comparison with CFD results shows that the thermal risk predictions are accurate for most of the systems (>80%). Therefore, the new analysis capability improves the physical insight gained into the thermal analysis and increases the prediction accuracy.

The third contribution of this thesis is the demonstration of the capability to analyze different ventilation concepts in conceptual design without using CFD. This capability was validated with the most complex case study, an avionics bay with fifteen systems and varying outlet configurations. With the TRA, one can identify the worst configurations from a thermal risk perspective. Compared to the CFD simulations, the overall reduction in time is from hours to seconds. The longest CFD simulation (design study) took almost 48 hours to complete. Using the TRA tool reduces the time for one analysis to under 1 minute. This reduction in analysis time is one of the main advantages of using TRA and enables the integration of the TRA into multidisciplinary design analysis and optimization environments typically used in conceptual design. TRA can be a part of multidisciplinary studies, including analysis on aircraft (such as weight or drag) and system levels (such as maintenance aspects or electromagnetic capabilities)

[67]. Thus, using this enhanced TRA, much better consideration of the ventilation effects on the thermal environment of systems is now possible during the conceptual design phase.

5.2 Limitations

Although the thermal risk prediction capability is enhanced and system-level details are added to the TRA, some limitations remain. The thermal risk prediction does not capture the 3D effect of the complex mainstream flow patterns, which shows in lack of symmetry in CFD results. Therefore, irregularly shaped equipment bays cannot be captured well with the current TRA. Including more complex geometry for the bays, such as curved aircraft zones, would make the TRA more accurate.

The validation of the mainstream flow analysis was done using the velocity and temperature plots. Quantitative comparison (flow velocity and mass flow rate) would provide a better understanding of the ranges of the MS numbers. Some systems were predicted to be at low thermal risk, but the CFD results put them at high thermal risk. This can be explained by the radiation heat transfer between systems which is not captured in the current TRA. The radiative heat transfer effect needs to be studied in more detail, which is explained in Section 5.3.

Although extensive CFD case studies have been performed to validate the updated TRA methodology, it has not been validated with test data from aircraft. However, validation with test data from aircraft manufacturers was performed in previous versions of the TRA [1,32]. Based on these previous results and for the scope of this thesis, the validation with CFD only was deemed appropriate.

While this thesis explores the worst case in the form of systems exceeding their maximum long term operating temperatures (T_{lim}), it does not consider cases where systems reach their survival temperatures for short periods of time (Short term operation high definition in DO160 [9]). Thus, only steady-state cases were considered and validated with steady-state CFD.

5.3 Future Work

Based on the limitations described above, future developments of the TRA should focus on the following three aspects.

The first aspect is to introduce the radiation into the system-level analysis of the TRA. Radiation heat transfer in real bodies is based on the grey body heat transfer law and depends majorly on the body's temperature (T^4). However, the temperature of a system is not a part of the input data in conceptual design. It can only be accurately determined in detailed design phases, from thermocouples or detailed CFD simulations. Thus, determining the exact amount of radiation heat transfer between two systems is not possible in TRA.

Although the exact radiation heat transfer between systems cannot be determined, there exists a way to determine if a single system is under an increased thermal risk in specific circumstances. Some of these circumstances have been introduced in [1]. Recall that the temperature limits analysis compared the system limit temperatures with the temperatures of the walls. If the

corresponding view factor is close to 1, and the temperature of the wall is higher than the system, then a higher thermal risk is predicted. This is due to heat transfer from the wall to the system ($T_w > T_{sys,lim}$). Thus, investigating DN such as the view factor could aid in shedding light on the system-to-system radiation heat transfer. This type of analysis is even more essential in the trend towards more electrification, where the electronics tend to be more and more packed. Thus, radiation between two surfaces is substantial.

The second aspect to future work in TRA can be improvements in its validation strategy. This includes moving from qualitative to quantitative comparisons. Quantitative comparisons with CFD can help gauge the numerical differences in parameters such as mass flow rate and velocity. This can help identify further limitations and increase the accuracy of TRA. Also, including complex bay geometries such as the curved fuselage-like shapes, in future versions of TRA could help eliminate the deviations from the CFD results.

The last part of the future work could include the short-term high temperature reached by a system. This type of thermal risk assessment is complex as the risk of reaching these temperatures would be based on transient conditions. It would require inputs such as time dependant system heat loads, time dependant ventilation characteristics (fan on/off,) and a transient CFD model or test data for validation.

5.4 Conclusion

The TRA predicts the thermal architecture of various system configurations in aircraft conceptual design. As the TRA does not use CFD, it is faster than thermal studies usually conducted in aircraft design. Therefore, this new thermal analyses capability is suitable for conceptual design, which helps to detect thermal issues early, allowing to find solutions to, e.g., increased heat loads occurring in more electric aircraft. Therefore, better requirements can be sent to the system suppliers, thus removing future roadblocks in development. Furthermore, this method can be integrated within a Multidisciplinary Design Analysis and Optimization (MDAO) framework, thus aiding in developing future more or all-electric aircraft technologies.

In summary, this thesis improves the TRA method by expanding its scope at the system level. Therefore, this thesis is contributing to helping the aviation industry achieve its goals for a sustainable future.

Bibliography

- [1] Sanchez, F., and Liscouët-Hanke, S. “Thermal Risk Prediction Methodology for Conceptual Design of Aircraft Equipment Bays.” *Aerospace Science and Technology*, Vol. 104, 2020, p. 105946. <https://doi.org/10.1016/j.ast.2020.105946>.
- [2] Sanchez, F., Liscouët-Hanke, S., Boutin, Y., and Beaulac, S. A Thermal Risk Assessment Approach for the Conceptual Design of Aircraft System Architectures. *AIAA Aviation 2019 Forum*, 2019.
- [3] Ahlers, M. F. Aircraft Thermal Management. In *Encyclopedia of Aerospace Engineering*, John Wiley & Sons, Ltd, Chichester, UK, 2011, pp. 1–13.
- [4] Schminder, J., Gårdhagen, R., Nilsson, E., Storck, K., and Karlsson, M. “Development of a Cockpit-Pilot Model for Thermal Comfort Optimization During Long-Mission Flight.” *AIAA Modeling and Simulation Technologies Conference*, No. January, 2016, pp. 1–10. <https://doi.org/10.2514/6.2016-0172>.
- [5] Sarlioglu, B., and Morris, C. T. “More Electric Aircraft: Review, Challenges, and Opportunities for Commercial Transport Aircraft.” *IEEE Transactions on Transportation Electrification*, Vol. 1, No. 1, 2015, pp. 54–64. <https://doi.org/10.1109/TTE.2015.2426499>.
- [6] Martin, H. “Electric Flight - Potential and Limitations.” *AVT-209 Workshop, Lisbon*, No. October 2012, 2012, pp. 1–30.
- [7] Xie, Y., Savvarisal, A., Tsourdos, A., and Zhang, D. “Review of Hybrid Electric Powered Aircraft, Its Conceptual Design and Energy Management Methodologies.” *Chinese Journal of Aeronautics*, Vol. 34, No. 4, 2021, pp. 432–450. <https://doi.org/10.1016/j.cja.2020.07.017>.
- [8] Madonna, V., Giangrande, P., and Galea, M. “Electrical Power Generation in Aircraft: Review, Challenges, and Opportunities.” *IEEE Transactions on Transportation Electrification*, Vol. 4, No. 3, 2018, pp. 646–659. <https://doi.org/10.1109/TTE.2018.2834142>.
- [9] RTCA-DO-160. “Environmental Conditions and Test Procedures for Airborne Equipment.” *Federal Aviation Administration (FAA)*, 2011, p. 16.
- [10] Sadraey, M. H. *AIRCRAFT DESIGN Aerospace Series List Design and Analysis of Composite Structures: With Applications to Aerospace Structures*. 2013 pp 49-50.
- [11] Donovan, A., Nuzum, S., Roberts, R. A., and Wolff, M. “Impact of High Energy Pulsed Systems on an Aircraft’s Power and Thermal Management System.” *57th AIAA/ASCE/AHS/ASC Structures, Structural Dynamics, and Materials Conference*, No. January, 2016, pp. 1–16. <https://doi.org/10.2514/6.2016-0672>.
- [12] Glickstein, M. R., Hodge, E. S., and Van Griethuysen, V. J. “Application of a New Modeling Tool for Evaluating Aircraft Thermal System Concepts.” *Collection of Technical Papers - 3rd International Energy Conversion Engineering Conference*, Vol. 2,

- No. August, 2005, pp. 1205–1212. <https://doi.org/10.2514/6.2005-5648>.
- [13] Doman, D. B. “Optimal Cruise Altitude for Aircraft Thermal Management.” *Journal of Guidance, Control, and Dynamics*, Vol. 38, No. 11, 2015, pp. 2084–2095. <https://doi.org/10.2514/1.G000845>.
- [14] Falck, R. D., Chin, J., Schnulo, S. L., Burt, J. M., and Gray, J. S. "Trajectory Optimization of Electric Aircraft Subject to Subsystem Thermal Constraints". In *18th AIAA/ISSMO Multidisciplinary Analysis and Optimization Conference*, American Institute of Aeronautics and Astronautics, 2017.
- [15] Kellermann, H., Lüdemann, M., Pohl, M., and Hornung, M. “Design and Optimization of Ram Air–Based Thermal Management Systems for Hybrid-Electric Aircraft.” *Aerospace*, Vol. 8, No. 1, 2021, p. 3. <https://doi.org/10.3390/aerospace8010003>.
- [16] Alyanak, E. J., and Allison, D. L. “Fuel Thermal Management System Considerations in the Aircraft Conceptual Design Process.” *57th AIAA/ASCE/AHS/ASC Structures, Structural Dynamics, and Materials Conference*, No. January, 2016, pp. 1–18. <https://doi.org/10.2514/6.2016-0670>.
- [17] Torres, F., and McCarthy, K. Lockheed Martin "Overview of the AFRL EXPEDITE Program: Power and Thermal Management System". In *AIAA Scitech 2020 Forum*, American Institute of Aeronautics and Astronautics, 2020.
- [18] German, B. J., Daskilewicz, M. J., and Doty, J. H. “Using Interactive Visualizations to Assess Aircraft Thermal Management System Modeling Approaches.” *11th AIAA Aviation Technology, Integration, and Operations (ATIO) Conference, including the AIAA Balloon Systems Conference and 19th AIAA Lighter-Than-Air Technology Conference*, No. September, 2011, pp. 1–13. <https://doi.org/10.2514/6.2011-7060>.
- [19] Jafari, S., and Nikolaidis, T. “Thermal Management Systems for Civil Aircraft Engines: Review, Challenges and Exploring the Future.” *Applied Sciences (Switzerland)*, Vol. 8, No. 11, 2018, pp. 1–16. <https://doi.org/10.3390/app8112044>.
- [20] van Heerden, A. S., Judt, D. M., Lawson, C. P., Jafari, S., Nikolaidis, T., and Bosak, D. "Framework for Integrated Dynamic Thermal Simulation of Future Civil Transport Aircraft". In *AIAA Scitech 2020 Forum*, American Institute of Aeronautics and Astronautics, 2020.
- [21] Kallath, H., Kholi, F. K., Ha, M. Y., Min, J. K., and Chetwynd-Chatwin, J. “Computational Study on the Aerodynamics of a Surface-Heated Wing for Thermal Management.” *AIAA Journal*, Vol. 58, No. 10, 2020, pp. 4339–4356. <https://doi.org/10.2514/1.J059220>.
- [22] Schnulo, S. L., Chin, J. C., Smith, A. D., and Dubois, "A. Steady State Thermal Analyses of SCEPTOR X-57 Wingtip Propulsion". In *17th AIAA Aviation Technology, Integration, and Operations Conference*, American Institute of Aeronautics and Astronautics, 2017.
- [23] Level, D., and Code, F. “TOICA Final Report – Publishable Summary.” *Education And Training*, Vol. 1, No. September, 2013, pp. 1–16.
- [24] European Commission FP7. Maaximus.

- [25] Butler, C., Newport, D., and Geron, M. “Optimising the Locations of Thermally Sensitive Equipment in an Aircraft Crown Compartment.” *Aerospace Science and Technology*, Vol. 28, No. 1, 2013, pp. 391–400. <https://doi.org/10.1016/j.ast.2012.12.005>.
- [26] Akin, A., and Kahveci, H. S. “An Optimization Study for Rotorcraft Avionics Bay Cooling.” *Aerospace Science and Technology*, Vol. 90, 2019, pp. 1–11. <https://doi.org/10.1016/j.ast.2019.04.029>.
- [27] Stancato, F., Santos, L. C. Dos, and Pustelnik, M. “Electronic Package Cooling Analysis in an Aircraft Using CFD.” *SAE Technical Papers*, Vol. Part F1298, No. September, 2017. <https://doi.org/10.4271/2017-01-2158>.
- [28] Liscouët-Hanke, S. *A Model-Based Methodology for Integrated Preliminary Sizing and Analysis of Aircraft Power System Architectures*. 2008.
- [29] Chakraborty, I. “Subsystem Architecture Sizing and Analysis for Aircraft Conceptual Design.” No. December, 2015, pp. 1–325.
- [30] Tfaily, A., Liscouet-Hanke, S., and Esdras, G. “Parametric 3D Modeling for Integration of Aircraft Systems in Conceptual Design.” *Candian Aeronautics and Space Institute Conference*, 2015, pp. 1–10.
- [31] Buckingham, E. “On Physically Similar Systems: Illustration of the Use of Dimensional Equations.” *Physical review*, Vol. 4, No. 4, 1914, pp. 345–376.
- [32] Sanchez, F., Liscouet-Hanke, S., Boutin, Y., and Beaulac, S. A Thermal Risk Assessment Approach for the Conceptual Design of Aircraft System Architectures. 2019.
- [33] Incropera, F. P., DeWitt, D. P., Bergman, T. L., and Lavine, A. S. *Fundamentals of Heat and Mass Transfer*. John Wiley & Sons, 2007.
- [34] Duval, W., and Balasubramaniam, R. “Convection Effects On Thermal Stratification Inside Enclosures Due To Wall Heat Flux.” *AIAA Aerospace Sciences Meeting and Exhibit*, 2008.
- [35] Davidson, J. H., Adams, D. a., and Miller, J. a. “A Coefficient to Characterise Mixing in Solar Water Storage Tanks.” *Solar Energy Engineering*, Vol. 116, No. 2, 1994, pp. 94–99.
- [36] Castell, A., Medrano, M., Solé, C., and Cabeza, L. F. “Dimensionless Numbers Used to Characterize Stratification in Water Tanks for Discharging at Low Flow Rates.” *Renewable Energy*, Vol. 35, No. 10, 2010, pp. 2192–2199. <https://doi.org/10.1016/j.renene.2010.03.020>.
- [37] Sinha, S. L., Arora, R. C., and Roy, S. “Numerical Simulation of Two-Dimensional Room Air Flow with and without Buoyancy.” *Energy and Buildings*, 2000. [https://doi.org/10.1016/S0378-7788\(99\)00047-X](https://doi.org/10.1016/S0378-7788(99)00047-X).
- [38] Papanicolaou, E., and Jaiuria, Y. “Electronic Components at Varying Relative Positions in a Cavity.” *Journal of Heat Transfer*, Vol. 116, No. 1986, 1994, pp. 960–970. <https://doi.org/10.1115/1.2911472>.
- [39] Gunes, H., Cadirci, S., and Gocmen, K. “Numerical Simulation of Mixed Convection in a

- Rectangular Cavity With Multiple Heat Sources.” 2018, pp. 1–10.
- [40] Sanchez, F., Liscouët-Hanke, S., Boutin, Y., Beaulac, S., and Dufresne, S. “Multi-Level Modeling Methodology for Aircraft Thermal Architecture Design.” *SAE Technical Papers*, 2018. <https://doi.org/10.4271/2018-01-1910>.
- [41] Sanchez, F., Huzaiifa, A. M., and Liscouët-Hanke, S. “Mainstream Flow Prediction for the Thermal Risk Assessment of Aircraft Systems in Conceptual Design.” *AIAA Aviation 2020 Forum*, 2020. <https://doi.org/10.2514/6.2020-2646>.
- [42] Sanchez, F., Huzaiifa, A. M., and Liscouët-Hanke, S. “Ventilation Considerations for an Enhanced Thermal Risk Prediction in Aircraft Conceptual Design.” *Aerospace Science and Technology*, Vol. 108, 2021, p. 106401. <https://doi.org/10.1016/j.ast.2020.106401>.
- [43] SAE. *Aerothermodynamic Systems Engineering and Design*. Warrendale, PA: Society of Automotive Engineers. SAE International, 1990.
- [44] Howell, J. R. *A Catalog of Radiation Configuration Factors*. McGraw-Hill Book, New York, 1982.
- [45] Bhise, T., Sanchez, F., and Liscouët-hanke, S. “Systems Radiation Consideration for Thermal Risk Assessment of Avionics Bays in Conceptual Design.” 2021, pp. 1–6.
- [46] Mainstream Flow. Oxford Dictionary.
- [47] Farj, M. A., Mohammed, S., Aftab, A., and Ahmad, K. A. “Parametric Study to Determine Optimum HVAC in a Hospital Operation Theatre Akademia Baru Parametric Study to Determine Optimum HVAC in a Hospital Operation Theatre.” No. September, 2018.
- [48] Ling, Z., Wang, F., Fang, X., Gao, X., and Zhang, Z. “A Hybrid Thermal Management System for Lithium Ion Batteries Combining Phase Change Materials with Forced-Air Cooling.” Vol. 148, 2015, pp. 403–409. <https://doi.org/10.1016/j.apenergy.2015.03.080>.
- [49] Fontana, É., Capeletto, C. A., and Mariani, V. C. “Numerical Analysis of Mixed Convection in Partially Open Cavities Heated from Below.” *International journal of heat and mass transfer*, Vol. 81, 2015, pp. 829–845. <https://doi.org/10.1016/j.ijheatmasstransfer.2014.11.011>.
- [50] Jankes, G., Skistad, H., and Tanasi, N. “Cfd Analysis and Airflow Measurements to Approach Large Industrial Halls Energy Efficiency : A Case Study of a Cardboard Mill Hall.” Vol. 43, 2011, pp. 1200–1206. <https://doi.org/10.1016/j.enbuild.2010.12.034>.
- [51] Babu, T. P. A., Sriram, G. S., Vadvadgi, A. S., and Siddeshwar, R. “Air Flow Modeling In a Mechanically Ventilated Room.” *International Refrigeration and Air Conditioning Conference*, 2008, p. 971.
- [52] Transfer, N. H., and Applications, P. A. “MIXED CONVECTION IN A PARTIALLY DIVIDED.” Vol. 7782, 2007. <https://doi.org/10.1080/10407789708914058>.
- [53] Babu, T. P. A., Sriram, G. S., Vadvadgi, A. S., and Siddeshwar, R. Air Flow Modeling In a Mechanically Ventilated Room. 2008.
- [54] Mc Adams, W. H. *Heat Transmission*. McGraw-Hill, New-York, 1985.

- [55] SIEMENS. STAR-CCM+. <https://www.plm.automation.siemens.com/global/en/products/simcenter/STAR-CCM.html>.
- [56] Yuce, B. E., and Pulat, E. “Forced, Natural and Mixed Convection Benchmark Studies for Indoor Thermal Environments.” *International Communications in Heat and Mass Transfer*, Vol. 92, No. February, 2018, pp. 1–14. <https://doi.org/10.1016/j.icheatmasstransfer.2018.02.003>.
- [57] Lewis, G. A., Mathieu, D., and Phan-Tan-Luu, R. “Pharmaceutical Experimental Design.” *Technometrics*, Vol. 42, No. 2, 2000, pp. 222–222. <https://doi.org/10.1080/00401706.2000.10486034>.
- [58] Hochkirchen, T. *Design and Modeling for Computer Experiments*. 2006.
- [59] Banerjee, S. K., Thomas, P., and Cai, X. “CATIA V5-Based Parametric Aircraft Geometry Modeler.” *SAE International Journal of Aerospace*, Vol. 6, No. 1, 2013, pp. 311–321. <https://doi.org/10.4271/2013-01-2321>.
- [60] CMC Electronics Inc. *Flexible Power and Advanced Technology in a Low-Cost Mission Processing and Display Generation System*.
- [61] CMC Electronics inc. FV-4000 Open Architecture Avionics Computer.
- [62] Moir, I., and Seabridge, A. *Aircraft Systems: Mechanical, Electrical, and Avionics Subsystems Integration*. 2011.
- [63] Gaska, T., Watkin, C., and Chen, Y. “Integrated Modular Avionics - Past, Present, and Future.” *IEEE Aerospace and Electronic Systems Magazine*, Vol. 30, No. 9, 2015, pp. 12–23. <https://doi.org/10.1109/MAES.2015.150014>.
- [64] Baily, S., Sullivan, N., and Savisaar, A. *Development of Avionics Installation Interface Standards*. 1981.
- [65] De Vahl Davis, G., and Jones, I. P. “Natural Convection in a Square Cavity: A Comparison Exercise.” *International Journal for Numerical Methods in Fluids*, Vol. 3, No. 3, 1983, pp. 227–248. <https://doi.org/doi:10.1002/flid.1650030304>.
- [66] Bombardier Business Aircraft. Global 7500. Bombardier, 2020.
- [67] Sanchez, F., Liscouët-Hanke, S., and Tfaily, A. “Improving Aircraft Conceptual Design through Parametric CAD Modellers – A Case Study for Thermal Analysis of Aircraft Systems.” *Computers in Industry*, Vol. 130, 2021. <https://doi.org/10.1016/j.compind.2021.103467>.

Publications Associated with This Thesis

1. Sanchez, F., Huzaifa, A. M., and Liscouët-Hanke, S. “Mainstream Flow Prediction for the Thermal Risk Assessment of Aircraft Systems in Conceptual Design.” *AIAA AVIATION 2020 FORUM*, 2020. doi:10.2514/6.2020-2646.
2. Sanchez, F., Huzaifa, A. M., and Liscouët-Hanke, S. “Ventilation Considerations for an Enhanced Thermal Risk Prediction in Aircraft Conceptual Design.” *Aerospace Science and Technology*, Vol. 108, 2021, p. 106401. doi:10.1016/j.ast.2020.106401

Appendix

This section contains the design tables for the case studies conducted in this thesis. These tables contain data on the geometrical and physical parameters of the configurations used for the CFD studies.

Table I lists the data related to the design study conducted for a single system 2D CFD study in section 3.2.1.

Table I: The design table containing the values of different parameters for the design study conducted for a 2D simple equipment bay for establishing the ranges of mainstream numbers and their corresponding mainstream numbers.

.Bay dimensions		System dimensions			Inlet/Outlet dimensions				Boundary Conditions					Mainstream Numbers		
<i>Hbay</i> (m)	<i>Wbay</i> (m)	<i>Rsys</i> (m)	<i>Xsys</i> (m)	<i>Ysys</i> (m)	<i>Hin</i> (m)	<i>Yin</i> (m)	<i>Hout</i> (m)	<i>Yout</i> (m)	<i>M</i> (kg/s)	<i>Qsys</i> (W)	<i>Tbot</i> (°C)	<i>Tin</i> (°C)	<i>Ttop</i> (°C)	<i>S1</i>	<i>S2</i>	<i>S*</i>
0.50	1.00	0.05	0.12	0.36	0.09	0.30	0.08	0.35	0.17	1228.72	29.08	15.17	72.58	1.22	0.12	(1,1)
0.50	1.00	0.05	0.33	0.32	0.21	0.11	0.21	0.11	0.31	748.70	32.52	23.66	37.96	8.96	0.33	(0,0)
0.50	1.00	0.05	0.16	0.13	0.20	0.16	0.18	0.25	0.43	1108.08	27.51	17.76	65.34	0.41	0.16	(0,1)
0.50	1.00	0.05	0.78	0.28	0.24	0.12	0.17	0.09	0.43	912.96	23.67	15.93	36.45	7.25	0.78	(0,1)
0.50	1.00	0.05	0.59	0.22	0.12	0.07	0.09	0.38	0.32	1253.65	39.31	26.58	57.01	1.98	0.59	(0,0)
0.50	1.00	0.05	0.63	0.15	0.07	0.20	0.20	0.37	0.28	443.20	54.43	23.20	76.02	0.28	0.63	(0,0)
0.50	1.00	0.05	0.53	0.20	0.10	0.43	0.12	0.14	0.34	116.05	50.60	24.72	53.68	0.66	0.53	(1,0)
0.50	1.00	0.05	0.19	0.40	0.16	0.17	0.22	0.16	0.49	794.61	46.42	18.90	69.61	5.96	0.19	(0,1)
0.50	1.00	0.05	0.83	0.31	0.15	0.22	0.06	0.41	0.24	651.00	59.66	16.82	42.67	1.04	0.83	(1,1)
0.50	1.00	0.05	0.56	0.12	0.17	0.31	0.07	0.30	0.27	1501.78	53.00	19.99	59.59	0.15	0.56	(0,0)
0.50	1.00	0.05	0.68	0.22	0.05	0.40	0.14	0.22	0.40	1608.21	31.68	26.14	78.68	0.54	0.68	(0,0)
0.50	1.00	0.05	0.29	0.33	0.19	0.21	0.11	0.35	0.35	292.79	43.98	27.67	46.56	1.47	0.29	(1,1)
0.50	1.00	0.05	0.23	0.25	0.23	0.23	0.13	0.30	0.23	1918.93	34.58	21.37	48.28	0.94	0.23	(1,1)
0.50	1.00	0.05	0.46	0.17	0.19	0.32	0.22	0.37	0.39	1047.01	20.83	28.25	31.49	0.23	0.46	(0,0)
0.50	1.00	0.05	0.50	0.24	0.11	0.38	0.11	0.10	0.16	1777.32	45.34	29.04	41.79	1.42	0.50	(1,0)
0.50	1.00	0.05	0.38	0.35	0.09	0.10	0.16	0.16	0.22	558.11	24.49	21.78	60.40	7.84	0.38	(0,0)
0.50	1.00	0.05	0.72	0.38	0.13	0.10	0.18	0.14	0.19	1822.82	49.54	20.71	52.31	10.38	0.72	(0,1)
0.50	1.00	0.05	0.83	0.20	0.23	0.26	0.25	0.13	0.46	211.37	57.28	18.37	70.62	1.31	0.83	(1,1)
0.50	1.00	0.05	0.41	0.11	0.06	0.47	0.24	0.19	0.38	1396.60	36.76	29.59	32.52	0.14	0.41	(0,0)
0.50	1.00	0.05	0.78	0.29	0.16	0.13	0.09	0.12	0.47	1625.61	40.30	25.18	64.09	5.27	0.78	(0,1)
0.50	1.00	0.10	0.17	0.32	0.09	0.30	0.08	0.35	0.17	1228.72	29.08	15.17	72.58	0.98	0.17	(1,1)
0.50	1.00	0.10	0.35	0.30	0.21	0.11	0.21	0.11	0.31	748.70	32.52	23.66	37.96	7.70	0.35	(0,0)

0.50	1.00	0.10	0.20	0.17	0.20	0.16	0.18	0.25	0.43	1108.08	27.51	17.76	65.34	0.71	0.20	(1,1)
0.50	1.00	0.10	0.74	0.27	0.24	0.12	0.17	0.09	0.43	912.96	23.67	15.93	36.45	6.80	0.74	(0,1)
0.50	1.00	0.10	0.58	0.23	0.12	0.07	0.09	0.38	0.32	1253.65	39.31	26.58	57.01	2.13	0.58	(0,0)
0.50	1.00	0.10	0.61	0.18	0.07	0.20	0.20	0.37	0.28	443.20	54.43	23.20	76.02	0.44	0.61	(0,0)
0.50	1.00	0.10	0.53	0.22	0.10	0.43	0.12	0.14	0.34	116.05	50.60	24.72	53.68	0.77	0.53	(1,0)
0.50	1.00	0.10	0.23	0.35	0.16	0.17	0.22	0.16	0.49	794.61	46.42	18.90	69.61	4.59	0.23	(0,1)
0.50	1.00	0.10	0.79	0.29	0.15	0.22	0.06	0.41	0.24	651.00	59.66	16.82	42.67	0.91	0.79	(1,1)
0.50	1.00	0.10	0.55	0.16	0.17	0.31	0.07	0.30	0.27	1501.78	53.00	19.99	59.59	0.28	0.55	(0,0)
0.50	1.00	0.10	0.66	0.23	0.05	0.40	0.14	0.22	0.40	1608.21	31.68	26.14	78.68	0.59	0.66	(0,0)
0.50	1.00	0.10	0.32	0.30	0.19	0.21	0.11	0.35	0.35	292.79	43.98	27.67	46.56	1.24	0.32	(1,0)
0.50	1.00	0.10	0.26	0.25	0.23	0.23	0.13	0.30	0.23	1918.93	34.58	21.37	48.28	0.94	0.26	(1,1)
0.50	1.00	0.10	0.46	0.19	0.19	0.32	0.22	0.37	0.39	1047.01	20.83	28.25	31.49	0.32	0.46	(0,0)
0.50	1.00	0.10	0.50	0.24	0.11	0.38	0.11	0.10	0.16	1777.32	45.34	29.04	41.79	1.48	0.50	(1,0)
0.50	1.00	0.10	0.39	0.32	0.09	0.10	0.16	0.16	0.22	558.11	24.49	21.78	60.40	6.39	0.39	(0,0)
0.50	1.00	0.10	0.69	0.34	0.13	0.10	0.18	0.14	0.19	1822.82	49.54	20.71	52.31	8.10	0.69	(0,0)
0.50	1.00	0.10	0.83	0.20	0.23	0.26	0.25	0.13	0.46	211.37	57.28	18.37	70.62	1.31	0.83	(1,1)
0.50	1.00	0.10	0.42	0.16	0.06	0.47	0.24	0.19	0.38	1396.60	36.76	29.59	32.52	0.28	0.42	(0,0)
0.50	1.00	0.10	0.75	0.27	0.16	0.13	0.09	0.12	0.47	1625.61	40.30	25.18	64.09	4.84	0.75	(0,1)

Table II contains the dimensions and the boundary conditions of the 3D avionics bay with a single outlet. The case study refers to section 4.2.

Table II: Dimension and values boundary conditions of the for the 3D avionics bay.

Entity	Dimension (m)	System 1	System 2	System 3	System 4	System 5	System 6	System 7	System 8	System 9
Systems	X_{sys}	0.58	0.76	0.94	0.58	0.76	0.94	0.58	0.76	0.94
	Y_{sys}	0.72	0.72	0.72	0.44	0.44	0.44	0.16	0.16	0.16
	H_{sys}	0.20	0.20	0.20	0.20	0.20	0.20	0.20	0.20	0.20
	W_{sys}	0.16	0.10	0.16	0.16	0.10	0.16	0.16	0.10	0.16
	L_{sys}	0.38	0.38	0.38	0.38	0.38	0.38	0.38	0.38	0.38
	Heat load (W)	250	150	250	250	150	250	250	150	250
Inlet	X_{in}	0.19	0.19	0.19	0.19	0.19	0.19	0.19	0.19	0.19
	Y_{in}	0.03	0.03	0.03	0.03	0.03	0.03	0.03	0.03	0.03
	Z_{in}	0	0	0	0	0	0	0	0	0
	H_{in}	0.05	0.05	0.05	0.05	0.05	0.05	0.05	0.05	0.05
	W_{in}	0.38	0.38	0.38	0.38	0.38	0.38	0.38	0.38	0.38
	L_{in}	0.38	0.38	0.38	0.38	0.38	0.38	0.38	0.38	0.38
	T_{in} (°C)	27	27	27	27	27	27	27	27	27
	M (kg/s)	0.05	0.05	0.05	0.05	0.05	0.05	0.05	0.05	0.05
Outlet	X_{out}	1.14	1.14	1.14	1.14	1.14	1.14	1.14	1.14	1.14
	Y_{out}	0.85	0.85	0.85	0.85	0.85	0.85	0.85	0.85	0.85
	Z_{out}	0	0	0	0	0	0	0	0	0
	H_{out}	0.05	0.05	0.05	0.05	0.05	0.05	0.05	0.05	0.05
	W_{out}	0.38	0.38	0.38	0.38	0.38	0.38	0.38	0.38	0.38
	L_{out}	0.05	0.05	0.05	0.05	0.05	0.05	0.05	0.05	0.05
Bay	H_{bay}	0.89	0.89	0.89	0.89	0.89	0.89	0.89	0.89	0.89
	W_{bay}	0.76	0.76	0.76	0.76	0.76	0.76	0.76	0.76	0.76
	L_{bay}	0.58	0.58	0.58	0.58	0.58	0.58	0.58	0.58	0.58
	T_{tw} (°C)	50	50	50	50	50	50	50	50	50
	T_{bw} (°C)	30	30	30	30	30	30	30	30	30
	$\Delta\theta = T_{tw} - T_{bw}$	20	20	20	20	20	20	20	20	20

Table III: Dimensions and values boundary conditions for the systems and the ventilation sources of all outlets in the 3D avionics rack with multiple outlets in section 4.3.

Entity	Dimension (m)	System 1	System 2	System 3	System 4	System 5	System 6	System 7	System 8
Systems	X_{sys}	-0.18	0	0.18	-0.18	0	0.18	-0.18	0
	Y_{sys}	1.28	1.28	1.28	1	1	1	0.72	0.72
	Z_{sys}	0.67	0.67	0.67	0.67	0.67	0.67	0.67	0.67
	H_{sys}	0.20	0.20	0.20	0.20	0.20	0.20	0.20	0.20
	W_{sys}	0.16	0.10	0.16	0.16	0.10	0.16	0.16	0.10
	L_{sys}	0.38	0.38	0.38	0.38	0.38	0.38	0.38	0.38
	Heat load (W)	250	150	250	250	150	250	250	150
Inlet	X_{in}	0	0	0	0	0	0	0	0
	Y_{in}	0.1	0.1	0.1	0.1	0.1	0.1	0.1	0.1
	Z_{in}	0.19	0.19	0.19	0.19	0.19	0.19	0.19	0.19
	H_{in}	0.05	0.05	0.05	0.05	0.05	0.05	0.05	0.05
	W_{in}	0.76	0.76	0.76	0.76	0.76	0.76	0.76	0.76
	L_{in}	0.38	0.38	0.38	0.38	0.38	0.38	0.38	0.38
	T_{in} (°C)	27	27	27	27	27	27	27	27
Outlet_1	M (kg/s)	0.27	0.27	0.27	0.27	0.27	0.27	0.27	0.27
	X_{out}	0	0	0	0	0	0	0	0
	Y_{out}	0.85	0.85	0.85	0.85	0.85	0.85	0.85	0.85
	Z_{out}	0.79	0.79	0.79	0.79	0.79	0.79	0.79	0.79
	H_{out}	0.05	0.05	0.05	0.05	0.05	0.05	0.05	0.05
	W_{out}	0.2	0.2	0.2	0.2	0.2	0.2	0.2	0.2
	L_{out}	0.05	0.05	0.05	0.05	0.05	0.05	0.05	0.05
Outlet_2	M (kg/s)	0.18	0.18	0.18	0.18	0.18	0.18	0.18	0.18
	X_{out}	0	0	0	0	0	0	0	0
	Y_{out}	1.11	1.11	1.11	1.11	1.11	1.11	1.11	1.11
	Z_{out}	1.09	1.09	1.09	1.09	1.09	1.09	1.09	1.09
	H_{out}	0.03	0.03	0.03	0.03	0.03	0.03	0.03	0.03
	W_{out}	0.32	0.32	0.32	0.32	0.32	0.32	0.32	0.32
	L_{out}	0.03	0.03	0.03	0.03	0.03	0.03	0.03	0.03
Outlet_3	M (kg/s)	0.05	0.05	0.05	0.05	0.05	0.05	0.05	0.05
	X_{out}	0	0	0	0	0	0	0	0
	Y_{out}	0.56	0.56	0.56	0.56	0.56	0.56	0.56	0.56
	Z_{out}	1.12	1.12	1.12	1.12	1.12	1.12	1.12	1.12
	H_{out}	0.03	0.03	0.03	0.03	0.03	0.03	0.03	0.03
	W_{out}	0.38	0.38	0.38	0.38	0.38	0.38	0.38	0.38
	L_{out}	0.03	0.03	0.03	0.03	0.03	0.03	0.03	0.03
Bay	H_{bay}	1.83	1.83	1.83	1.83	1.83	1.83	1.83	1.83
	W_{bay}	0.76	0.76	0.76	0.76	0.76	0.76	0.76	0.76
	L_{bay}	0.85	0.85	0.85	0.85	0.85	0.85	0.85	0.85
	T_{tw} (°C)	50	50	50	50	50	50	50	50
	T_{bw} (°C)	30	30	30	30	30	30	30	30
	$\Delta\theta = T_{tw} - T_{bw}$	20	20	20	20	20	20	20	20

Entity	Dimension (m)	System 9	System 10	System 11	System 12	System 13	System 14	System 15
Systems	X_{sys}	0.18	-0.18	0	0.18	-0.18	0	0.18
	Y_{sys}	0.72	0.44	0.44	0.44	0.16	0.16	0.16
	Z_{sys}	0.67	0.67	0.67	0.67	0.67	0.67	0.67
	H_{sys}	0.20	0.20	0.20	0.20	0.20	0.20	0.20
	W_{sys}	0.16	0.16	0.10	0.16	0.16	0.10	0.16
	L_{sys}	0.38	0.38	0.38	0.38	0.38	0.38	0.38
	Heat load (W)	250	250	150	250	250	150	250
Inlet	X_{in}	0	0	0	0	0	0	0
	Y_{in}	0.1	0.1	0.1	0.1	0.1	0.1	0.1
	Z_{in}	0.19	0.19	0.19	0.19	0.19	0.19	0.19
	H_{in}	0.05	0.05	0.05	0.05	0.05	0.05	0.05
	W_{in}	0.76	0.76	0.76	0.76	0.76	0.76	0.76
	L_{in}	0.38	0.38	0.38	0.38	0.38	0.38	0.38
	T_{in} (°C)	27	27	27	27	27	27	27
	M (kg/s)	0.27	0.27	0.27	0.27	0.27	0.27	0.27
Outlet_1	X_{out}	0	0	0	0	0	0	0
	Y_{out}	0.85	0.85	0.85	0.85	0.85	0.85	0.85
	Z_{out}	0.79	0.79	0.79	0.79	0.79	0.79	0.79
	H_{out}	0.05	0.05	0.05	0.05	0.05	0.05	0.05
	W_{out}	0.2	0.2	0.2	0.2	0.2	0.2	0.2
	L_{out}	0.05	0.05	0.05	0.05	0.05	0.05	0.05
	M (kg/s)	0.18	0.18	0.18	0.18	0.18	0.18	0.18
Outlet_2	X_{out}	0	0	0	0	0	0	0
	Y_{out}	1.11	1.11	1.11	1.11	1.11	1.11	1.11
	Z_{out}	1.09	1.09	1.09	1.09	1.09	1.09	1.09
	H_{out}	0.03	0.03	0.03	0.03	0.03	0.03	0.03
	W_{out}	0.32	0.32	0.32	0.32	0.32	0.32	0.32
	L_{out}	0.03	0.03	0.03	0.03	0.03	0.03	0.03
	M (kg/s)	0.05	0.05	0.05	0.05	0.05	0.05	0.05
Outlet_3	X_{out}	0	0	0	0	0	0	0
	Y_{out}	0.56	0.56	0.56	0.56	0.56	0.56	0.56

	<i>Zout</i>	1.12	1.12	1.12	1.12	1.12	1.12	1.12
	<i>Hout</i>	0.03	0.03	0.03	0.03	0.03	0.03	0.03
	<i>Wout</i>	0.38	0.38	0.38	0.38	0.38	0.38	0.38
	<i>Lout</i>	0.03	0.03	0.03	0.03	0.03	0.03	0.03
	<i>M (kg/s)</i>	0.05	0.05	0.05	0.05	0.05	0.05	0.05
<i>Bay</i>	<i>Hbay</i>	1.83	1.83	1.83	1.83	1.83	1.83	1.83
	<i>Wbay</i>	0.76	0.76	0.76	0.76	0.76	0.76	0.76
	<i>Lbay</i>	0.85	0.85	0.85	0.85	0.85	0.85	0.85
	<i>T_{tw} (°C)</i>	50	50	50	50	50	50	50
	<i>T_{bw} (°C)</i>	30	30	30	30	30	30	30
	$\Delta\theta = T_{tw} - T_{bw}$	20	20	20	20	20	20	20

Table IV lists each system's CS and SW values for the case study conducted in section 4.3.

Table IV: CS and SW numbers for all the systems with respect to each ventilation source for the avionics bay with multiple outlets.

System	Inlet			Outlet_1			Outlet_2			Outlet_3		
	CSin (x)	CSin (y)	SWin (z)	CSout (x)	CSout (z)	SWout (y)	CSout (x)	CSout (y)	SWout (z)	CSout (x)	CSout (y)	SWout (z)
System 1	-0.47	136.13	0.26	3.67	-0.65	0.17	6.96	4.19	0.08	6.96	100.89	0.08
System 2	-1.43	136.13	0.26	-0.13	-0.65	0.17	-0.56	4.19	0.08	-0.56	100.89	0.08
System 3	-0.47	136.13	0.26	3.67	-0.65	0.17	6.96	4.19	0.08	6.96	100.89	0.08
System 4	-0.47	78.89	0.26	3.67	-0.65	0.34	6.96	0.88	0.08	6.96	36.82	0.08
System 5	-1.43	78.89	0.26	-0.13	-0.65	0.34	-0.56	0.88	0.08	-0.56	36.82	0.08
System 6	-0.47	78.89	0.26	3.67	-0.65	0.34	6.96	0.88	0.08	6.96	36.82	0.08
System 7	-0.47	37.09	0.26	3.67	-0.65	0.50	6.96	28.44	0.08	6.96	3.61	0.08
System 8	-1.43	37.09	0.26	-0.13	-0.65	0.50	-0.56	28.44	0.08	-0.56	3.61	0.08
System 9	-0.47	37.09	0.26	3.67	-0.65	0.50	6.96	28.44	0.08	6.96	3.61	0.08
System 10	-0.47	10.72	0.26	3.67	-0.65	0.67	6.96	86.87	0.08	6.96	1.28	0.08
System 11	-1.43	10.72	0.26	-0.13	-0.65	0.67	-0.56	86.87	0.08	-0.56	1.28	0.08
System 12	-0.47	10.72	0.26	3.67	-0.65	0.67	6.96	86.87	0.08	6.96	1.28	0.08
System 13	-0.47	-0.21	0.26	3.67	-0.65	0.84	6.96	176.16	0.08	6.96	29.81	0.08
System 14	-1.43	-0.21	0.26	-0.13	-0.65	0.84	-0.56	176.16	0.08	-0.56	29.81	0.08
System 15	-0.47	-0.21	0.26	3.67	-0.65	0.84	6.96	176.16	0.08	6.96	29.81	0.08

Table V lists the predicted thermal risk scoring for the case study performed in section 4.3.

Table V-a: Thermal risk table for the avionics rack with multiple outlets- Case 1.

Case 1								
System	Ventilation TR ₁	Stratification TR ₂	Mainstream TR ₃	System Integration TR ₄	Temperature Limits TR ₅	Heat Removal Potential TR ₆	Thermal Risk Score	Thermal Risk
System 1	1	1	3	3	1	1	9	Medium risk
System 2	1	1	2.25	3	1	1	6.75	Medium risk
System 3	1	1	3	3	1	1	9	Medium risk
System 4	1	1	3	2	1	1	6	Medium risk
System 5	1	1	3	2	1	1	6	Medium risk
System 6	1	1	3	2	1	1	6	Medium risk
System 7	1	1	3	2	1	1	6	Medium risk
System 8	1	1	3	2	1	1	6	Medium risk
System 9	1	1	3	2	1	1	6	Medium risk
System 10	1	1	3	1	1	1	3	Low risk
System 11	1	1	3	1	1	1	3	Low risk
System 12	1	1	3	1	1	1	3	Low risk
System 13	1	1	1	1	1	1	1	Low risk
System 14	1	1	1	1	1	0.012	0.012	Low risk
System 15	1	1	1	1	1	1	1	Low risk

Table V-b Thermal risk table for the avionics rack with multiple outlets- Case 2.

Case 2								
System	Ventilation TR ₁	Stratification TR ₂	Mainstream TR ₃	System Integration TR ₄	Temperature Limits TR ₅	Heat Removal Potential TR ₆	Thermal Risk Score	Thermal Risk
System 1	1	1	3	3	1	1	9	Medium risk
System 2	1	1	2.25	3	1	1	6.75	Medium risk
System 3	1	1	3	3	1	1	9	Medium risk
System 4	1	1	3	2	1	1	6	Medium risk
System 5	1	1	3	2	1	1	6	Medium risk
System 6	1	1	3	2	1	1	6	Medium risk
System 7	1	1	4	2	1	1	8	Medium risk
System 8	1	1	3	2	1	1	6	Medium risk
System 9	1	1	4	2	1	1	8	Medium risk
System 10	1	1	4.5	1	1	1	4.5	Low risk
System 11	1	1	3.75	1	1	1	3.75	Low risk
System 12	1	1	4.5	1	1	1	4.5	Low risk
System 13	1	1	1	1	1	0.056	0.056	Low risk
System 14	1	1	1	1	1	0.056	0.056	Low risk
System 15	1	1	1	1	1	0.056	0.056	Low risk

Table V-c Thermal risk table for the avionics rack with multiple outlets- Case 3

Case 3								
System	Ventilation TR ₁	Stratification TR ₂	Mainstream TR ₃	System Integration TR ₄	Temperature Limits TR ₅	Heat Removal Potential TR ₆	Thermal Risk Score	Thermal Risk
System 1	1	1	3	3	1	0.19	1.71	Medium risk
System 2	1	1	2.25	3	1	0.19	1.2825	Low risk
System 3	1	1	3	3	1	0.19	1.71	Medium risk
System 4	1	1	4	2	1	1	8	Medium risk
System 5	1	1	3	2	1	1	6	Medium risk
System 6	1	1	4	2	1	1	8	Medium risk
System 7	1	1	3	2	1	1	6	Medium risk
System 8	1	1	3	2	1	1	6	Medium risk
System 9	1	1	3	2	1	1	6	Medium risk
System 10	1	1	3	1	1	1	3	Low risk
System 11	1	1	3	1	1	1	3	Low risk
System 12	1	1	3	1	1	1	3	Low risk
System 13	1	1	1	1	1	1	1	Low risk
System 14	1	1	1	1	1	0.01	0.01	Low risk
System 15	1	1	1	1	1	1	1	Low risk

Table V-d: Thermal risk table for the avionics rack with multiple outlets- Case 4

Case 4								
System	Ventilation TR ₁	Stratification TR ₂	Mainstream TR ₃	System Integration TR ₄	Temperature Limits TR ₅	Heat Removal Potential TR ₆	Thermal Risk Score	Thermal Risk
System 1	1	1	3	3	1	0.48	4.32	Low risk
System 2	1	1	2.25	3	1	0.48	3.24	Low risk
System 3	1	1	3	3	1	0.48	4.32	Low risk
System 4	1	1	4	2	1	0.48	3.84	Low risk
System 5	1	1	3	2	1	0.48	2.88	Low risk
System 6	1	1	4	2	1	0.48	3.84	Low risk
System 7	1	1	4	2	1	0.48	4.8	Low risk
System 8	1	1	3	2	1	0.48	3.6	Low risk
System 9	1	1	4	2	1	0.48	4.8	Low risk
System 10	1	1	5	1	1	0.11	0.55	Low risk
System 11	1	1	3.75	1	1	0.11	0.4125	Low risk
System 12	1	1	5	1	1	0.11	0.55	Low risk
System 13	1	1	1	1	1	0.11	0.11	Low risk
System 14	1	1	1	1	1	0.11	0.11	Low risk
System 15	1	1	1	1	1	0.11	0.11	Low risk